NOTE TO USERS

14

Investigation of Aircraft Yaw Motion Control

NICOLAS ULYSSE

A Thesis

in

The Department

of

Mechanical and Industrial Engineering

Presented in Partial Fulfillment of the Requirements

for the Degree of Master of Applied Science at

Concordia University

Montreal, Quebec, Canada

August 2003

Your file Votre référence
ISBN: 0-612-83885-4
Our file Notre référence
ISBN: 0-612-83885-4

ABSTRACT

Investigation of Aircraft Yaw Motion Control

Nicolas Ulysse

During production flight tests, a number of aircrafts of different types and constructors have exhibited small and uncommanded yaw shudders or 'kicks' which in some instances were accompanied by minute, poorly damped oscillations.

In a continuation of a collaborative research study carried out by Concordia University and Bombardier Aerospace, this thesis aims to understand and eventually eliminate this phenomenon. Based on previous work done on a detailed flight model that concludes that the yaw 'kicks' are most likely initiated by uncommanded small deflections of the rudder, this thesis investigates the possibility that discontinuous non-linearities in the rudder control system might be at the root of the problem. The research in this study is conducted through modeling and virtual testing of the rudder control system, and are also aims at producing an "industrially viable" model.

The research involved the modeling of the system including various non-linearities, as well as the integration of the hydraulic servo actuators, concluding with the validation of the model. Finally, an extensive "trial-and-error" investigation was performed where variations of the non-linearities within realistic/actual tolerances were used to instantiate a number of different model configurations, each of them being virtually "flown". This thesis demonstrates that under certain condition, the system can self-initiate a rudder deflection of the order of magnitude expected.

ACKNOWLEGEMENTS

The author wishes to express his gratitude to his supervisors Dr. J. Svoboda and Dr. Gordon for their guidance, support, and patience in completing this project and for their precious help in correcting this thesis.

The invaluable assistance of the simulation group at Bombardier Aerospace, including Enrique Davaze, Tony d'Amore and François Godin for their advices and help is greatly appreciated. Last but not the least, the author wishes to thank Carlos Trinidad, strategic technology group, Bombardier Aerospace, for his advice in coordinating the Concordia and Bombardier project.

My friends Jian Chen, Narendra Gollu, Gilles Huard and Dong Sheng Wang at the CIC were always there to provide me with invaluable support when needed and contributed to make this work a pleasant and memorable experience.

This would be incomplete without a word for my family in France: without them, I would not have gone this far in my studies. I also wish to thank Nathalie Gratton; for her love and understanding.

TABLE OF CONTENT

LIST OF TABLES AND FIGURES

TABLES:

FIGURES:

LIST OF VARIABLES

$A_{actuator}$ Surface of the actuator

$A_{orifice}$ Area of control valve orifice

b Wing span

$\bar{c}$ Mean aerodynamic chord

C Orifice flow coefficient

C_x Aircraft overall longitudinal force coefficient

C_y Aircraft overall side force coefficient

C_z Aircraft overall vertical force coefficient

C_L Rolling moment coefficient

C_M Pitching moment coefficient

C_N Yawing moment coefficient

g Gravity acceleration

h Solver integration step

I_c Cable installation factor

I_{xx} Aircraft moment of inertia about the X body axis

I_{yy} Aircraft moment of inertia about the Y body axis

I_{zz} Aircraft moment of inertia about the Z body axis

I_p Pendulum moment of inertia

J Jacobian matrix

L_a Lagrangian

L Net rolling moment acting in the aircraft about the Y body axis

l_{stroke} Stroke length of the PCU actuator

L_c	Cable length
m	Aircraft mass
m_p	Pendulum mass
M	Net pitching moment acting in the aircraft about the Y body axis
N	Net yawing moment acting on the aircraft about the Z body axis
p	Aircraft roll rate about the z body axis
q	Aircraft pitch rate about the y body axis
Q	Column matrix of externally applied force
q_p	Generalized coordinate vector
r	Aircraft yaw rate about the z body axis
S	Aircraft wing surface area
T	Kinetic energy
U_0	Reference flight speed
u, $\dot{u}$	Longitudinal speed and acceleration
u_p	Time derivative of pendulum x position
δW_{nc}	Virtual work done by non-conservative forces
V	Potential energy
v, $\dot{v}$	Lateral speed and acceleration
v_p	Time derivative of pendulum y position
w, $\dot{w}$	Vertical speed and acceleration
w_p	Time derivative of pendulum orientation
X	Longitudinal force
x_p	Pendulum x position

Y	Lateral force
$\overline{Y}$	State vector
y_p	Pendulum y position
Z	Vertical force
α	Angle of attack
β	Angle of sideslip
δ_c	Cable elongation
ϵ	Integration error tolerance
μ_d	Dynamic coefficient of friction
$\beta_{effective}$	Effective bulk modulus of the PCU actuator
θ	Pitch angle
θ_p	Pendulum orientation
λ	Column matrix of the Lagrange multiplier
μ_s	Static coefficient of friction
δa	Aileron deflection
δr	Rudder deflection
ρ	Mass density of powering fluid
ϕ	Roll angle
Φ_q	Jacobian matrix of the constraint equations
ψ	Yaw angle

LIST OF ACRONYMS AND ABBREVIATIONS

A/C	Aircraft
BDF	Backward Differentiation Formula
BL	Buttock Line
DOE	Design Of Experiment
DOF	Degree Of Freedom
FAA	Federal Aviation Administration
FEM	Finite Element Modelisation
FS	Fuselage Station
HM	Hinge Moment
MLW	Maximum Landing Weight
MTOW	Maximum Take-Off Weight
ODE	Ordinary Differential Equation
PCU	Power Control Unit
PSD	Power Spectral Density
SL	Sea Level
VPFCS	Virtual Primary Flight Control System
WL	Water Line

1 Introduction

Machine design in the earliest period of the industrial era involved a large amount of testing and trial and error reasoning. Engineers had to find answers, results, and solutions to problems where scientific knowledge and opinion were often limited, and the development of empirical laws through extensive testing was frequently the only path to a successful design.

The rapid rise in digital computer technology in the second half of the 20th century allowed scientists and engineers to build meaningful models of complex systems and to reproduce physical system behaviors; this then led to computer simulation.

For the engineer, simulation enabled the creation of virtual prototypes and as a result, allowed for the testing and comparison of different solutions at the earliest stages of design at a low cost and with limited risks. Another consequence of enacting simulations is the possibility to investigate the behavior of a machine in a virtual environment at the production stage, when implementing the actual test would be too difficult or costly. Using a virtual environment also allows for full control of all of the parameters when reality obviously only allows limited access and control to the engineer.

This work is an attempt to make use of all of these possibilities to contribute to the solving of an actual industry problem, the understanding of which has presented a challenge for many years.

1.1 Problem Definition

In the past, a number of aircrafts of different types and constructors have been affected by small inexplicable anomalies in their yaw motions, anomalies usually referred

as yaw activities. One type of such an occurrence is commonly called the yaw kick: a small, fast and uncommanded movement. The other type consists of minute yaw oscillations, occurring at a frequency around one cycle per second (*Figure 1.1*).

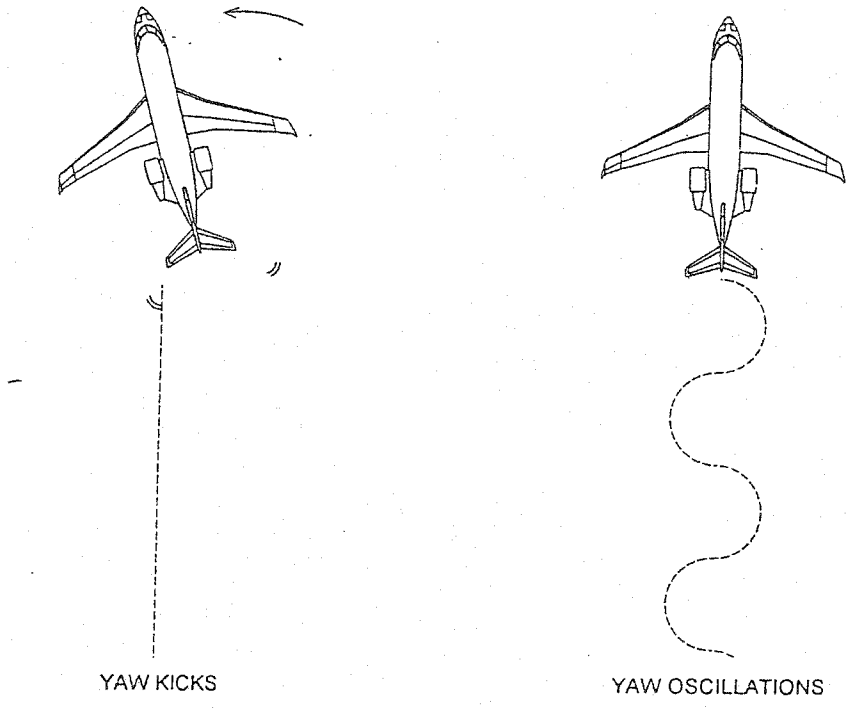

Figure 1.1 -Yaw Activity

Yaw activities are not dangerous; however, they can be annoying for both passengers and crew since the aircraft behaves in an uncommanded and unpredictable manner [1]. Additionally, delivery of the aircraft can been subsequently delayed if the customer judges the level of yaw activity too high, thereby increasing costs.

1.1.1 Yaw Activity

A major concern with yaw activity is the difficulty to reproduce it during flight tests, which explains a chronic lack of experimental data. In addition the phenomena

could affect only a small percentage of the production of particular aircraft design, which explains why tracking procedures engaged by flight test departments did not lead to any significant results. Moreover, production aircrafts are not equipped with adequate instrumentation and test aircrafts do not consistently experience yaw activity.

It is therefore very difficult to characterize under what conditions these phenomena are occur but they normally arise under the following circumstances:

1. High dynamic pressure
2. Between 10 000 and 30 000 feet [2]

Yaw kicks on which this study focuses have been characterized by lateral accelerations of the order of 0.01 g [2]. Though it might seems very small, the human body was found to be very sensitive to lateral acceleration and even though no international regulation exists in aerospace on the matter, ISO standards [3] for building do consider such small magnitudes to be noticeable.

Most of the time engineers were able to eliminate these phenomena that anyway have stayed a low priority issue and did not generate any detailed investigations thanks to their small impact.

1.2 Previous Work and Findings

With the wish to completely characterize this phenomenon, and possibly integrate the findings in its future design, Bombardier Aerospace, a world leader manufacturer of business/regional aircrafts has engaged a long-term collaboration with Concordia University to investigate the issue [1]. Bombardier Aerospace would therefore offer Concordia a controlled access to one of its earliest design characteristics.

As shown in *Figure 1.2*, possible causes for yaw activity could be classified in three categories:

- Aerodynamic Causes: non-linearity in the roll damping has in the past been the source of such phenomena as wing rock, which does have similarities with the yaw oscillations phenomena [1]. Also, unsymmetrical stalling of the winglets was first investigated as a cause of the yaw kick. All this issues were therefore investigated and rejected in the past: they are not considered in this work.
- Autopilot/Yaw Damper: it seems that yaw kick were experienced with yaw damper both on and off. Nevertheless, no record was found testifying whether the turn coordination function, also performed by the yaw damper, but which cannot be switched off directly from the cockpit, was off. As Sperry, the subcontractor in charge of the design and production of the yaw damper is refusing to give the design details, this option could not be further investigated
- The Yaw Control System: it converts the pilot feet motion to the rudder rotation, through a number of linkages and pulleys, and is usually hydraulically boosted. This is the part of the mechanism of interest in this study.

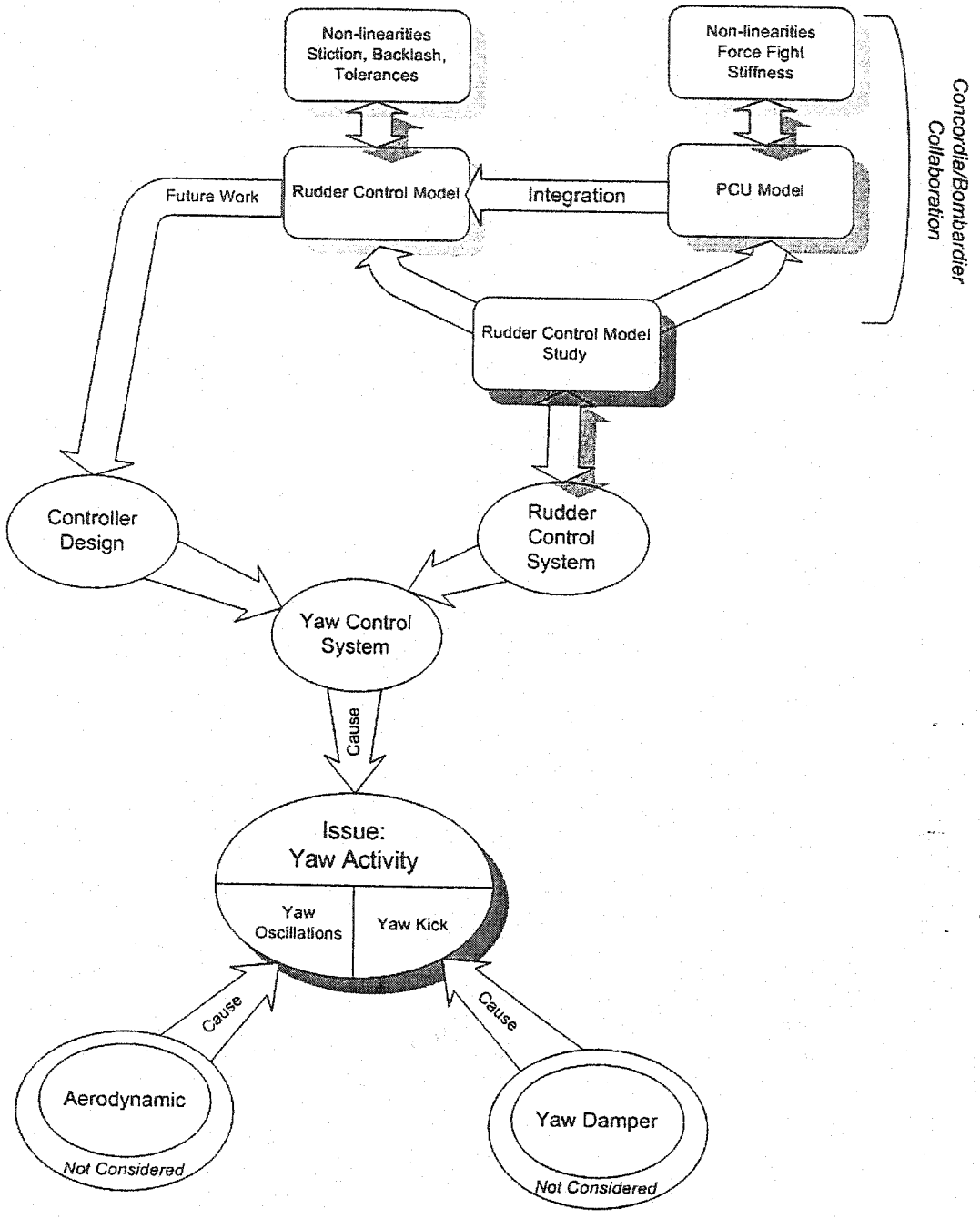

Figure 1.2 -Problem Solving Map

Earlier attempts to find an aerodynamic cause were unsuccessful. This has led to the conviction that the cause must originate in a failure of the yaw control mechanism:

this are these investigations that were taken care of by Concordia, and that are detailed in the top half of *Figure 1.2*.

Of key role in the choosing of this final cause for investigation were computer simulations of the aircraft dynamic by Concordia University, showing that a rudder input of **0.5 degrees** was sufficient to produce an aircraft response close to yaw kicks (*Figure 1.3*) as witnessed in flight, with the expected lateral acceleration of 0.01g [1].

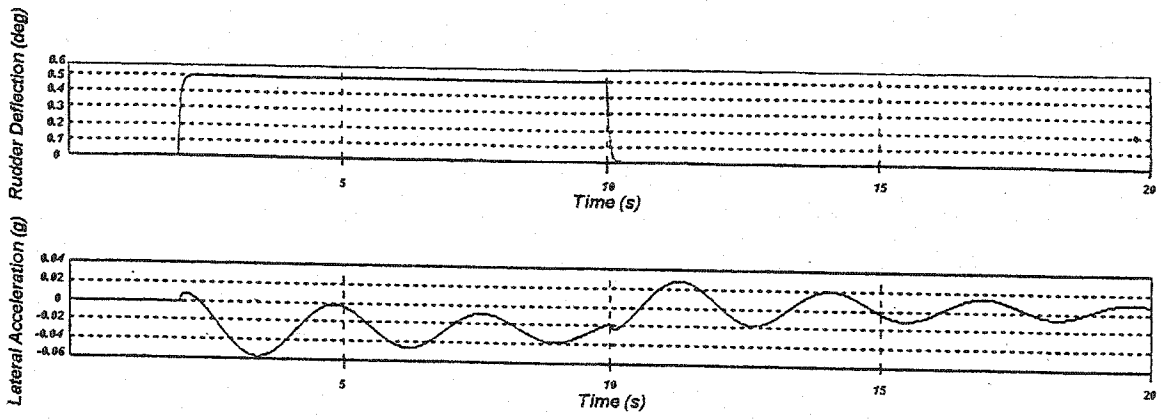

Figure 1.3 -Yaw Kick Simulation

Concordia originally regarded yaw kick and yaw oscillation as two linked phenomena.

The route initially considered was to develop a new control algorithm using modern non-linear control strategies in order to suppress yaw activity, without alteration of the mechanism [1]. This would have also been sustained by the parallel development of a detailed model of the yaw control system. This approach, however, proved to be difficult to implement in actual aircraft design, and was abandoned. Yet, detail modeling and research on the yaw control part was still considered a priority (*Figure 1.2*).

Backlash, dead spot and cable stretching, and introducing non-linearity in a control system have been known to be a cause of limit cycle oscillation, if not system

instability [5]. These are therefore serious candidates as the cause for the yaw activity that oriented the research on their modeling, and on extensive testing of the resulting model. This model was therefore be able, not only to reproduce the normal behavior of the system, but also to include the various discontinuous non-linearities suspected to produce yaw kick under conditions that were still to be identified.

Early investigation had pointed the key role of the Power Control Units in the system dynamic. This Concordia University, to the development and validation of a detailed model of the Power Control Units and an investigation of their dynamic (PCU's are the hydraulic servo actuators located at the end of the rudder control system providing force/power amplification of the control inputs) [4]. This work suggests that the PCU should not be incriminated in association with the problematic of uncommanded yaw activity.

1.3 Thesis Objective

From the background work discussed in *Section 1.2* made it possible to clearly define the objectives of this thesis. It was indeed decided to focus the study effort primarily at the yaw kick phenomenon. This was to be achieved in the following steps:

- To develop a dynamic model of the rudder control system on ADAMS, integrating the hydraulic systems, and capitalizing on Concordia findings on PCU. This model is to be "industry viable", while being of sufficient accuracy and flexibility to conduct the second step of this study.
- Using this model, investigate whether non-linearities in the rudder control system might self-initiate a rudder deflection of the characteristic and magnitude defined in Section 1.2.

The goal of this project is therefore to investigate whether non-linearity in the system, whose most likely sources were identified as cable stretching or clearance in the mechanical linkage or friction, may initiate a brisk uncommanded motion of the rudder. At the same time, the project seeks to produce a model whose characteristics would be compliant with Bombardier general needs.

1.4 Outline

The next section is an attempt to gather and summarizes general knowledge about aircraft dynamics and control, and on a flight model used in this study. Based on this considerations *Section 3* studies the yaw control system: its requirements, and architecture, indeed preparing for the detailed review of the rudder control system model, in *Section 4*. This section also includes validation procedures and results of the model, paving the way for the last section: investigation on the behavior of the rudder control system model with non-linearities.

2 Aircraft Dynamic and Modeling

An airplane is a dynamic system with six degrees of freedom with each of them subjected to various coupling effects. An airplane is also subjected to a variety of complex aerodynamic forces, and is a very intricate machine encompassing a wide range of interrelated systems. Finally, the airplane is carefully designed to fulfill a particular type of mission, whether it is to carry a few passengers on a short-range distance trip, or to carry 450 people all around the globe. It appears obvious that modeling such a machine involves many challenges, not the least being the ability to choose the right set of assumptions in order to build the proper model for the design issue studied.

2.1 Aircraft Dynamic

2.1.1 Flight Forces and Equilibrium

An airplane in flight is the center of a continuous tug of war between four forces (*Figure 2.1*), which can be divided into:

- Aerodynamic forces ⇒Lift and Drag
- Weight
- Propulsion forces

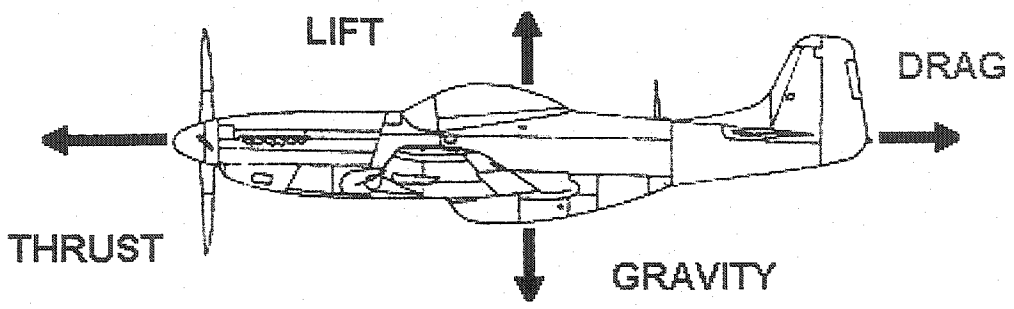

Figure 2.1 - Forces of Flight

The lift is a consequence of the airflow around the particular profile of the wing. Opposing gravity, it pulls the aircraft into the air. Drag is the logic consequence of the lift and opposes aircraft motion: it is counteracted by the thrust.

2.1.2 Reference Axis

Because the aircraft is subjected to so many different types of forces and allowed to move in six degrees of freedom, special care must taken to define the proper naming convention, while the choice of the optimal reference frame from which to derive the equations is crucial.

The origin of the axis is usually positioned at the aircraft center of gravity. The naming convention for the degrees of freedom is illustrated in *Figure 2.2*.

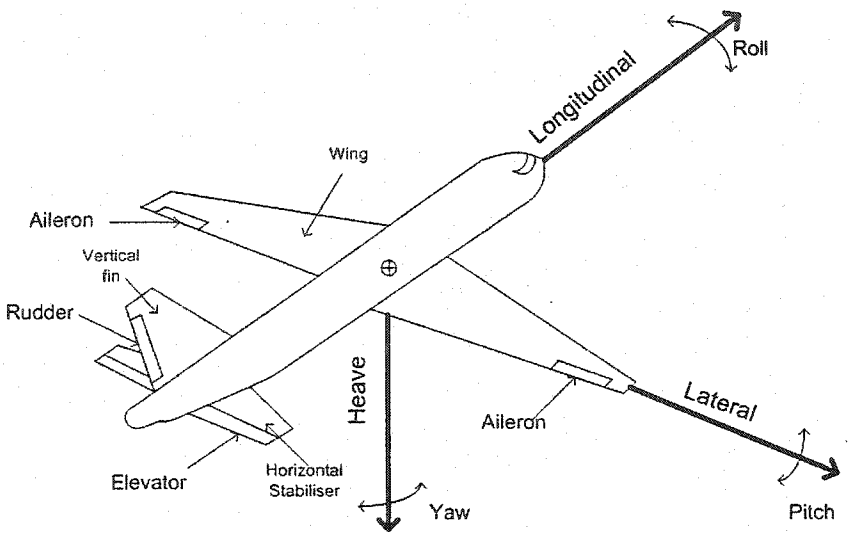

Figure 2.2 - Aircraft Movements and Primary Flight Controls

Flight controls have become more complex, but for the purposes of this document, we will limit them to the following typical control surfaces (as shown in *Figure 2.2*):

- Aileron, controlling the rolling motion: their asymmetrical deflection is inducing differential lift on each wing.
- Elevator, controls the pitching motion, by changing the lift of the horizontal stabilizer.
- Rudder, which controls the yawing motion. It is used for co-ordination of airplane movement, for correction of asymmetric thrust, cross-wing effect….

In aircraft dynamics, there are two important axis systems commonly used: body axes and inertia axes [5]:

- **Body Axes System** *(O,Xb,Yb,Zb)*: fixed to the airframe, it uses the aircraft's center of gravity as an origin, and if the aircraft has a plane of symmetry, it

coincides with the OXbYb plane, as shown in *Figure 2.3*. Hence, moment and product of inertia will remain constant in respect to time.

- **Stability Axes System** *(O,Xs,Ys,Zs):* is a special case of the body axes and is widely used to study airplane motion involving small disturbances from a steady reference condition [6]. In reference to *Figure 2.3*, β is called the sideslip angle, and α the angle of attack. These two angles also express the aircraft's orientation relative to airflow.

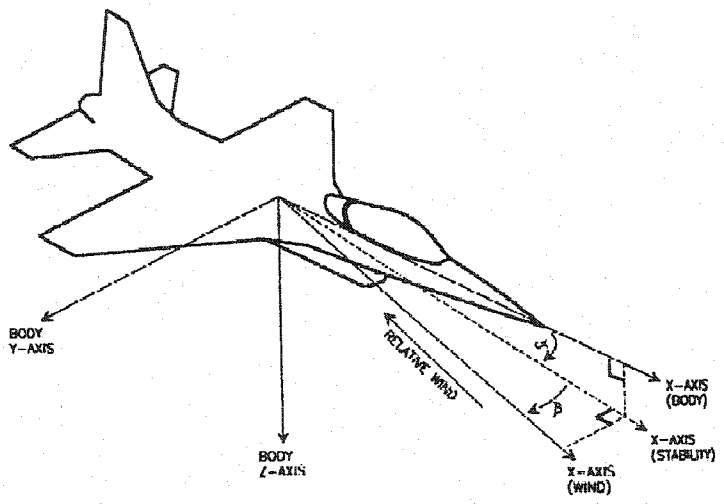

Figure 2.3 -Aircraft Stability and Body Axes [8]

- **The Navigational Axes System** *(O,Xe,Ye,Ze):* is fixed to the earth. This is important, because acceleration forces are calculated in respect to the earth. In aircraft dynamics, where navigation is not of interest, and does not involve a study on long period motion, the navigational axes system is considered a Newtonian reference (*Figure 2.4*). Considering it a Newtonian reference frame, the effect of the earth 's rotation is neglected, which is notably small for fast moving machines during a short period of time [6].

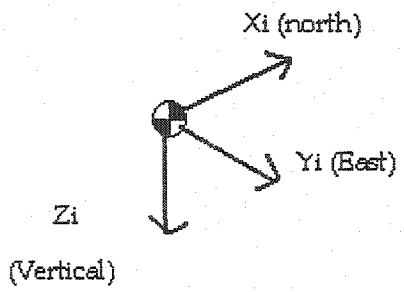

Figure 2.4 - Navigational Axis System

Finally, *Figure 2.5* summarizes the notations used in the calculation of the equation of motions.

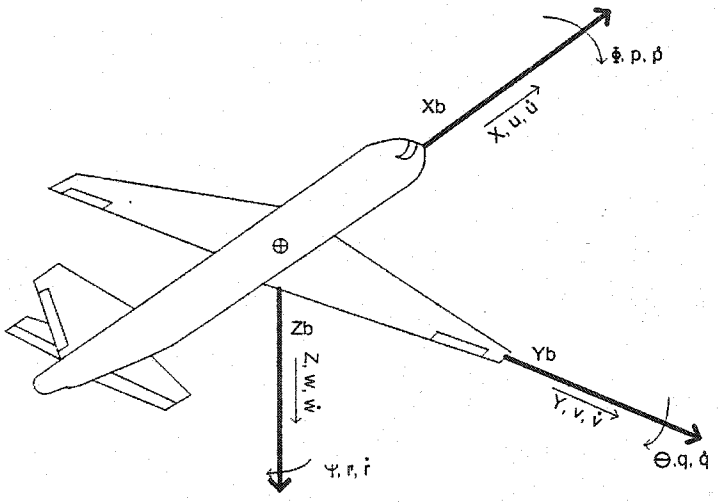

Figure 2.5 - Standard Notations

2.1.3 The Equations of Motion

2.1.3.1 Introduction

The equations governing the equations of motion are based on Newton's laws of motion. Deriving them from a space-fixed frame would induce many difficulties because the inertia would continuously vary with time. They are therefore usually derived in the body reference frame (*Section 2.1.2).* Although doing so simplifies the equations

with m being the aircraft mass, g denoting the gravity acceleration, I_{xx}, I_{yy} and I_{zz} the aircraft's moment of inertia in respect to the body frame reference, X, Y, Z the applied forces, and L, M, N the applied moment projected on the body reference frame.

The motion of the aircraft can be computed by solving these equations. The reader should note the cross coupling between longitudinal and lateral equations.

2.1.3.4 Lateral Stability

For the study of aircraft stability and control it is common practice to derive a simplified equation, describing the aircraft's response to disturbances with reference to an initial straight and level, unaccelerated flight. It is usually assumed that disturbances are small compared to the disturbed variables.

It is also common practice to introduce dimensionless coefficients to express the forces and moment. These coefficients are usually referred to as stability derivatives and are defined as in *Eqn. (2)*:

$$\Delta C_x = \frac{\Delta X_x}{\frac{1}{2} * \rho * U_0^2 * S} \quad \Delta C_l = \frac{\Delta L}{\frac{1}{2} * \rho * U_0^2 * S * b}$$

$$\Delta C_y = \frac{\Delta Y}{\frac{1}{2} * \rho * U_0^2 * S} \quad \Delta C_m = \frac{\Delta M}{\frac{1}{2} * \rho * U_0^2 * S * \bar{c}} \qquad \textit{Eqn. (2)}$$

$$\Delta C_z = \frac{\Delta Z}{\frac{1}{2} * \rho * U_0^2 * S} \quad \Delta C_n = \frac{\Delta N}{\frac{1}{2} * \rho * U_0^2 * S * b}$$

the suffix o being the steady flight conditions and Δ the disturbances.

Furthermore, three new assumptions are introduced:

- Instantaneous forces and moment depend on the instantaneous values of the motion variables

- Aerodynamic forces and moment vary linearly with motion variables
- Lateral forces and moment (Y , L, N) depend only on lateral-directional variables (u, α, q) *(valid at small angle of slide slip)*

Using the Taylor series expansion, the two last hypotheses can be used approximate the stability derivatives defined in *Eqn. (2)* to *Eqn. (3)*:

$$\Delta C_y = \frac{\partial C_y}{\partial \beta}\Delta\beta + \frac{\partial C_y}{\partial \Phi}\Delta\Phi + \frac{\partial C_y}{\partial \dot{\beta}}\Delta\dot{\beta} + \frac{\partial C_y}{\partial p}p + \frac{\partial C_y}{\partial r}r + \frac{\partial C_y}{\partial \delta_a}\delta_a + \frac{\partial C_y}{\partial \delta_r}\delta_r + \ldots$$

$$\Delta C_l = \frac{\partial C_l}{\partial \beta}\Delta\beta + \frac{\partial C_l}{\partial \Phi}\Delta\Phi + \frac{\partial C_l}{\partial \dot{\beta}}\Delta\dot{\beta} + \frac{\partial C_l}{\partial p}p + \frac{\partial C_l}{\partial r}r + \frac{\partial C_l}{\partial \delta_a}\delta_a + \frac{\partial C_l}{\partial \delta_r}\delta \qquad \textit{Eqn. (3)}$$

$$\Delta C_n = \frac{\partial C_n}{\partial \beta}\Delta\beta + \frac{\partial C_n}{\partial \Phi}\Delta\Phi + \frac{\partial C_n}{\partial \dot{\beta}}\Delta\dot{\beta} + \frac{\partial C_n}{\partial p}p + \frac{\partial C_n}{\partial r}r + \frac{\partial C_n}{\partial \delta_a}\delta_a + \frac{\partial C_n}{\partial \delta_r}\delta_r + \ldots$$

However, in order to make them non-dimensional, stability derivatives relatively to β, p and r are usually defined as follow using the shorter notation of *Eqn. (4)*:

$$C_{?\dot{\beta}} = \frac{\partial C_?}{\partial(\frac{\dot{\beta}b}{2U_0})}$$

$$C_{?p} = \frac{\partial C_?}{\partial(\frac{pb}{2U_0})} \qquad \textit{Eqn. (4)}$$

$$C_{?r} = \frac{\partial C_?}{\partial(\frac{rb}{2U_0})}$$

Still using the same hypotheses, *Eqn. (1)* can be further simplified and separated into two sets of independent equations: three for the longitudinal motions, and three for lateral motions. Furthermore, it means the lateral/longitudinal cross coupling is neglected

Eqn. (1) can then be used to derive the ***lateral-directional equations of motion for small disturbances*** (The reader might refer to [6] for the detailed derivation), as given in *Eqn. (5)*:

$$\begin{aligned}
&(m_1\frac{d}{dt}-b_1C_{y\dot{\beta}}\frac{d}{dt}-C_{y\beta})\Delta\beta-(b_1C_{yp}\frac{d}{dt}+C_{y\phi})\Delta\phi+(m_1\frac{d}{dt}-b_1C_{yr}\frac{d}{dt})\Delta\Psi=C_{y\delta r}\Delta\delta r+C_{y\delta a}\Delta\delta a\\
&(-C_{l\beta}-b_1C_{l\dot{\beta}}\frac{d}{dt})\Delta\beta+(-b_1C_{lp}\frac{d}{dt}+I_{xz}\frac{d^2}{dt^2})\Delta\phi+(-b_1C_{lr}\frac{d}{dt}-I_{xz}\frac{d^2}{dt^2})\Delta\Psi=C_{l\delta r}\Delta\delta r \qquad \textit{Eqn. (5)}\\
&(-C_{n\beta}-b_1C_{n\dot{\beta}}\frac{d}{dt})\Delta\beta+(-b_1C_{np}\frac{d}{dt}+I_{xz}\frac{d^2}{dt^2})\Delta\phi+(-b_1C_{nr}\frac{d}{dt}-I_{xz}\frac{d^2}{dt^2})\Delta\Psi=C_{n\delta r}\Delta r
\end{aligned}$$

with δ_a denoting the aileron deflection, while δ_r stands for the rudder deflection.

We may then derive a state-space equation from *Eqn. (5)*, whose validity has been demonstrated for the study of aircraft dynamics and control [6]. The form of the equation in this document is consistent with [6]:

$\dot{X} = AX + BU$ With,

$$X = \begin{pmatrix} \Delta\beta \\ \Delta\Phi \\ p \\ \Delta\Psi \\ r \end{pmatrix}, \text{ And } U = \begin{pmatrix} \Delta\delta a \\ \Delta\delta r \end{pmatrix} \qquad \textit{Eqn.(6)}$$

In our case, at cruise condition (36000ft, Mach 0.8), and medium weight:

$$A = \begin{pmatrix} -0.14 & & 0.045 & 0 & -0.99 \\ 0 & 0 & 1 & 0 & 0 \\ -17.55 & 0 & -2.39 & 0 & 0.15 \\ 0 & 0 & 0 & 0 & 1 \\ 1.69 & 0 & -0.22 & 0 & -0.22 \end{pmatrix}$$

$$\text{and } B = \begin{pmatrix} 0.00437 & 0.0325 \\ 0 & 0 \\ 9.538 & 3.86 \\ 0 & 0 \\ 0.662 & -2.79 \end{pmatrix}$$

Hence, the eigenvalues for A can be computed as follow:

- 0
- -2.6458
- $-0.0580 \pm 1.7618i$

The last eigenvalue corresponds to *Dutch-Roll* oscillation, which means oscillation with a very small damping ratio of 0.033, and a slow natural frequency of 1.76 rad/s.

Aircraft behavior during a *Dutch-Roll* is illustrated in *Figure 2.6* (to completely understand the *Dutch-Roll*, one should also imagine damped oscillation of the aircraft around yaw axis).

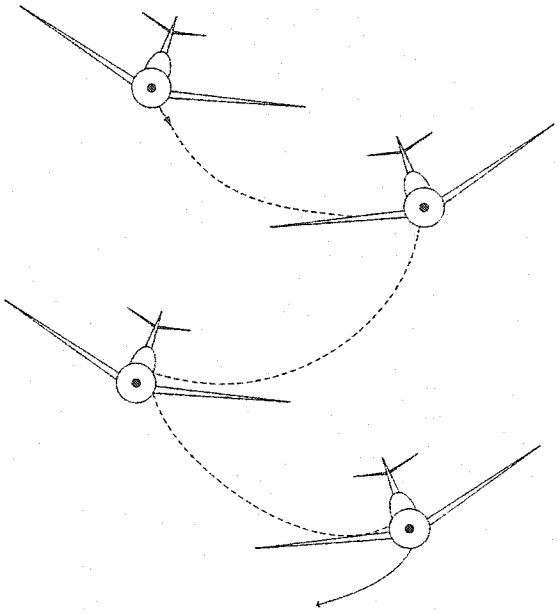

Figure 2.6 - Physical Motion of an Airplane during a *Dutch-Roll*

This emphasizes the need for an artificial way to dampen the aircraft motion: this is the purpose of the yaw damper.

The eigenvalue -2.6458 is accounting to what is referred as the *roll convergent mode*. As this mode is usually heavily dampened, it is most of the time not noticeable.

0 is referring to a very slight instability referred as *spiral stability mode* and is exaggerated here due to some approximations in the aerodynamic coefficients and in the hypotheses done during derivation of *Eqn. (5)*. What is in reality a very slight instability is however usually not considered as a problem and easily corrected by the pilot.

2.1.3.5 Yaw Damper

The yaw damper is in charge of artificially damping yaw and roll oscillations associated with a Dutch-roll; it usually carries out these tasks through a classical closed loop feedback control on the rudder. Since correct measurement of the sideslip angle is usually not available [5], the feedback is usually performed on the yaw rate, as measured

with a rate gyro (also required for inertial navigation systems). The feedback also usually includes a washout filter: this high pass filter will ensure that the controller won't counteract pilot input (pilot's bandwidth is usually estimated to 4 rad/s) [7]. *Figure 2.7* gives an illustration of this standard implementation of a yaw damper.

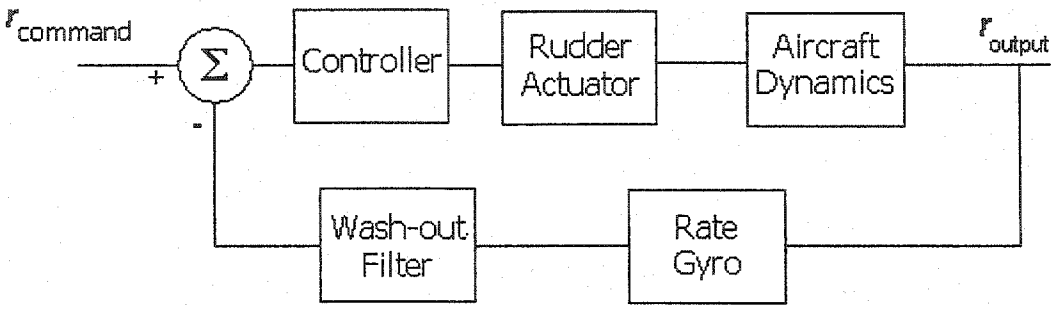

Figure 2.7 – Yaw Damper Block Diagram

2.2 Flight Model

For the purposes of the project, Bombardier has provided Concordia University with a flight model of a particular aircraft design. This model was developed in order to study the aircraft's dynamics and stability under different loading and mission conditions. Since it is used in the project to collect data on the aircraft dynamics and therefore fill the blank left by the lack of experimental data, it is important to understand its possibilities and limitations.

2.2.1 MatrixX

The model was built using MatrixX, a software package whose possibilities and architecture is comparable to Matlab. It includes Xmath, a mathematical analysis, visualization, and scripting package, and is complemented with SystemBuild (Simulink

in the Matlab suite), which provides the user with the easy-to-use "block type" interface to build models.

Xmath and SystemBuild run concurrently, which allows the user to simultaneously edit SystemBuild models, perform Xmath analysis or SystemBuild simulations, and display graphics.

2.2.2 Flight Model Architecture

The flight model dynamic computation is based on *Eqn. (1)*. It is therefore directly derived from Newton's law, with the earth's curvatures and rotation neglected, and is suitable for study of the aircraft motion around equilibrium condition. *Figure 2.8* gives a view of the model at its higher hierarchical point, and gives a rough idea of the choices that were made by the designer in order to divide the model of this complex system into a number of separated entities. The choices that were made for the division into subsystems is consistent and can be found in the pertinent literature [9].

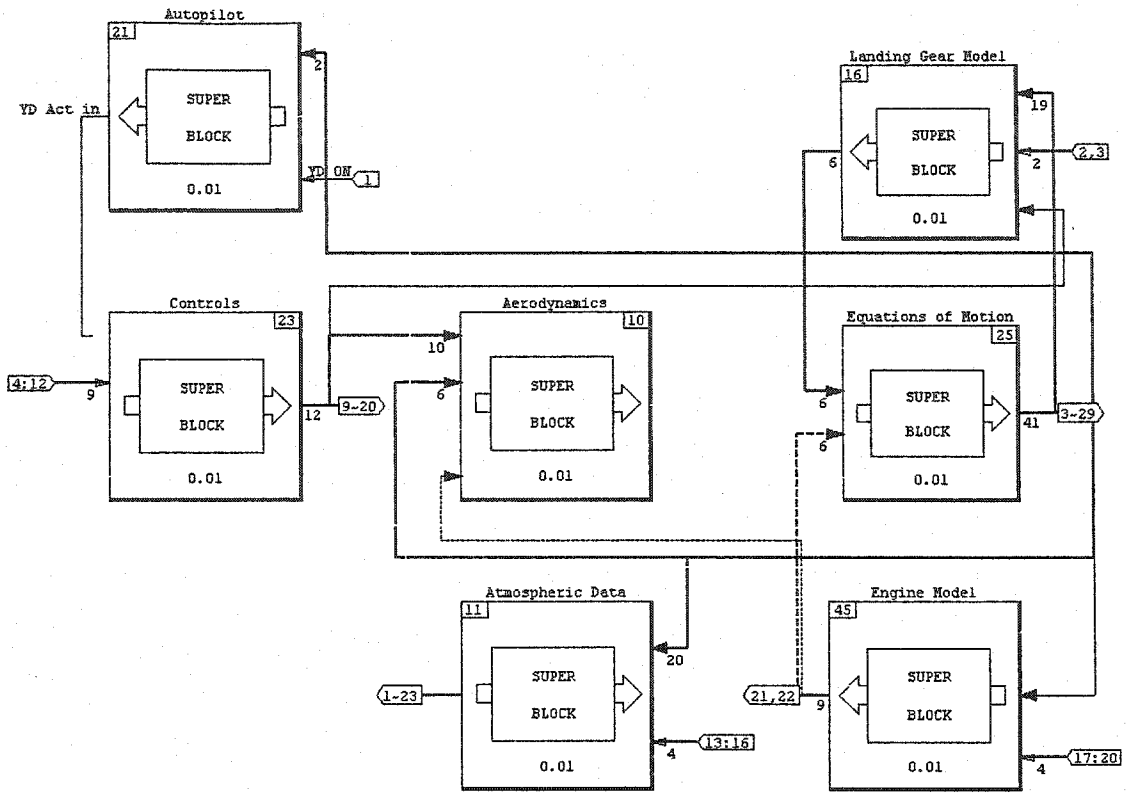

Figure 2.8 - Flight Model Higher Overall View

As can be seen on *Figure 2.8*, the main blocks are:

- **Equations of Motion** (Based on *Eqn. (1)*, also including frame transformations from body axis to stability axis)
- **Aerodynamics** (aerodynamic forces computation)
- **Engine Model** (engine's behavior and performance model)
- **Landing Gear Model** (landing gear aerodynamic forces and kinematics)
- **Atmospheric Data** (atmospheric variables following ISA standards)
- **Controls** (control kinematics, from pilot input to surfaces displacements)
- **Autopilot** (autopilot logic and yaw damper)

Aerodynamic forces are computed from stability derivatives whose values were extracted from flight test data, and inserted in the model with the help of look-up tables.

2.2.3 Turbulence Model

The flight model includes a Von Karman turbulence model, located within the Atmospheric Data block (used during simulation in *Section 5*). The Von Karman model provides a power series distribution approximation of the gust velocity during turbulences, and is one common way to model gust. It is also considered to be the approximation that produces the best match with experimental data, and is therefore widely used during design [10] to estimate the loads on the aircraft.

Further information on the subject may be found in Appendix A.

2.2.4 Simulation Procedure

The flight model is a discrete model, with a sampling period of 0.01s. The sequence of events carried out when a simulation is launched is as follows:

1. A MatrixX script that contains the aircraft configuration data (total mass, fuel mass, initial attitude, speed, altitude...) passes these values on to a series of "pre-simulation" blocks in the model, thus initializing the variables in the model.
2. Another script separates fixed and floating state variables, preparing the model for the use of the *trim* function. *trim* is used to find the trimmed input, state and output values for equilibrium points of the model. It can bring the model to a steady-state reference, without actually simulating it [11]

3. The model is simulated. A number of functions are "pre sorting" the huge amount of data generated.

The model inputs are listed in *Table 2.1*:

Input No.	Label Name	Description	Units	Sign Convention
1	YD_ON	Flag indicating that the Yaw Damper is ON	non dimensional	1= ON; 0= OFF
2	LH Brakes	LH Pilot's Toe Brake input	non dimensional	1= full braking, 0= off
3	RH Brakes	RH Pilot's Toe Brake input	non dimensional	1= full braking, 0= off
4	Flap_Cmd	Flap deflection	degrees hingewise	always positive
5	Stab_Cmd	Stabilizer deflection	degrees hingewise	+'ve leading edge up
6	LGear_Cmd	Normalized Gear Position	non dimensional	1= fully extended 0= stowed and locked
7	Tiller	Nose Wheel Steering Wheel displacement	degrees	+'ve aircraft nose right
8	Pedal pos	Pilot's pedal displacement	inches	+'ve aircraft nose left
9	Wheel pos	Pilot's wheel displacement	degrees	+'ve right wing down
10	Column pos	Pilot's column displacement	inches	+'ve aircraft nose down
11	Ground_Spoiler	Ground Spoiler Command	degrees hingewise	+'ve always, max 40 deg
12	Flight Spoiler	Flight Spoiler Command	degrees hingewise	+'ve always, max 40 deg
13	Wind_X	North-to-South wind component	knots	+'ve from the North
14	Wind_Y	East-to-West wind component	knots	+'ve from the East
15	Wind_Z	Vertical wind component	knots	+'ve UP
16	TURBON	Turbulence discrete	non dimensional	1= ON, 0= OFF
17	LH_PLA_Cmd	Left hand Engine Power Lever Angle	degrees	+'ve forward thrust
18	RH_PLA_Cmd	Right hand Engine Power Lever Angle	degrees	+'ve forward thrust

Table 2.1 - Flight Model Inputs [12]

Of great importance to this work are the inputs to the flight controls, accessible through time dependant curves within the script in charge of simulating the model. One should also note the input to the rudder control system, represented by the pedal displacement: the next chapter will provide a closer look at this particular system.

3 Yaw control System Architecture

Yaw is controlled in aircraft by the rudder pedals (see *Figure 3.1*). Pushing the left pedal will yaw the aircraft to the left, while pushing the right pedal will have the reverse effect. Additionally, the cockpit pedals usually include wheel brakes. The aircraft is usually controlled on its other two axes by using a wheel (see *Figure 3.1*), whose rotation controls the rolling motion while pushing the wheel back and forth is controls the pitch.

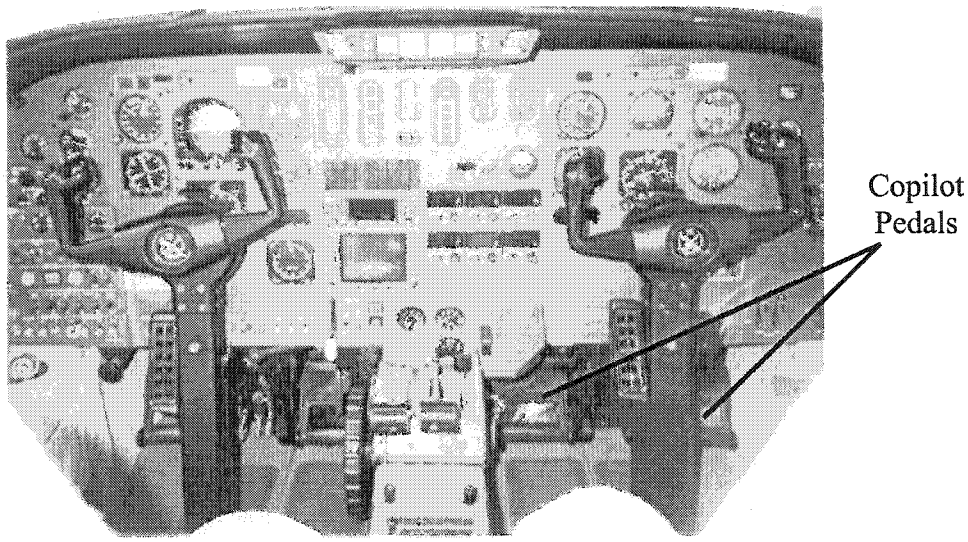

Figure 3.1 – Citation II Cockpit [13]

3.1 Flight Control Requirements

3.1.1 Aircraft Handling

The design of flight controls has advanced considerably since their initial development; in the earliest biplanes flown, flight was controlled by warping wings and control surfaces and by attaching a system of wires to the controls in the cockpit (note the

multiplicity of rigging and control wire on *Figure 3.2*).). This rudimentary system was of course barely adequate. Designers quickly began to use articulated control surfaces, but the use of wires and pulleys to link them to the pilot's control is still partly in use on the design of interest in this thesis.

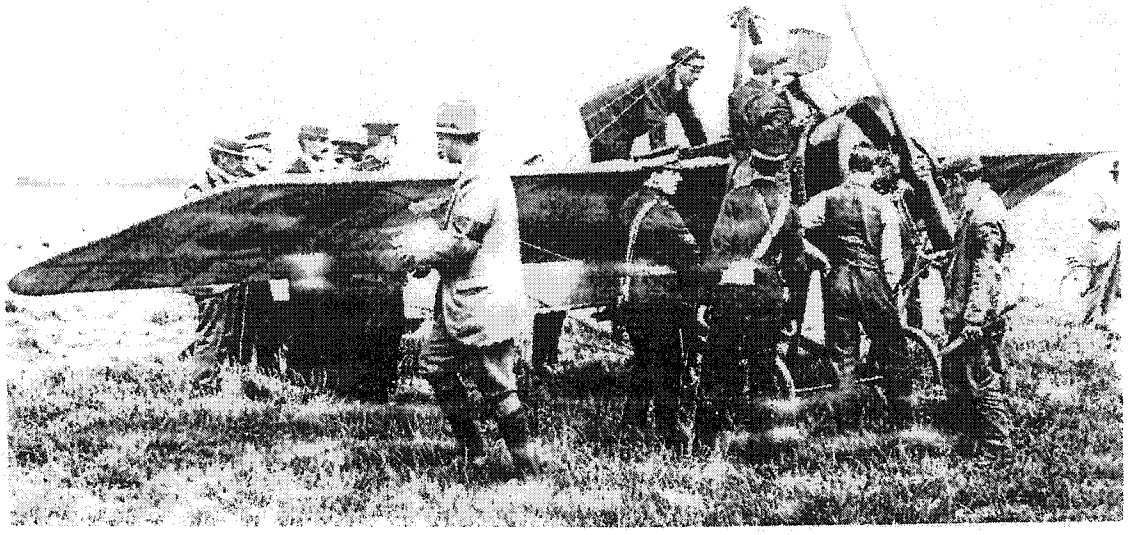

Figure 3.2 - Morane Saulnier Refueling in 1913 [14]

As the top speed advanced to the transonic region and the weight of aircraft increased, the pilot physical effort became inefficient for control of the aircraft over the entire airplane-operating envelope (*Table 3.1*) This led to hydraulically powered control surfaces. This is the case here, where three independent Power Control Units (*Figure 3.3*) a provide a force/power amplification of the rudder control inputs.

	Maximum pilot effort (N)	Minimum pilot effort (N)	Greatest force pilots care to exert for a short while (N)
On one side of rudder bar	130	105	270 (push)
Simustaneously on each side of rudder bar	180	180	

Table 3.1 – Pilot Characteristics [15]

New designs also required friction and backlash to be kept as low as possible. Friction is obviously altering pilot control and may lead to over control and imprecision. [15] estimates the maximum felt friction (at the pedals) for a correct yaw control to be 6 lbf (27.2 N). Backlash should also be avoided: it is not only impacting the pilot's "feel", but may also result in flutter: a high frequency oscillation of the rudder surface. It is therefore highly undesirable.

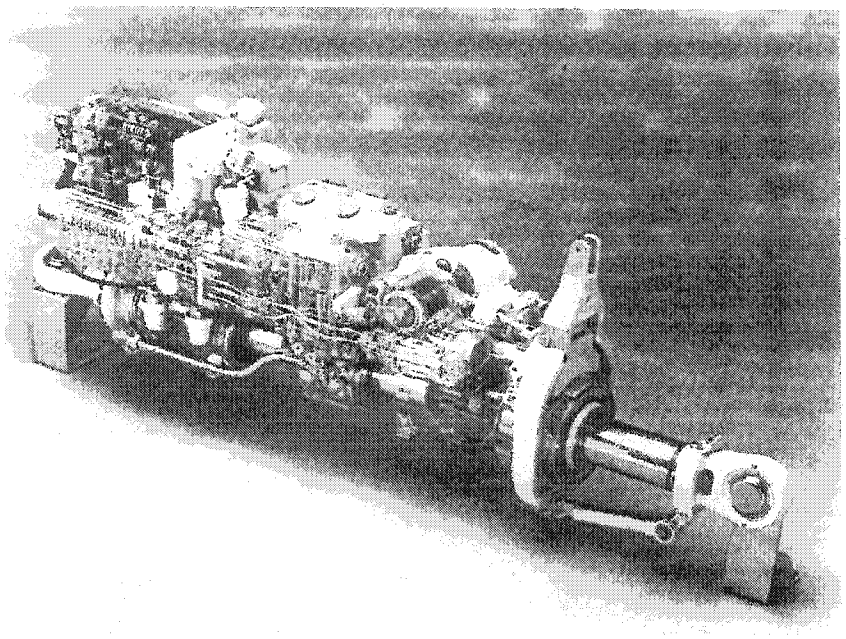

Figure 3.3 - Tornado Rudder Actuator [14]

The issue of backlash is connected to another very important topic for flight control design: that of the "feel", or the perception of the pilot/copilot of the controls. By divorcing the pilot from the true effort required to fly the aircraft, it became possible to undertake maneuvers that could overstress the aircraft. It is therefore necessary to include in the control a mechanism providing artificial feel to the crew and is discussed in *Section 3.2.2.1*.

An additional issue that appeared with the increasing speed characteristics of the latter stage of aircraft development (World War two period) is the appearance of roll/yaw coupling effects such as the Dutch-roll (see *Section 2.1.3.4*), emphasizing the need for artificial damping. Two Yaw Dampers, also ensuring turn coordination function, provide this artificial damping on the particular design studied here.

3.1.2 Security

When designing any aircraft system, there are two points the designers should always keep in mind: weight and security.

One can easily imagine the result of losing one or more flight control during flight, or even worse: having a surface stuck in a deflected position, therefore quickly bringing the aircraft into an uncontrollable situation.

The FAA states that: "The failure of mechanical parts (such as piston rods and links), and the jamming of power cylinders, must be considered unless they are extremely improbable." [16]. This greatly contributes to making the flight control system a very complicated mechanism: a lot of possible failure cases must be considered, and the system must respond in a correct way to these failures.

3.2 Yaw Control Architecture

3.2.1 System Overview

A sketch of the rudder control system of the studied here can be seen in *Figure 3.4*. Starting from the pedals, the inputs from both the pilot's and copilot's sides are added and conveyed to two quadrants (pilot and copilot) through a number of push-pull rods and cranks.

These quadrants, located at the front of the aircraft, drive two aft quadrants through cables and a series of pulleys. These two parallel systems (pilot and copilot) are protected from jam by a system that isolates the failed cable from the rest of the system (Anti-Jam Breakout mechanism on *Figure 3.4*,with more details given in *Section 3.2.2.3*).

The two aft quadrants's rotations are in turn driving the rotation of a single bell crank through a summing mechanism (see *Section 3.2.2.4* for details)

From this point the load is conveyed through a load limiter to a system that mixes the pilot's and copilot's input with those of the electrical trim system and yaw dampers. This is then conveyed to the torque tube that drives the three PCUs, and the displacement of the pistons ensures the rotation of the rudder.

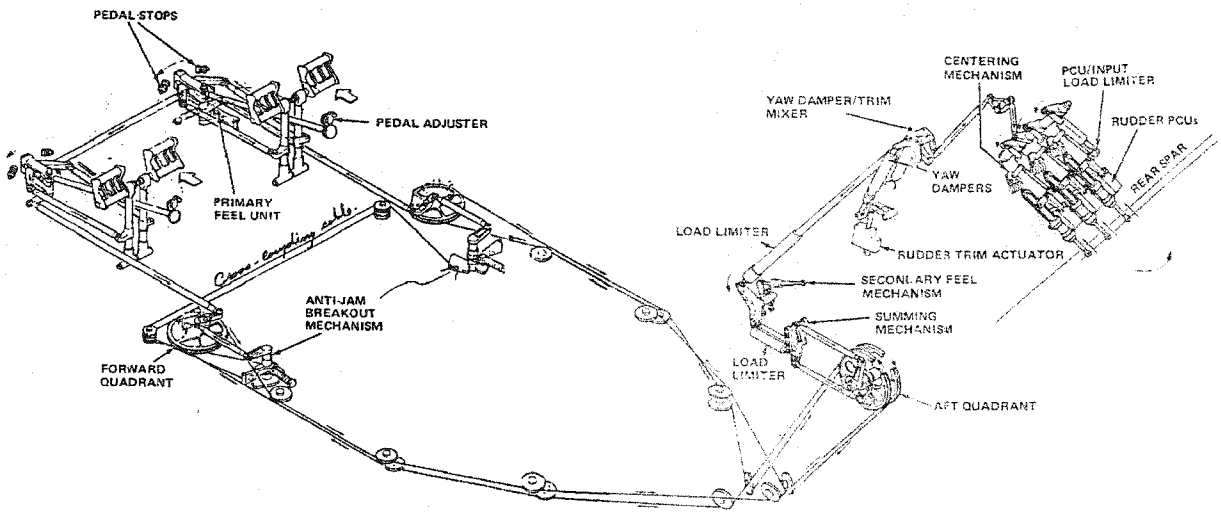

Figure 3.4 –Rudder Control System [18]

3.2.2 Systems

3.2.2.1 Feel Unit

Feel is provided in this design through a cam, and a spring-loaded roller follower system (*Figure 3.5* is illustrates the primary feel unit). The feel mechanisms ensure pilot feeling, but also centers the control. The main disadvantage of this system is that it does not function to reproduce the feeling of aircraft speed or altitude and it therefore divorces the pilot from any "true" feeling of the aircraft's behavior.

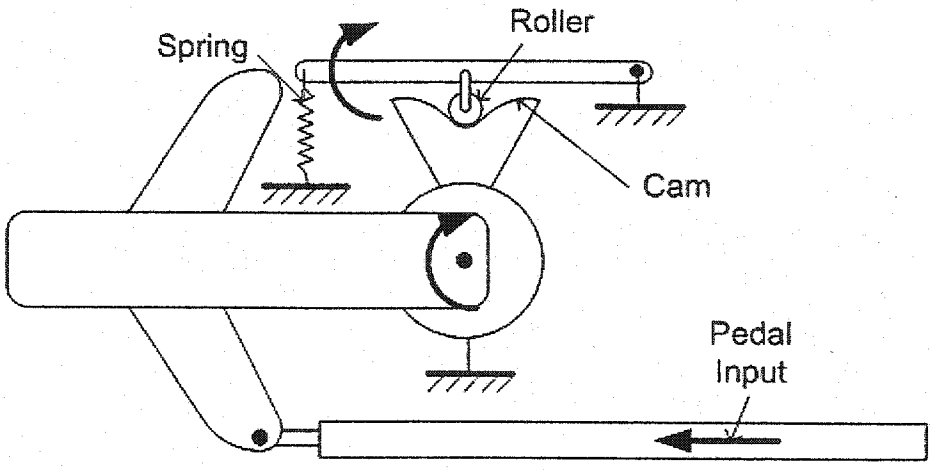

Figure 3.5 – Feel Unit Assembly Principle

3.2.2.2 Stops & Pedal Adjustment

The Stops and Pedal adjustment system encompasses adjustable pedal stops limiting pedal motion, as well as stops on the torque tube to limit input to the PCU.

A drive shaft, operated by a hand crank on the aft face of each rudder bar console, provides a means for the flight crew to shift to the neutral position of the rudder bar, therefore enabling stature adjustment.

3.2.2.3 Anti-Jam Break-Out Mechanism

The anti-jam breakout mechanism and cross-coupling cable ensure that in the event of a cable jam, the input from the other side is still transmitted, and the cable circuit which is free to move is displaced twice the normal amount for a given rudder pedal input.

3.2.2.4 Summing Mechanism

This mechanism ensures that there is a mixing of the pilot and copilot signals (*Figure 3.6*). In normal operation, it converts this double input into a single input. In the case of a cable circuit being severed, it ensures (through the load limiter bungee) that the signal from the safe side will still be transmitted in a normal fashion, at a normal amplitude.

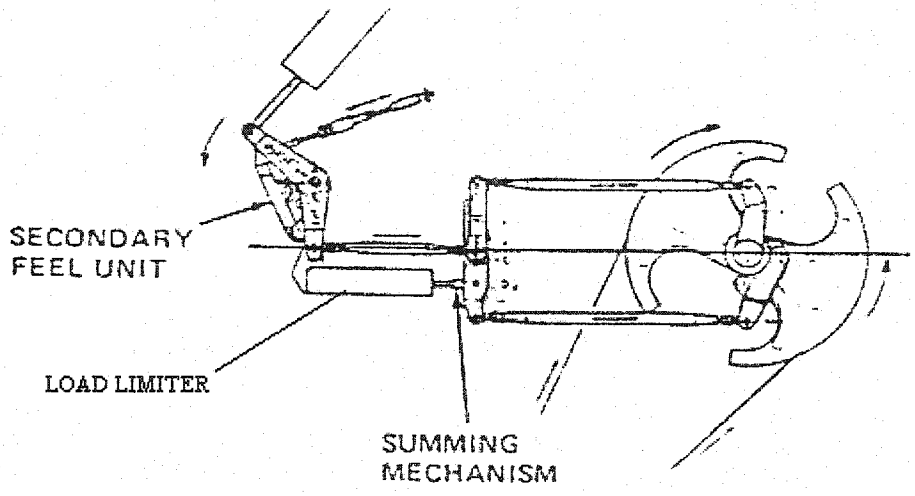

Figure 3.6 – Summing Mechanism System [4]

3.2.2.5 Load Limiter

The load limiter, located just after the secondary feel unit, protects the overall system from overload. Load limiters located at the input of each PCU ensure that in the

event of a valve jam, input command will still be transmitted to the remaining PCU. The two combined PCUs will overpower the jammed valve PCU so that rudder control is maintained.

3.2.2.6 Yaw Damper/Trim Mixer

The mixer installation provides the means for yaw damping and trim signal to be added to the primary rudder control inputs. Parallel arrangement of the yaw dampers in conjunction with the yaw damping control system characteristics provides for continued yaw damping should one damper channel fail.

3.2.2.7 PCU Centering Mechanism

A centering mechanism is provided for each PCU. In the event of an input command disconnect, the centering mechanism returns the affected PCU to a neutral position. During normal operation, the centering mechanism is continuously activated by the input command.

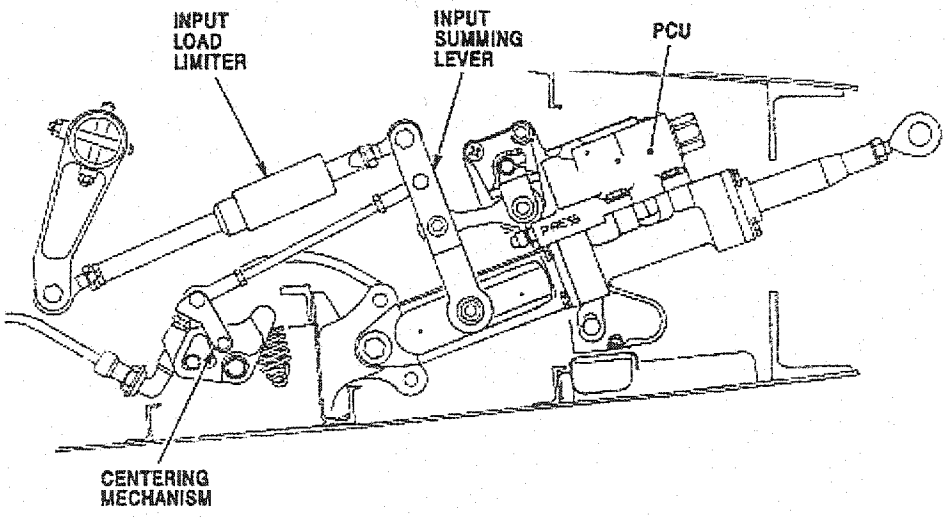

Figure 3.7 – PCU Centering Spring [4]

3.3 Aircraft Hydraulic

Hydraulic systems are used to transmit power. Hence, they must include:

- A pump, which is the unit that puts work into the fluid lines.
- Pipes, to transmit this work to another place.
- Actuators for transforming the moving fluid under pressure back into mechanical power.

Section 3.1.1 has shown that the rudder control of an aircraft such as the one of interest in this work has to encompass hydraulic boosting. For the reasons stated in *Section 3.1.2*, this job is done here by three independents Power Control Unit, which could be referred as servo actuator swith mechanical feedback.

3.3.1 Hydraulic System

An aircraft's hydraulic system is of the *constant pressure* type: pressure is available in the circuit at a constant value of 3000 psi (210 bars). This type of system is often used to supply multiple servo systems, as is the case for aircraft flight controls. *Figure 3.8*, gives an idea of the basic configuration of this type of system (a detailed discussion of the system is beyond the scope of this work), including relief valve, filter check valve, compensator (see *Section 3.3.2* for more details), control valve, actuator and pump.

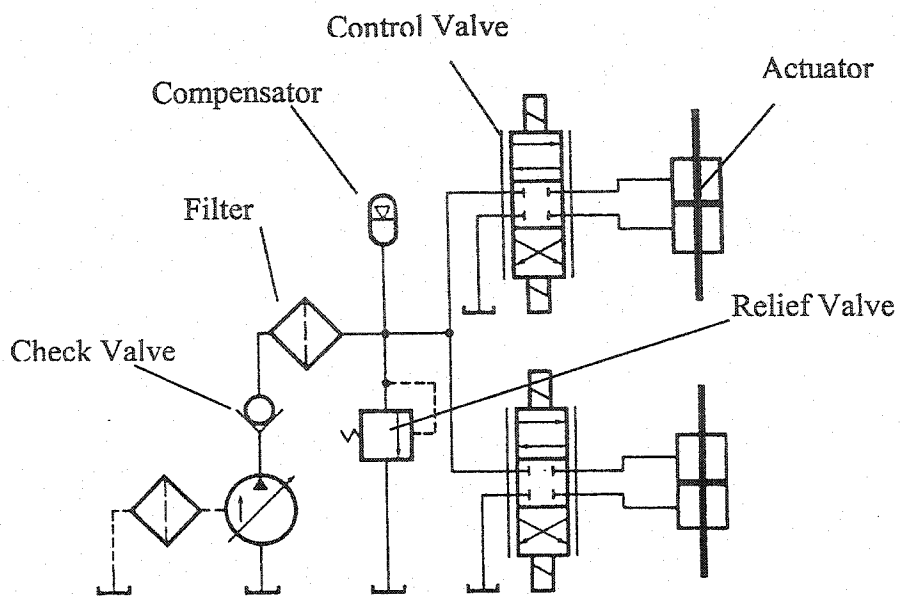

Figure 3.8 – Constant Pressure System [17]

In the design studied here, the flight control hydraulic system encompasses three fully independent systems, and each control surface is powered by at least two of them. One alone is sufficient for maintaining continued operation [18].

3.3.2 Power Control Unit

At the ends of the hydraulic systems are the Power Control Units, enhancing pilot efforts. Located at the top of the vertical fin in this case, they include both the control valve and the actuator. One of them is sketched in *Figure 3.9* with its main components. One can see on this drawing that there is still a mechanical connection between the pilot and the rudder surface, therefore ensuring part of the "feel".

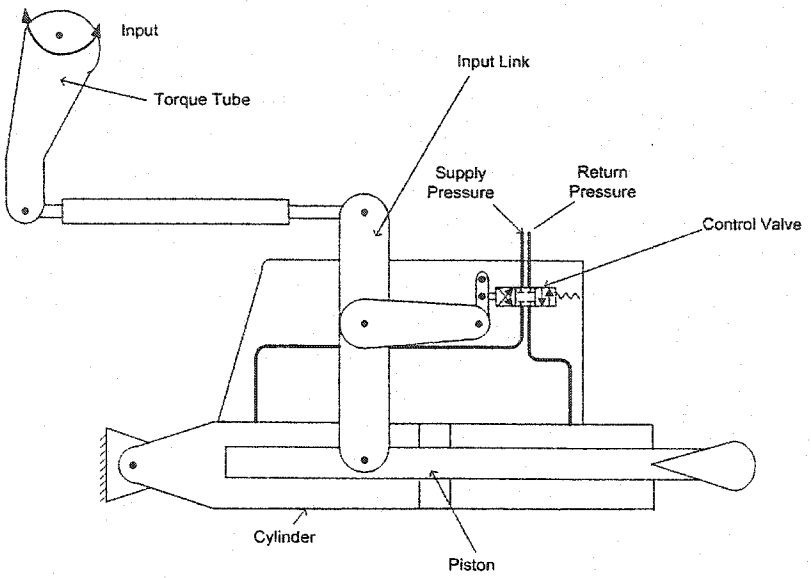

Figure 3.9 – Power Control Unit

The control valve has the important role of distributing the fluid in the cylinder and thereby controls the displacement of the actuator. A so-called *spool* is translating with reference to the *sleeve (*see *Figure 3.10),* therefore varying the size of the orifice that connects the pressure and return line to the two chambers of the actuator.

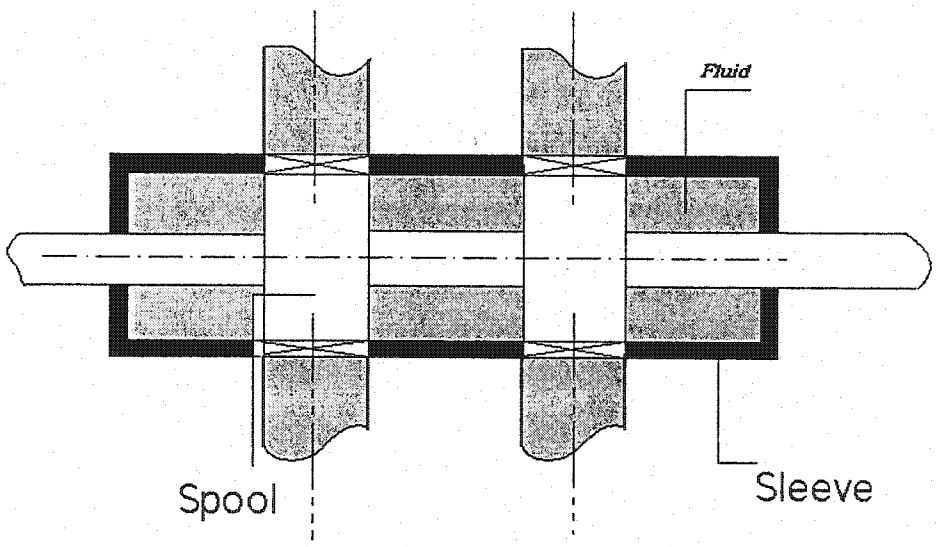

Figure 3.10 – Control Valve

The torque tube, connected to a push-pull rod, receives the input from the pilot pedal. The difference between this pilot/copilot input and the actuator position commands the motion of the spool, as illustrated in *Figure 3.11*:

- Torque tube rotation first induces a rotation of the input link around point A.
- This in turns moves the control valve, building up pressure on one side of the piston: the piston retracts, and the input link turns around point B.
- Finally, the control valve returns to neutral: The piston has retracted.

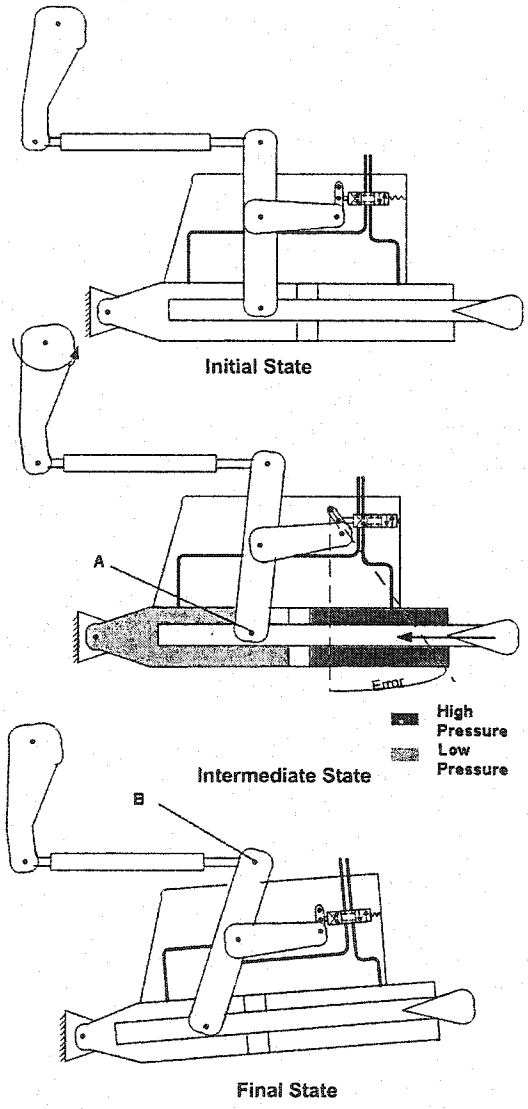

Figure 3.11 – PCU Operation

The PCU's control valve kinematics have been slightly simplified on *Figure 3.9 & Figure 3.11*. In reality, they involve a set of rods to ensure a correct ratio of the valve displacement for a given input link rotation (more detail available in [4]). It also incorporates the so-called rate stop, limiting the maximum displacement of the control valve.

Finally, *Figure 3.12* gives us a complete hydraulic schematic of the PCU.

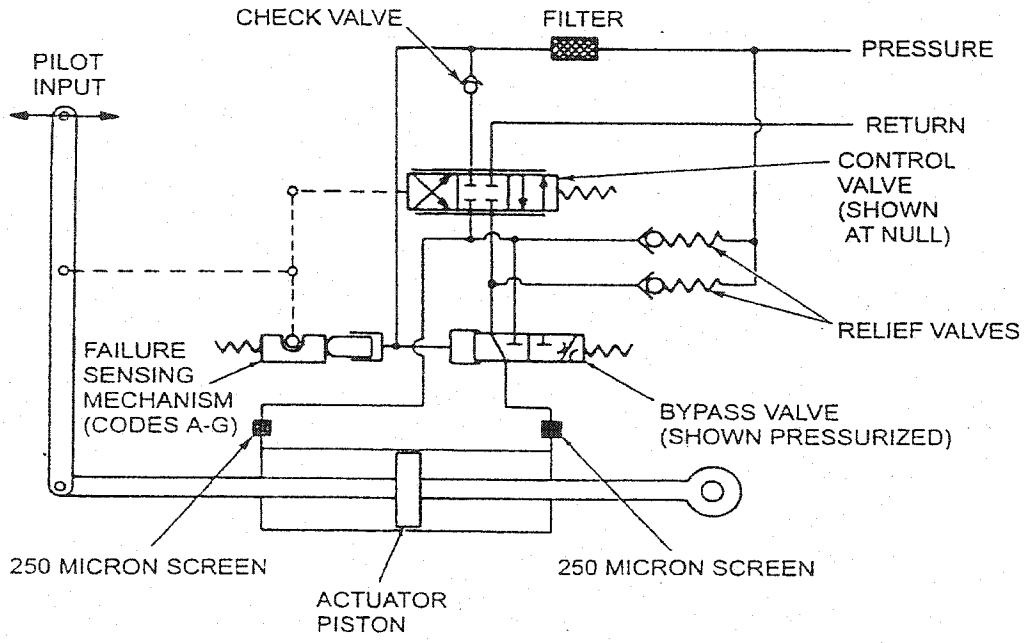

Figure 3.12 – PCU Hydraulic Schematic [4]

Apart from the control valve, the PCU encompasses a number of components, mainly to ensure the safety of the aircraft in case of partial failure of the mechanism, and are common to this type of system (*Section 3.3.1*).

The check valve prevents reverse flow of the hydraulic fluid back into the hydraulic system pump. A bypass valve permits the flow between the cylinder chambers

to circulate in close-loop in case of hydraulic system failure, ensuring the free motion of the actuator if there is a control valve failure.

Anti-cavitation valves are check valves connected to the return line and are designed so that the minimum pressure in the PCU hydraulic system is the same as the return pressure (between 75 to 160 psi). These check valves help avoid the formation of damaging bubbles in the PCU hydraulic system.

4 Modeling of the Rudder Control System

Supporting the yaw kicks investigation, this work also aims to develop an industrially viable model of the rudder control part of the system they provided.

Bombardier Aerospace has been working with the ADAMS software package for years, and they have developed expertise in the field of flight controls modeling using this software. It seems obvious that the value of this work could greatly benefit by adopting the same standards, grouped under the generic name of VPFCS (Virtual Primary Flight Control System). Additionally, MSC names ADAMS a world leader in the field of mechanical system simulation: the reasoning behind using ADAMS as the "modeling platform" is therefore evident.

4.1 ADAMS/*Solver* Characteristics

Large displacement and rotations that occur in the dynamic performance of spatial mechanical systems lead to a nonlinear mathematical model: formulation and analysis of this model might represent a difficult challenge. The model presented in this work is also including backlash (a well known type of non-linearity) and detailed non-linear friction

model. Such systems are therefore expressed mathematically by systems of nonlinear differential equations whose analytical solution is more than often unavailable, therefore commanding the use of numerical methods. Most of the modeling work illustrated in this section was done using ADAMS, whose solver makes use of such techniques. For that reason, it seemed important to present a brief review of the software's characteristics and limitations, while examining ADAMS 's computation engine equation formulation and solving methods.

4.1.1 ADAMS Architecture

ADAMS introduces a complete solution for mechanical system simulation and study. It is also a complete suite of softwares; those used during this project are as follows:

- ADAMS/*View*: friendly user interface used to build models. It associates each part with 3-D solid geometry, therefore greatly enhancing the system representation and the user experience.
- ADAMS/*Solver:* is the computational engine in charge of solving the equations (see *Section 4.1.3*)
- ADAMS/*Post-Processor:* used for plotting and analyzing ADAMS/*solver* results

4.1.2 Formulation of the Equations

Newton's Second Law becomes very difficult to use when large-scale multi-body systems are considered, and it is not very suitable for computer-solved problems. A

Lagrangian formulation is therefore usually preferred: though it is not intuitive, it is much more convenient for numerical formulation and solving.

Three important notions are important in order to understand the Lagrangian dynamic:

- The *virtual work* of a force, which is defined to be the dot product of the force with the virtual change in the vector displacement of the point of application of the force.
- The *generalized Coordinates*: a set of variables that completely define the location and orientation of each body in the system.
- The notion of *kinematic constraint:* which accounts for the mechanical joints in between the bodies or specified motion trajectory.

From Newton's second law and the principle of virtual work, the *Hamilton Principle* [19] can be derived (*Eqn. (7)*):

$$\delta \int_{t_1}^{t_2} L_a dt + \int_{t_1}^{t_2} \delta W_{nc} dt = 0 \qquad \textit{Eqn. (7)}$$

with:

- L_a is the Lagrangian of the dynamical system, and is defined as: $L_a = \sum_{j=1}^{N} T_j - V_j$ for multibody systems (T and V stand for kinetic and potential energy respectively)
- δW_{nc} is the virtual work done by non-conservative forces acting on the system.

The Hamilton principle therefore states that the variation of kinetic and potential energy, plus the virtual work done by non-conservative force from time t_1 to t_2 is null,

under the assumption that the difference between the virtual and true path at t_1 and t_2 is null.

Using the *calculus of variation techniques* [19] (which defines the less energetic path in between two instants) and *Eqn. (7)*, one can derive *Eqn. (8)*:

$$\frac{d}{dt}\left(\frac{\delta L_a}{\delta \dot{q}}\right) - \frac{\delta L_a}{\delta q} + \Phi_q^T \lambda = Q \qquad \textit{Eqn. (8)}$$

Eqn. (8) is referred to as the Lagrange-Euler equation, and is the formulation used by ADAMS [20], with:

- q_p as the column matrix of generalized coordinate
- The Jacobian matrix $\Phi_q = \frac{\delta \Phi}{\delta q}$ of the constraint equations is made up of the partial derivatives of the expressions for the constraints in respect to the generalized coordinates. Φ_q is used for coupling the constraint equation into the force equation: $\Phi_q^T \lambda$ is therefore accounting for the constraint forces, with λ a column matrix of the Lagrange multiplier.
- Q is a column matrix containing the externally applied, non-conservative forces in the model.

The use of the Lagrange multiplier is a sign of a so-called *augmented formulation*, and is common when using the Lagrange equation for a computer formulation. The system is expressed in terms of a dependant coordinate as well as constraint forces [19]. An example on a simple one-body system will better illustrate this formulation. For a simple "one body" system such as a pendulum (*Figure 4.1*), in a two dimensional (planar) world, we chose the general coordinates vector q_p as (position and orientation of a rigid body in a 2 dimension space):

$$q_p = \begin{pmatrix} x_p \\ y_p \\ \theta_p \end{pmatrix}$$

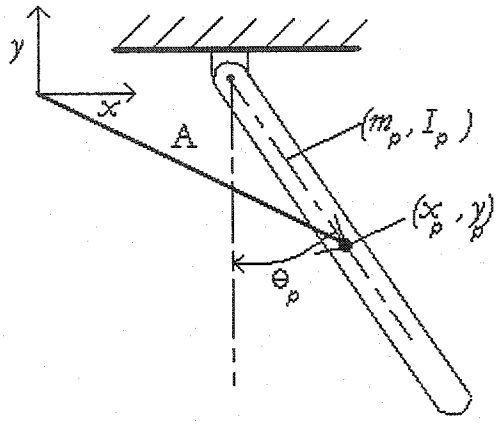

Figure 4.1 – Pendulum Schematic

The Euler-Lagrange equation (*Eqn. (8)*) is used to convert the constraint equation into the coupling term, therefore forming the three force balance equations, to which is added the two constraint (revolute joint of the pendulum) equations [20] leading to *Eqn. (9)*:

$$\left.\begin{array}{l} m_p\ddot{x}_p + \lambda_1 \\ m_p\ddot{y}_p + \lambda_2 + m_p g \\ I_p\ddot{\theta}_p + \lambda_1 l * \sin\theta_p - \lambda_2 l * \cos\theta_p \\ x_p - A_1 - l * \cos\theta_p \\ y - A_2 - l * \sin\theta_p \end{array}\right\} = 0 \qquad \textit{Eqn. (9)}$$

This system of second order differential equations is later formulated as a first order system by introducing a new variable for each second order term (*Eqn. (10)*):

$$\begin{array}{l} u_p = \dot{x}_p \\ v_p = \dot{y}_p \\ w_p = \dot{\theta}_p \end{array} \qquad \textit{Eqn. (10)}$$

Finally, the simple pendulum problem has been formulated as a system of height non-linear implicit differential algebraic equations (DAE) with a state vector of dimension 8 *Eqn. (12)*). Rewritten in compact form it gives *Eqn. (11):*

$$G(\overline{Y},\dot{\overline{Y}},t)=0 \qquad \textit{Eqn. (11)}$$

with,

$$\overline{Y}=\begin{bmatrix} u_p \\ v_p \\ w_p \\ x_p \\ y_p \\ \theta_p \\ \lambda_1 \\ \lambda_2 \end{bmatrix} \qquad \textit{Eqn. (12)}$$

4.1.3 Solving the Equations

Eqn. (11) is not readily transformable into an explicit system of ordinary differential equation (ODE) in the form of *Eqn.* (13):

$$\dot{\overline{Y}}=f(\overline{Y},t) \qquad \textit{Eqn.}\ (13)$$

standard solver formulation therefore does not apply to solve this type of problem. Thus, the ADAMS/*Solver* employs integrator that does accept equations in the implicit form: the DAE's are transformed into a system of linear equation by approximating each derivative in the column matrix $\dot{\overline{Y}}$ with a backward differentiation formula (BDF) [20].

4.1.3.1 The Integration Algorithm

The column matrix of the dependant variable is known as the state vector for the mechanical system. An ADAMS solution consists of the evaluation of the state vector Y_n

(the term is used somewhat loosely here, since it includes Lagrange multipliers) at the discrete times $t_0 < t_1 < ... < t_{n-1} < t_n < ... < t_{end}$ distributed (perhaps evenly over a specified interval).

The solution to the system of *Eqn. (11)* is first computed for *j=0,1,...,n-1* (or given by the initial conditions).

$$g(\bar{Y}_j, \dot{\bar{Y}}_j, t_j) = 0 \qquad \textit{Eqn. (14)}$$

the integration algorithm then specifies a value for $h = t_n - t_{n-1}$ and computes the solution to *Eqn. (15)* to within a given integration error tolerance $\varepsilon > 0$.

$$g(\bar{Y}_n, \dot{\bar{Y}}_n, t_n) = 0 \qquad \textit{Eqn. (15)}$$

for each of the entries in $\bar{Y}$, a predictor polynomial of order *k* is formed either

- From the initial conditions if the problem is just starting
- By an interpolation of the previously computed values

The predictor polynomials are used to estimate the value and the first derivative of each unknown at time t_n [20]. Continuing the pendulum example of *Section 4.1.2*, considering a first order predictor polynomial, and assuming that the state vector and its derivative at iteration n-1 are known and defined as in *Eqn. (16)*:

$$Y_{n-1} = \begin{pmatrix} u_{p\,n-1} \\ v_{p\,n-1} \\ w_{p\,n-1} \\ x_{p\,n-1} \\ y_{p\,n-1} \\ \theta_{p\,n-1} \\ \lambda_{1\,n-1} \\ \lambda_{2\,n-1} \end{pmatrix} \quad \text{and} \quad \dot{Y}_{n-1} = \begin{pmatrix} \dot{u}_{p\,n-1} \\ \dot{v}_{p\,n-1} \\ \dot{w}_{p\,n-1} \\ \dot{x}_{p\,n-1} \\ \dot{y}_{p\,n-1} \\ \dot{\theta}_{p\,n-1} \\ \dot{\lambda}_{1\,n-1} \\ \dot{\lambda}_{2\,n-1} \end{pmatrix} \qquad \textit{Eqn. (16)}$$

Therefore, the predictor would yield the following initial value for the state vector (again, assuming a first order predictor the purposes of simplification):

$$\bar{Y}_n^0 = \begin{pmatrix} u_{p_n}^0 = u_{p_{n-1}} + \dot{u}_{p_{n-1}} h \\ v_{p_n}^0 = v_{p_{n-1}} + \dot{v}_{p_{n-1}} h \\ w_{p_n}^0 = w_{p_{n-1}} + \dot{w}_{p_{n-1}} h \\ x_{p_n}^0 = x_{p_{n-1}} + \dot{x}_{p_{n-1}} h \\ y_{p_n}^0 = y_{p_{n-1}} + \dot{y}_{p_{n-1}} h \\ \theta_{p_n}^0 = \theta_{p_{n-1}} + \dot{\theta}_{p_{n-1}} h \\ \lambda_{1_n}^0 = \lambda_{1_{n-1}} + \dot{\lambda}_{1_{n-1}} h \\ \lambda_{2_n}^0 = \lambda_{2_{n-1}} + \dot{\lambda}_{2_{n-1}} h \end{pmatrix} \qquad \textit{Eqn. (17)}$$

the superscript 0 indicates the predicted estimate of the solution at time t_n. Starting from $\bar{Y}_n^0$, a Newton-Raphson algorithm repeatedly corrects the solution until the convergence criterion is satisfied and is determining Y_n^m using *Eqn. (18)*:

$$\bar{Y}_n^m = \bar{Y}_n^{m-1} + \Delta \qquad \textit{Eqn. (18)}$$

$$\text{till } \|\Delta\| < s\varepsilon \qquad \textit{Eqn. (19)}$$

with ϵ the integration error tolerance, and s a scale factor which is depending on the predictor polynomial order.

The predicted values are generated independently for each component of the solution after which the Newton-Raphson algorithm is used to solve the system of equation simultaneously [20]. Using the current notation, the Newton-Raphson algorithm can be written as in *Eqn. (20):*

$$\bar{Y}_n^m = \bar{Y}_n^{m-1} - J^{-1} * G(\bar{y}_n^{m-1}, \frac{\bar{y}_n^{m-1} - \bar{y}_n}{h}, t_n)$$

$$\text{or } \Delta = J^{-1} * G(\bar{y}_n^{m-1}, \frac{\bar{y}_n^{m-1} - \bar{y}_n}{h}, t_n) \qquad \textit{Eqn. (20)}$$

the new values of Δ are computed till the condition of *Eqn. (19)* is met.

Continuing the pendulum example of *Section 4.1.2* and using the first order backward differentiation formula ($\dot{q}_p = \frac{q_p - q_{p_{n-1}}}{h}$) to evaluate the state variable derivatives, the Jacobian matrix of the system can be computed to be:

J=

$$\begin{pmatrix} \frac{m_p}{h} & 0 & 0 & 0 & 0 & 0 & 1 & 0 \\ 0 & \frac{m_p}{h} & 0 & 0 & 0 & 0 & 0 & 1 \\ 0 & 0 & \frac{I_p}{h} & 0 & 0 & 0 & l\sin\theta_p & -l\cos\theta_p \\ -1 & 0 & 0 & \frac{1}{h} & 0 & 0 & 0 & 0 \\ 0 & -1 & 0 & 0 & \frac{1}{h} & 0 & 0 & 0 \\ 0 & 0 & -1 & 0 & 0 & \frac{1}{h} & 0 & 0 \\ 0 & 0 & 0 & 1 & 0 & l\sin\theta_p & 0 & 0 \\ 0 & 0 & 0 & 0 & 1 & -l\cos\theta_p & 0 & 0 \end{pmatrix} \qquad \textit{Eqn. (21)}$$

One should note that the Jacobian matrix is very sparse: which is certainly one of the reasons justifying the choice of *LU* decomposition [23] to solve *Eqn. (20)*.

Finally, the corrected values are compared to the predicted values of the components of the state vector to check for compliance with the user-specified integration error tolerance ϵ. The difference between the predicted and corrected value is also used to estimate the optimum time step and the optimum order for the predictor polynomials and backward differentiation formulas. If the error tolerance is satisfied, ADAMS proceeds to the next integration step with the improved value of the time step and order.

4.2 Rudder Control Model

4.2.1 Architecture

The model presented in this section benefits from an earlier model that served as a base for the modeling of the rudder control system. Nevertheless, software updates had made it obsolete, and as it had been developed for different purposes, it was not incorporating the features necessary for this work. Therefore, only the geometry (yet partially revised to include design changes), and part of the inertia data were kept.

The rudder control system model is illustrated in *Figure 4.2*

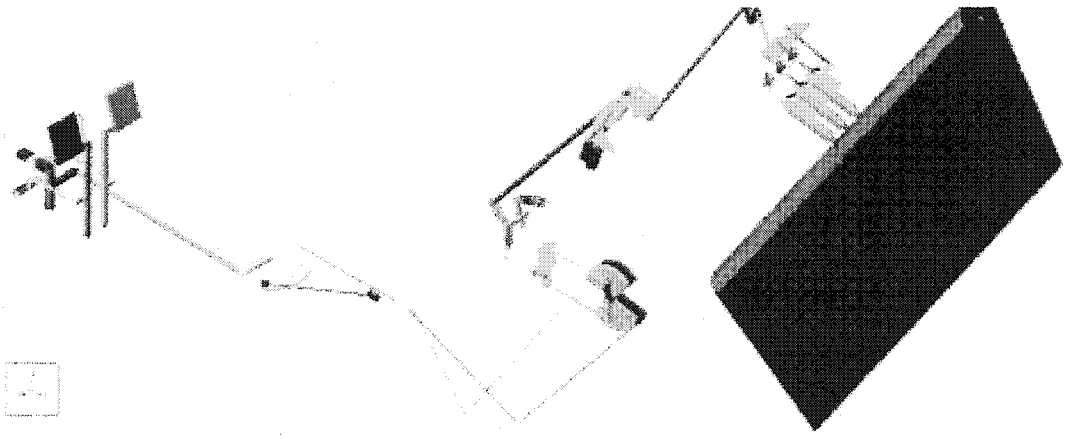

Figure 4.2 – Rudder Control Model in ADAMS

The present model includes the following simulated elements:

- All rigid moving parts (pedals, link, quadrant levers, summing mechanism...). *Figure 4.3* to *Figure 4.7* illustrate all the parts that have been modeled with their names (in italics).

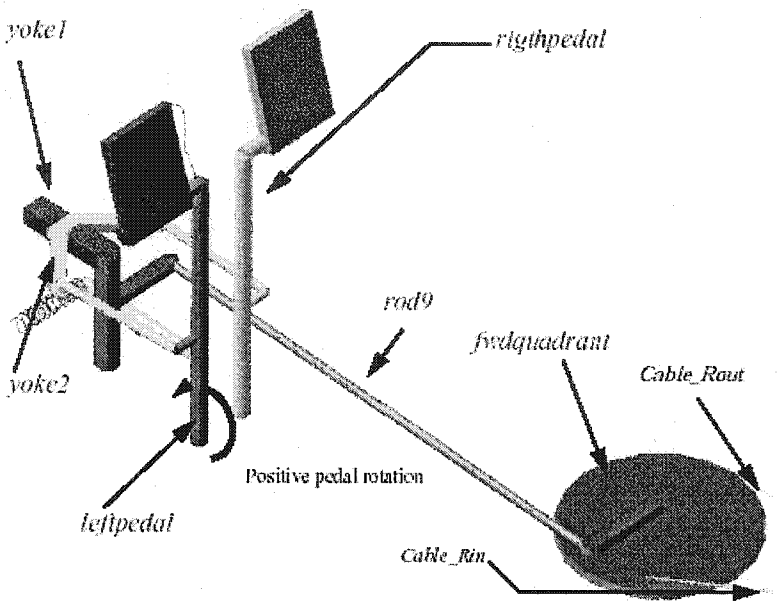

Figure 4.3 – Cockpit Section Layout

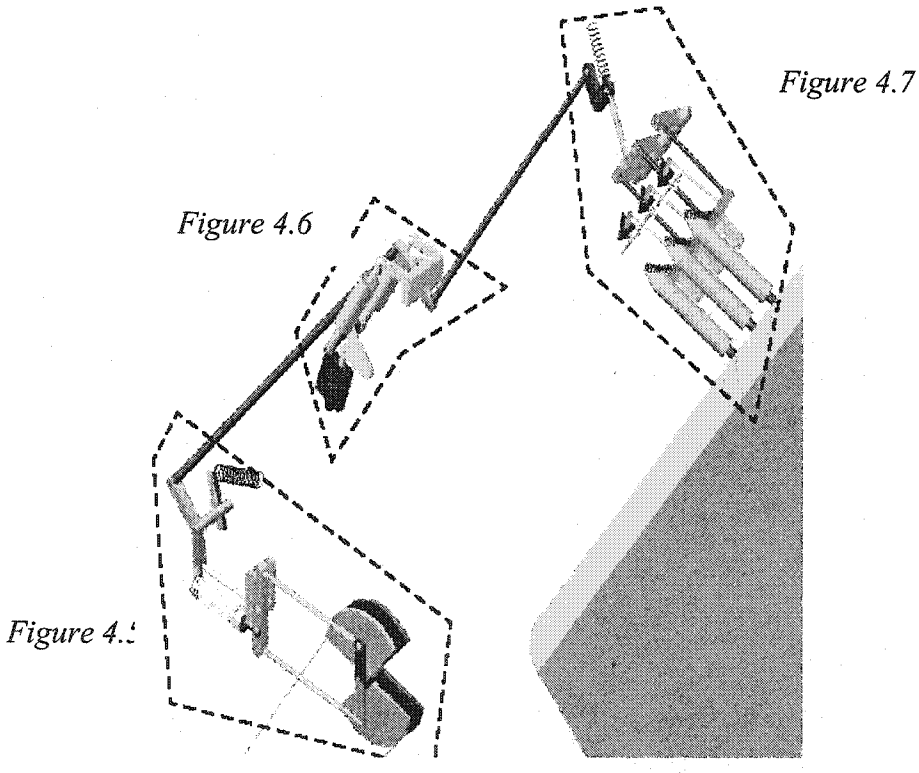

Figure 4.4 – Aft Section Layout

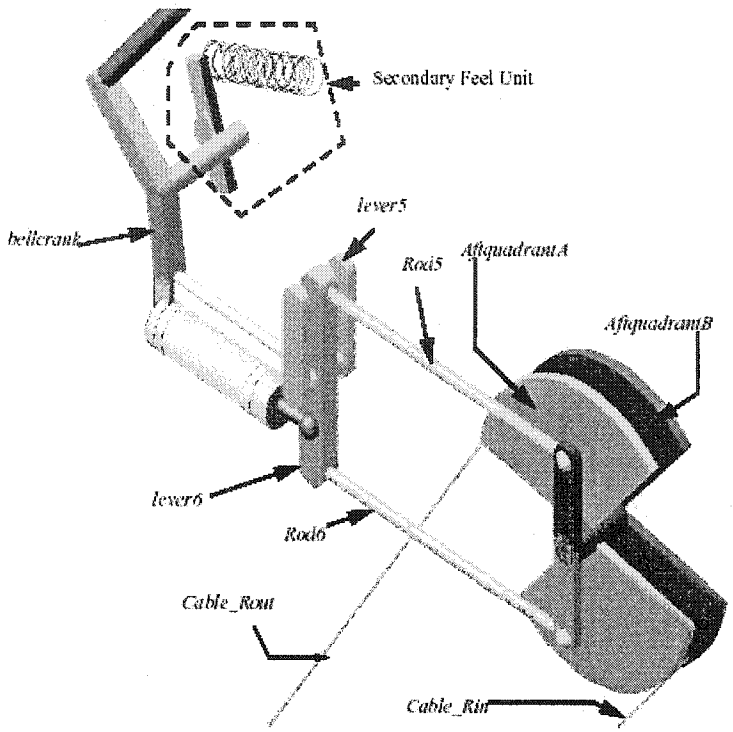

Figure 4.5 – Summing Mechanism Model

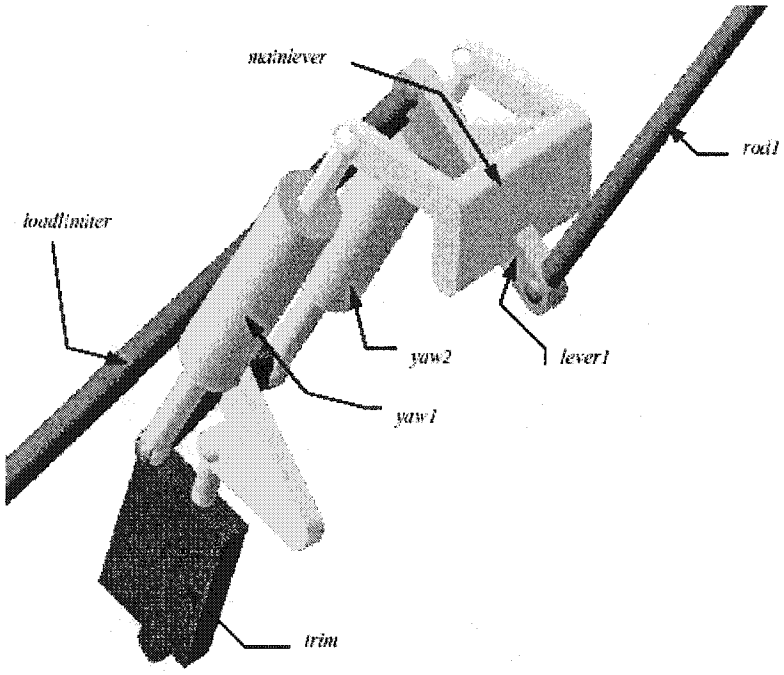

Figure 4.6 – Trim and Yaw Damper Mixer

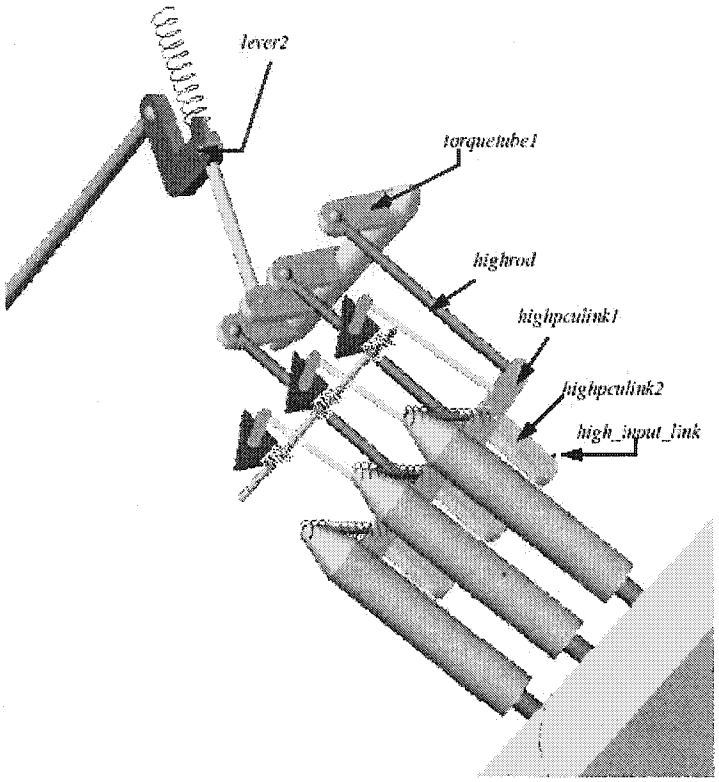

Figure 4.7 – Power Control Units Model

4.2.2 Limitations

The limitations of the model are as follows

1. Only the copilot's side is modeled (this is the side incorporating the Primary Feel Mechanism). Since both crew members are not supposed to act on the pedals simultaneously, the other half remains passive. Modeling both sides was therefore considered unnecessary for this work. All relevant inertia data and cable friction were doubled accordingly.
2. Cable damping characteristics are not modeled: its impact is recognized as limited and no data was available for modeling.
3. Cable routing is not modeled.

4. Joint and cable friction are kept constant (not dependant on cable tension), the details can be found in *Section 4.2.5.6.*
5. Cable stiffness/elongation does not change as a function of temperature (*Section 4.3.1*).
6. Since no systems compliance has been modeled (such a case was considered in [4]), the 3 PCU's are not modeled as independent systems, but as a single force (tripled) returned by the SUBROUTINE, and acts on the high PCU.

4.2.3 Assumptions

The assumptions used when building the model are as follow:

1. All parts are assumed to be rigid and homogeneous bodies.
2. The Boeing Design Manual's [21] appropriate minimum stiffness curves were used to define the cable characteristics (*Section 4.3.1*).
3. The aerodynamic hinge moment load is modeled as a spline function of rudder rotation for a specific aircraft flight condition, as generated from the flight model (as designated in *Section 2.2*). It therefore does not account for the aircraft dynamic and response to rudder rotation.
4. The mass properties were calculated manually and were in the original model. They therefore incorporate subsequent approximations, and cannot claim for the precision a 3D CAD software (such as CATIA and ProEngineer to name a few) can bring.
5. The pilot and copilot sides were assumed to be symmetrical.

4.2.4 Inputs/Outputs

4.2.4.1 Input Commands

The model has been set-up to be driven in various different ways via a user-friendly dialog box (*Figure 4.8*). The dialog box enables the engineer to control many aspects of the model configuration and run a number of preset analysis types. The model is however fully reversible and can be force or motion driven at any point in the model with minimal adjustment. The command parameters may also be adjusted if necessary.

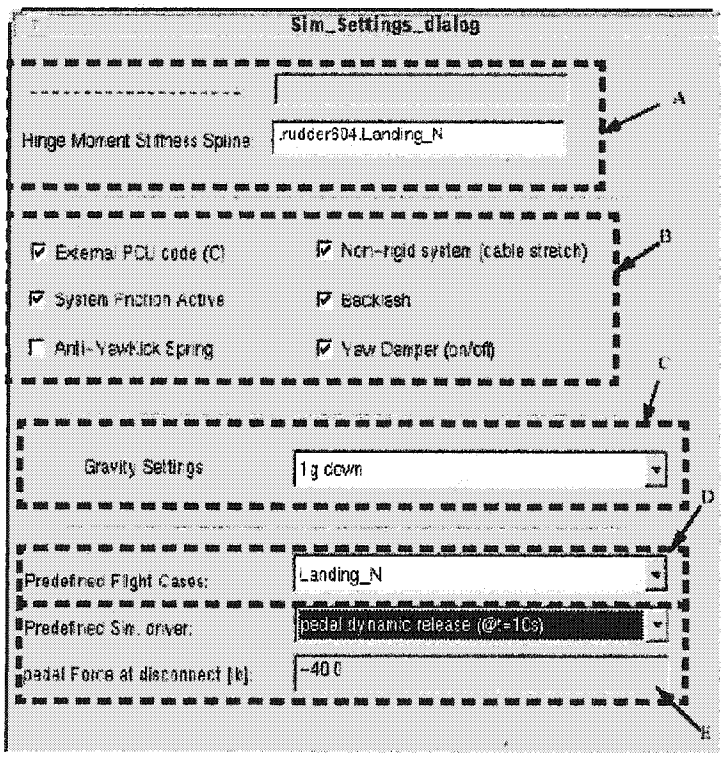

Figure 4.8 – Simulation Settings Dialog Box

The different numbered areas numbered in *Figure 4.8* are briefly described below:

A. General Settings

Table 4.1 is listing the two parameters adjustable to the user from the "simulation Settings" dialog box.

Pedal Force CMD Magnitude	Pedal force limit for the pedal rate sweep (Only active when a certain simulation driver is selected, see E)
Hinge Moment Stiffness Spline	Aerodynamic hinge moment spline (Corresponding to the flight case selected, see D)

Table 4.1 – Model General Settings

B. System Configuration

Table 4.2 is listing the different system configuration options offered to the user

External PCU Code	**Set**	Use a custom ADAMS solver build library build with the PCU C code
	Unset	Default ADAMS solver is used, PCU hydraulic characteristics arenot modeled
System Friction Active	**Set**	System friction enabled
	Unset	System friction disabled
Non-Rigid System	**Set**	Cable models are enabled
	Unset	Cable models are disabled
Yaw Damper	**Set**	Yaw damper active
	Unset	Yaw damper unactive
Anti Yaw-Kick Springs	**Set**	Anti yaw kick springs active
	Unset	Anti yaw kick springs unactive
Backlash	**Set**	All backlash in the sytem are active, dynamic solver settings changed (see chapter 3.3.3)
	Unset	All backlash unactive

Table 4.2 – System Configuration Options

C. Gravity Settings

Three choices are offered:

1. No gravity
2. Gravity active, one g down
3. Test Data: a set of spline submits each part to the relevant aircraft acceleration, depending on its location in the aircraft frame and on the aircraft's center of gravity location (see *Section 4.2.5.8* for details)

D. Predefined Flight Case

This list offers a choice of a number of hinge moment curves corresponding to common flight cases as defined by the flight science group. Selecting any one of the choices ensures the proper hinge moment spline is selected for the hinge moment curve (*Section 4.2.5.7*)

E. Predefined Simulation Diver

This feature allows the user to run the most common types of analysis (pedal constant rate sweep, pedal release test....) without any modifications to the model. When selected, the necessary fields open in the dialog box and one may choose an example rate or a maximum force. The right simulation script (a script in ADAMS/*solver* language) then activates or deactivates the necessary feature for the test.

4.2.4.2 Input Parameters

Table 4.3 lists the input parameters. Entered as ADAMS state variables, they may be varied during simulation time and programmed to follow a particular curve.

Variable Name	Description
Var_adjs	Pedal Adjustment (in)
Var_Trim	Trim Actuator Displacement (in)

Table 4.3- Model Input Variables

4.2.4.3 Main Output Measures

Table 4.4 lists the main measures of the model parameters the user has access to. ADAMS authorizes any new measure of the model state variable to be recorded, plotted and studied with a minimum of manipulations.

Measure Name	Description	Unit
PedalRotation	Left pedal rotation	deg
PedalDisplacement	Left pedal displacement @ 16 in	in
PedalTorque	Left pedal torque	lb.in
REV_fwdquadrant_ROTATION	Rotation of the forward quadrant	deg
Cable_Rin_stretch_value	Stretch of theinner Cable	in
Cable_Rout_stretch_value	Stretch of the outter Cable	in
Torque_tube_rotation	Rotation of the torque tube	deg
High_PCUlink_angle	Angle of the high PCU input link	deg
High_PCU_Xv	Displacement of the PCU control valve	in
High_PCU_Xa	Displacement of the PCU piston	in
High_PCU_Xa_dot	Speed of the PCU piston	in/s
Rudder_rotation	Rotation of the rudder	deg

Table 4.4 – Model Main Output Measures

4.2.4.4 Coordinate and Unit Systems, Conventions

The model uses the imperial unit system. All of the element positions and orientations are defined in the Cartesian coordinate system and Euler angle system (BODY 3-1-3) respectively. The X, Y and Z coordinates correspond to the following in the aircraft body reference frame: Fuselage Station (FS), Water Line (WL), Buttock Line (BL), and Water Line (WL) respectively (*Figure 4.9*).

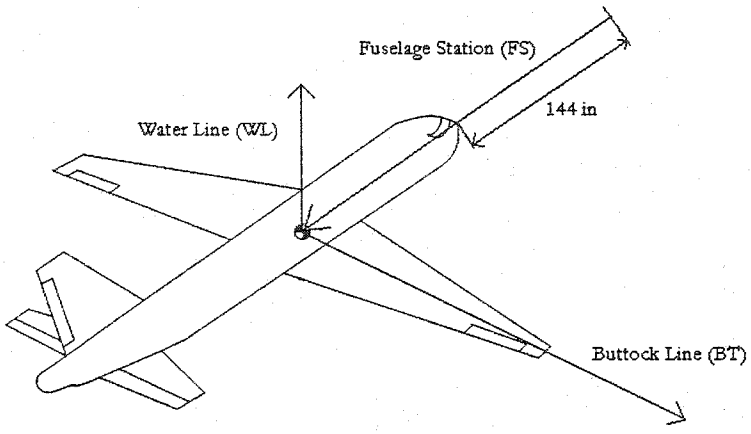

Figure 4.9 – Aircraft Reference

The units used in the model are as follows:

Length	**Inch**
Mass	pound mass
Force	pound force
Time	second
Angle	degree
Frequency	hertz

Table 4.5 – Unit System

Finally, the sign conventions chosen in the model are as follow:

- Left pedal forward travel is defined positive.
- Rudder trailing edge left is defined positive.
- The other main parts in the model follow the left pedal forward convention.

4.2.5 Rudder Model Configuration

The model is customized to enable multiple combinations of options and system configuration. The model is primarily constructed with PARTS, CONTRAINTS (joints, couplers, motions), and FORCES (cable, loads, stops, springs...).

4.2.5.1 Parts

An ADAMS part consists of a rigid non-deformable body with some attached geometry. The parts mass properties (weight, inertia and center of mass location) were included in the original model and have been left unchanged, except for the rudder (as the original model was not including PCU hydraulic, including rudder inertia data was unnecessary).

4.2.5.2 Constraints

Constraints define how parts are attached to one another and how they are allowed to move relative to one another. These elements include joints, motion generators and couplers.

4.2.5.3 Joints

The joint types used to construct the model consist of revolute (1 rotational Degree of Freedom DOF), U-joint (2 rotational DOF's), Spherical (3 rotational DOF's), and translational joints (1 translational DOF) and can be seen in *Figure 4.10.*

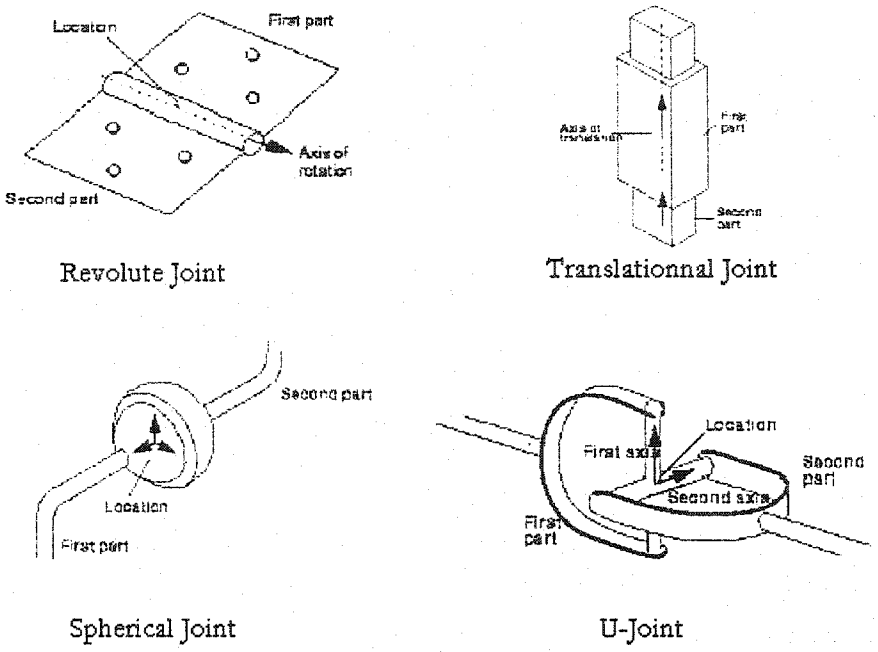

Figure 4.10 – Joint Types

4.2.5.4 Motions

A motion generator dictates the movement of a part as a function of time. It supplies whatever force is required to make the part satisfy the motion. The model includes motions for the pedal adjustment, the trim and yaw damper actuators.

4.2.5.5 Forces

Forces define loads and compliances on parts. Forces do not absolutely prohibit or prescribe motions, they therefore do not add or remove degrees of freedom (DOF) from

the system. The model includes forces to model the cable system, friction, mechanical stops, various springs, bungee, artificial feel units and the aerodynamic hinge moment load.

4.2.5.6 Friction

VPFCS locates the two main sources of friction in the primary flight control system in:

- Cable friction, encompassing:
- Cable/sheave friction
- Pulley bearing friction (the cable routing encompassing the twelve of them on each side, see *Figure 3.4*)
- Cable/eyeball pressure seal friction, since during its routing, the cable leaves the pressured part of the fuselage.
- PCU control valve friction

Cable/sheave and bearing static friction are both computed using the same empirical formula and table [21], valid for this type of certified cable and pulley arrangement. It therefore will not be discussed here. Cable pre-tension on the system is 100lbs.This signifies that the system is very stiff, and that cable tension fluctuations are limited and most of the time fall within a range of 10% of this value. The impact of cable tension fluctuation on the friction is therefore limited, and within the range of the error of the estimation of the cable static friction. Following VPFCS practice, cable friction was therefore input as a preload in ADAMS, and is not a function of the cable tension fluctuation. The small amplitude of the motions studied in this thesis is another justification for this assumption.

The cable/eyeball pressure seal amount was estimated from common assumptions on the friction coefficient and the cable tension and weight: accounting for only 1% of the cable friction, the amount is therefore negligible.

The only data available form the PCU control valve friction is it static friction: it is indeed very low, and account for only a very small part of the total friction in the system.

Finally the total friction in the mechanism as seen at the pedals is below 5 lbs, and is therefore around what is expected (*Section 4.1.1*). Minor discrepancies were found with experimental data (*Section 4.4.5*) that can reasonably be explained by the friction in the connections. The necessary friction was therefore added to the model, and distributed in the mechanism (*Figure 4.11*).

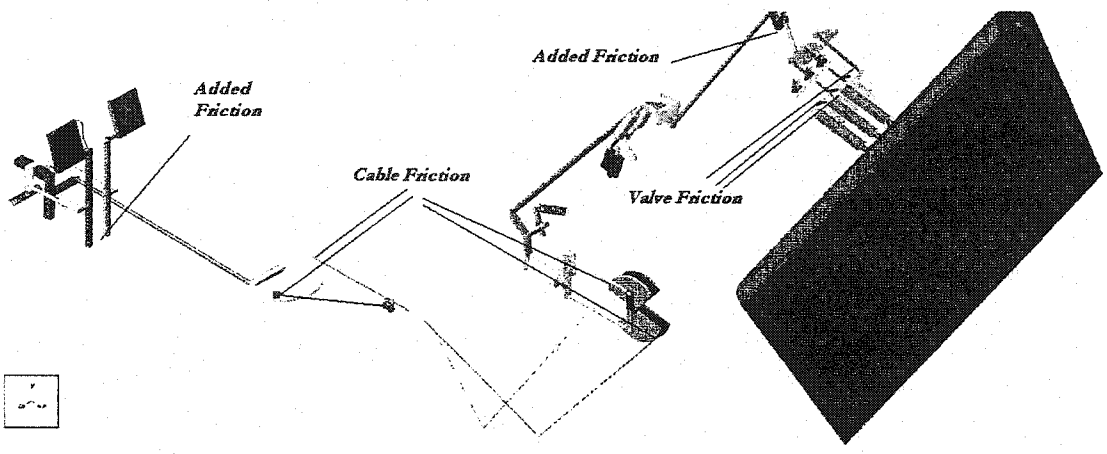

Figure 4.11 – Friction Distribution in the Model

Friction has been lumped into those elements (*Figure 4.11*) with the Joint Friction ADAMS built-in feature. *Section 4.3.1* gives more details about how the cable was modeled, and how friction was combined in this model. The frictional force/moment acts

to oppose the relative motion in the joint. The friction force calculations are specified as a function of the specified preload only; they do not include joint reaction forces.

The PCU subroutine encompasses friction in its code with a coulomb friction of 0.9 lbs, and a viscous friction of 25.2 lbf.s/in [4].

4.2.5.7 Aerodynamic Hinge Moment

The aerodynamic hinge moments have been modeled as torque spline-functions with the rudder rotation as the independent variable. The hinge moment curves are generated from the MatrixX flight model (*Section 2.2*) provided by Flight Sciences for a number of operating flight condition, including Mach, dynamic pressure, and slide slip angle.

4.2.5.8 Gravity/Aircraft Body Accelerations

ADAMS comes with a transparent gravity function that applies a unidirectional force at the center of mass marker of each part. The force direction and gravity acceleration (the resultant weight on each part of course depends on its mass) are chosen as a general setting, and therefore cannot be varied during simulation time.

Bombardier had developed a macro that could be used to simulate the impact of the aircraft acceleration on the part dynamic. It attaches a three-component force vector to every part center of mass marker (aligned with the aircraft global reference). The magnitudes of these forces may be kept constant (1 g down setting) or be a function of the three state variables *X_accel_FUN*, *Y_accel_FUN*, and *Z_accel_FUN*. This allows the user to model the impact of the aircraft acceleration on the control system dynamics, for example during a turn. When a 1 G acceleration is requested in the simulation setting

dialog box (Section 4.2.4), the x-axis and z-axis G-forces are set to zero and the y-axis component is set to -1 (down). This of course neglects the fact that each and every part of the system is subject to a different acceleration, depending on its location in the aircraft. Since yaw kick is a very brief phenomena of small amplitude and characterized by a yawing motion, this macro was further improved for the purposes of this project.

The macro developed for this project is active when requesting "test data" in the simulation setting dialog box, in the gravity section (*Section 4.2.4*) and requires the following data (*Table 4.6*) to be imported into the model, from either experimental or simulation results.

Variable	Unit
U	in/s
V	in/s
W	in/s
Nx	in/s^2
Ny	in/s^2
Nz	in/s^2
P	rad/s
Q	rad/s
R	rad/s
$\dot{P}$	rad/s^2
$\dot{Q}$	rad/s^2
$\dot{R}$	rad/s^2

Table 4.6 – Input to the Acceleration Macro

Signification of the variables in *Table 4.6* can be found in *Section 2.1.2*. They can easily be imported from a text file - with the variable value versus the time- to an ADAMS spline curve (an ADAMS data format associating arrays of 2 values, for example a variable depending on time).

With this option, the G force for each part now depends on its position relative to the aircraft's center of gravity and is defined by *Eqn. (22)* (Newton's law in a moving reference frame):

$$\begin{aligned} Nx &= -Nx + 2QW - 2RV + (X_g - X_m)(Q^2 + R^2) - Z_m(-\dot{R} + QP) + (Y_g - Y_m)*(\dot{Q} + RP) \\ Nz &= Ny + 2RU - 2PW + (X_g - X_m)(-\dot{R} + QP) - Z_m(-R^2 + P^2) + (Y_g - Y_m)*(\dot{P} + RQ) \\ Ny &= -Nz + 2PU - 2QU + (X_g - X_m)(-\dot{Q} + PR) + Z_m(\dot{P} + QR) + (Y_g - Y_m)*(P^2 + Q^2) \end{aligned} \qquad \textit{Eqn. (22)}$$

All the positions in *Eqn. (22)*, as well as the acceleration on the left hand side of the equal sign are referring to the model convention (*Section 4.2.4.4*). Imported values (*Table 4.6*) are in the body reference frame, since they usually come from the flight model or test data. The "g" subscript refers to the aircraft's center of gravity location, while "m" refers to the part's center of gravity location.

4.2.6 Systems

This section aims at summarizing the techniques used to model the different systems.

4.2.6.1 Feel Units

The two feel units consist of a cam profile, drawn on a mechanism part, whose rotation is followed by a roller that puts a set of two parallel springs in tension. The cam profile was drawn as a spline geometry, and is a part of the rotating element. The roller is

a circle geometry element (no mass), while a contact force (see Appendix B) models its contact with the cam.

4.2.6.2 Control Stops

Pedals stops (one on each side) are modeled using IMPACT functions in forces. Aft, (torque tube), and PCU control valve stop, are modeled using BSTOP functions within torque components.

4.3 System Hydraulic and Non-Linearity Modeling

4.3.1 Flight Control Cable Model

Flight control cables are modeled as force spline functions with the cable deformation as an independent variable. A cable run is defined as a cable section with both ends rigidly fixed to a quadrant.

A cable construction kit developed by Bombardier was used to create the two cable runs present in the rudder control system [22]. The kit creates two new parts (cable ends) for each cable run on the circumference of the end quadrants (located in polar coordinate (r, Θ) on the xy-plane of the revolute joint). These parts are then constrained with a pair of translation and gear joints to couple their translational displacement with the quadrant rotation (*Figure 4.12* illustrates this layout for one end of the cable). Single component forces attached on each cable end part calculate the cable tension as a function of cable installation elongation (preload), length, installation rigidity factor and the relative displacement of the two cable ends. The cable tension is assumed equal in magnitude at both ends and conforms to *Eqn. (23)*:

$$Force = (\frac{1}{I_c}) * AKISPL(\frac{\delta_c}{L_c} + InstalledElongation) \qquad Eqn.\ (23)$$

here, I_c is the installation factor that accounts for the tolerance in the cable stiffness, δ_c is the cable elongation and L_c the cable length.

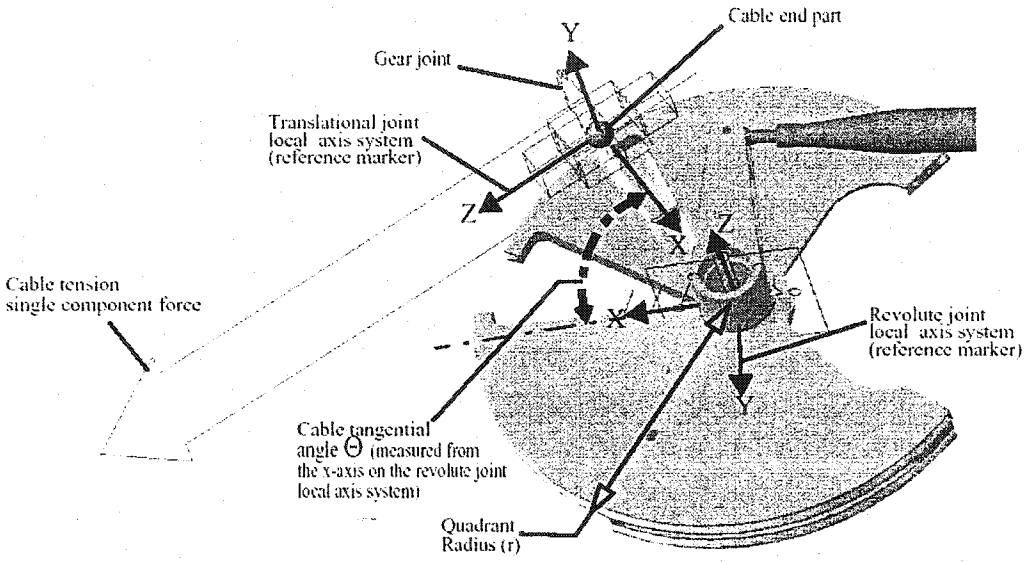

Figure 4.12- Cables Construction Kit Layout

There are two cable runs in the fuselage section consisting of 1/8 inch 7X19 stainless steel cables (*Figure 4.13*).

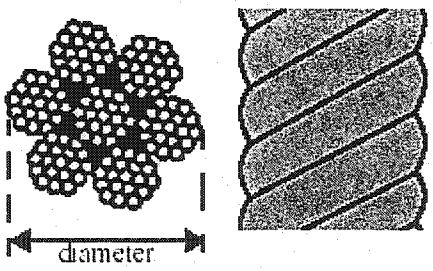

Figure 4.13- 1/8 inch 7X19 Stainless Steel Cables Section [22]

The maximum elongation (minimum stiffness) curves are active by default in the model, since by experience, they tend to be the closest to experimental values. *Figure*

4.14 demonstrates the cable's elongation characteristics, which prove to be slightly non-linear.

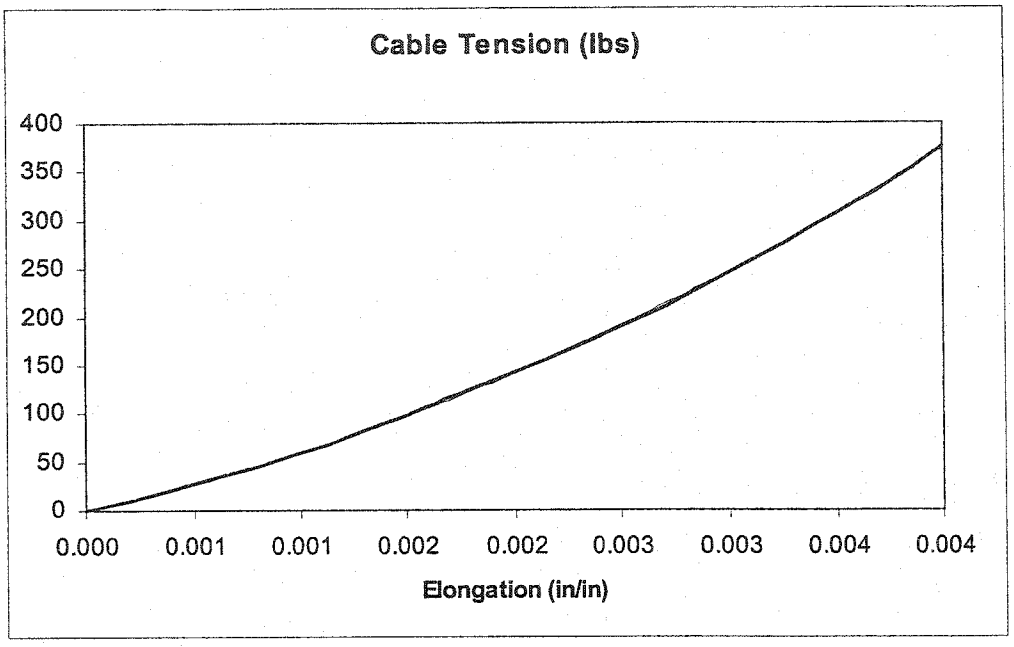

Figure 4.14 – Cable Elongation Characteristic [21]

4.3.2 PCU Model

Section 3.3.2 has recognized the PCU as a key component of the rudder control system and *Section 1.2* discussed the success of the previous collaboration between Concordia and Bombardier Aerospace on developing of a MatrixX model of rudder PCU's.

This work considers the rudder control in its totality, and the problem of integrating the ADAMS modeled mechanic with the PCU hydraulic logically arose.

One option considered was to use a particular ADAMS module, ADAMS/*Control*, to connect the MatrixX model of the PCU with the ADAMS model of the rudder control mechanic. This had a number of inconveniences:

- When doing co-simulation with MatrixX and ADAMS using ADAMS/*control*, it is MatrixX that is controlling the simulation. This is not very suitable for this project, since the PCU, though important, is still only one component of the system.
- Co-simulation as performed using ADAMS/*control* might encounter a number of problem when used with non-linear systems, as it is the case in this project. In particular, [23] warns the user against the use of co simulation when the model contains the IMPACT function. The ADAMS/*solver* indeed performs symbolic factorization of the system's Jacobian matrices before inverting it (using standard LU decomposition) for the purpose of solving the differential equation *Eqn. (15)* (*Section 4.1*). Major changes in the system's configuration usually implies refactorization of this matrix during the simulation (CONTACT force suddenly varies),and this is not appreciated by the "driving" software (MatrixX).
- It usually leads to an increased CPU charge and therefore a longer simulation time, compared to the solution adopted.

Finally, and partly for the above-mentioned reasons, co-simulation is not the method chosen and defined in the VPFCS project, and the resulting solution would therefore not be fully compatible with Bombardier needs.

Instead, the PCU hydraulic model is written in C language, following a Bombardier developed template. This code is based on an electrical network analogy, and therefore provides a very flexible and stable solution for calculating the pressure flow

rate within the PCU. This model is then integrated into ADAMS in the form of a so-called "user-defined subroutine".

This type of subroutine is compiled and integrated into the ADAMS/*solver* and thereby defines a new user-defined solver. This means that when the user is calling for a simulation, it will not call for the standard executable ADAMS/*solver*, but rather for a derived version of it that has the PCU code embedded in it. Hence, it is still ADAMS driving the simulation and authorizing for the use of ADAMS parameterization procedures.

The following section will first cover the MatrixX Concordia University developed model, and will then review how it was used as a basis for the C code model implementation.

Validation of this model will be reviewed later in this document (*Section 4.4.3*), in the section covering the validation of different original components and the overall model.

4.3.2.1 MatrixX Model

The specifications for the PCU control valve model are based on the validated model developed by Concordia [3].

This validated model was built using SystemBuild, the control system block editing solution for the MatrixX software suite (this product is equivalent to Simulink in the Matlab software package), in order to permit easy integration with the flight model. This model that was also used by Concordia to complete the study of yaw activity phenomenon in relation to the PCU dynamic [3].

The purpose here is not to present a detailed review of the PCU model architecture, but rather to review the assumptions and modeling choices that made when it was developed, thus justifying its consistency with the model adopted in this work, later reviewed in *Section 4.3.2.2.*

Figure 4.17 presents the architecture of the SystemBuild model, as seen in [4].

This model only covers the components active during the normal working of the PCU, which includes the control valve and actuator, but excludes failure sensing mechanism, relief valve and bypass valve.

For this project, ADAMS is in charge of modeling and solving the equations of the mechanical part of the PCU. *Figure 4.17* highlights the input and the output of the hydraulic part, which are of interest in this section: the control link dynamic, and PCU actuator dynamic are modeled in ADAMS.

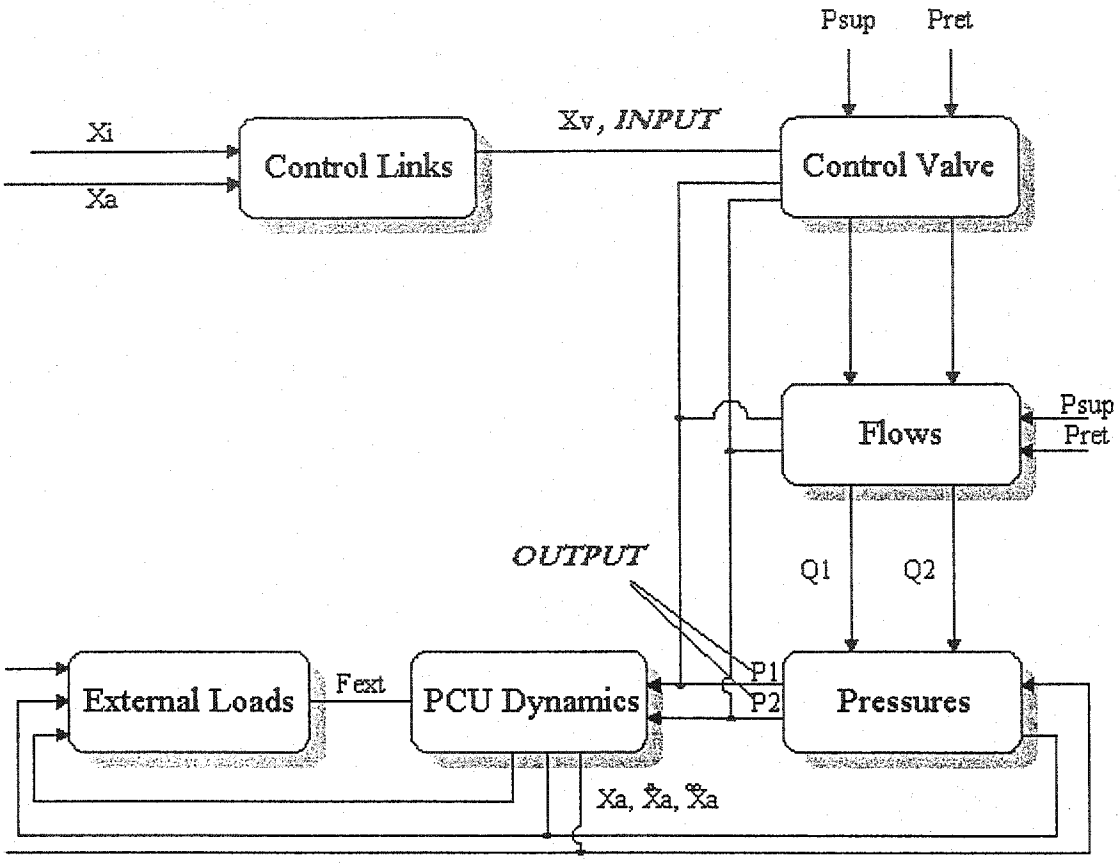

Figure 4.15 - Principle Schematic of a Control Valve Model, MatrixX Model [4]

The *control valve* block calculates the position of the control valve, which distributes the flow through the chambers, as a function of the error, as it was defined *in Figure 3.11*. The control valve dynamic is neglected in regard to the actuator dynamic: it is represented by a simple gain block. A dead band block in the sleeve motion models the possible overlap of the sleeve and spool.

Flow in the control valve orifice, computed by the *flows* block in *Figure 4.15* is built around *Eqn. (24)* [17] which can be derived using Torricelli's equation for a frictionless flow through an orifice:

$$Q = \left(C \cdot A_{orifice} \cdot X_V\right)\sqrt{\frac{2 \cdot \Delta P}{\rho}} \qquad \textit{Eqn. (24)}$$

where ρ is the mass density of the fluid, $A_{orifice}$ is the area of the orifice, and C is the orifice coefficient. C is necessary because the actual flow path past the orifice is actually smaller in cross section than the orifice itself and to account for friction, and its computation is dependant on the Reynolds number (turbulent flow assumption in that case [4]). Finally, Xv represents the spool displacement. This equation also assumes that the valve is operating in the linear portion of its control motion.

Losses in the pressure and return line are neglected, by comparison with the high hydraulic pressure in the system.

Finally, pressure in the actuator chambers is computed from the flow rate values using *Eqn. (25)* [17]:

$$Q = \frac{A_{actuator} * l_{stroke}}{\beta_{effective}} * \frac{dP}{dt} \qquad \textit{Eqn. (25)}$$

where $A_{actuator}$ is the surface of the actuator, l_{stroke} the stroke length of the actuator and $\beta_{effective}$ is the effective bulk modulus of the PCU actuator. From these pressures, it is easy to compute for the force at the piston, a product of pressure difference in the two chambers times the piston area. This force should be the output of the user-defined subroutine in the C code PCU model.

4.3.2.2 C Code PCU Model

This model was built around a template developed by Bombardier using the very same numerical values around which Concordia University MatrixX Model was built.

This section will therefore aim at reviewing the few differences in these two approaches. A first difference that was partly exposed when commenting *Figure 4.15* is the scope covered by the C-code PCU model To better understand this difference, a look at *Figure 4.16* clarifies which part of the system is modeled in ADAMS, and which part is done by the external subroutine.

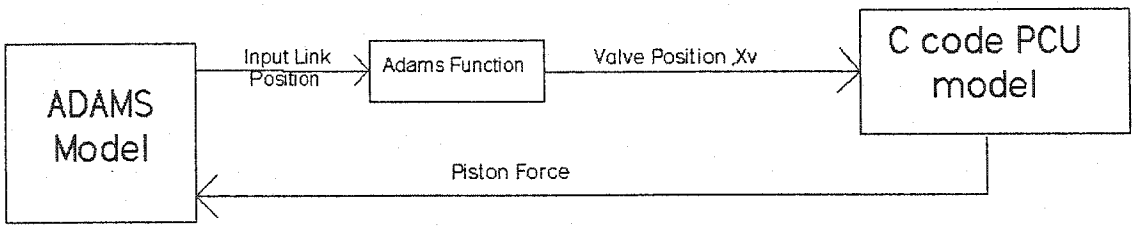

Figure 4.16 – Relationship between the ADAMS and PCU Model

The positional error between the PCU command (summing lever pilot input end displacement) and the PCU actuator position (summing lever lower end) is mechanically transmitted through the valve input link to move the spool inside the control valve. The mechanics of the spool valve linkage are not modeled in ADAMS, but rather computed by an ADAMS/*view* function that computes the spool valve position as a function of the input link (*Figure 4.17*), according to the geometry of the linkage system (details may be found in [4]).

In addition to the closed loop mechanical kinematics, the mechanism of the PCU control valves includes rate stops modeled with a BISTOP function (see Appendix B) located at the revolute joint of the input link (*Figure 4.17*).

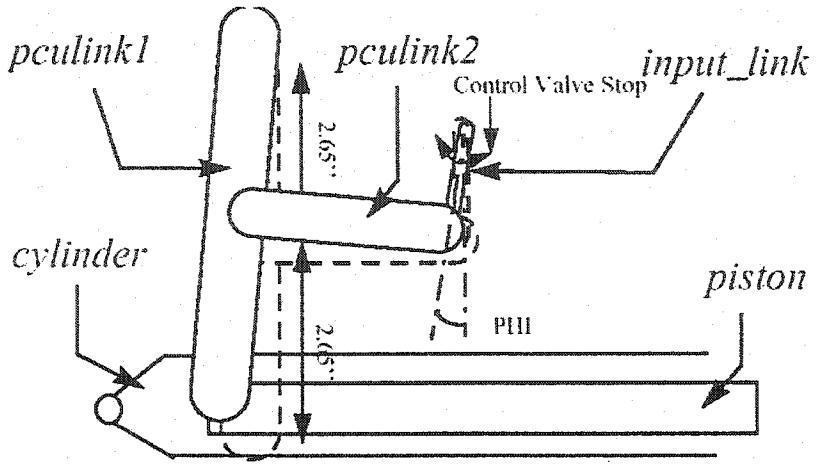

Figure 4.17 – Control Valve Schematic

The hydraulic actuator forces are calculated by the external user subroutine that models the PCU hydraulic circuit using an electrical circuit equivalent nodal representation. Each of the metering port of the valve are modeled under the same assumption as those stated in *Section 4.3.2.1*, and give a resistor in the electrical circuit equivalent. For the complete control valve, this gives a configuration similar to a Wheatstone bridge [17], as can be seen in *Figure 4.18*. Computation of the pressure in the actuator chambers is then based on the same compressed fluid formula, as seen in *Section 4.3.2.1*, and therefore find an electrical equivalent in a conductance.

The user subroutine calculates the hydraulic pressure at four control volumes (nodes) in the hydraulic circuit and the hydraulic conductance and capacitance for each flow branches. *Figure 4.18* shows a nodal diagram of one PCU (for a hydraulic schematic, see *Figure 3.12*).

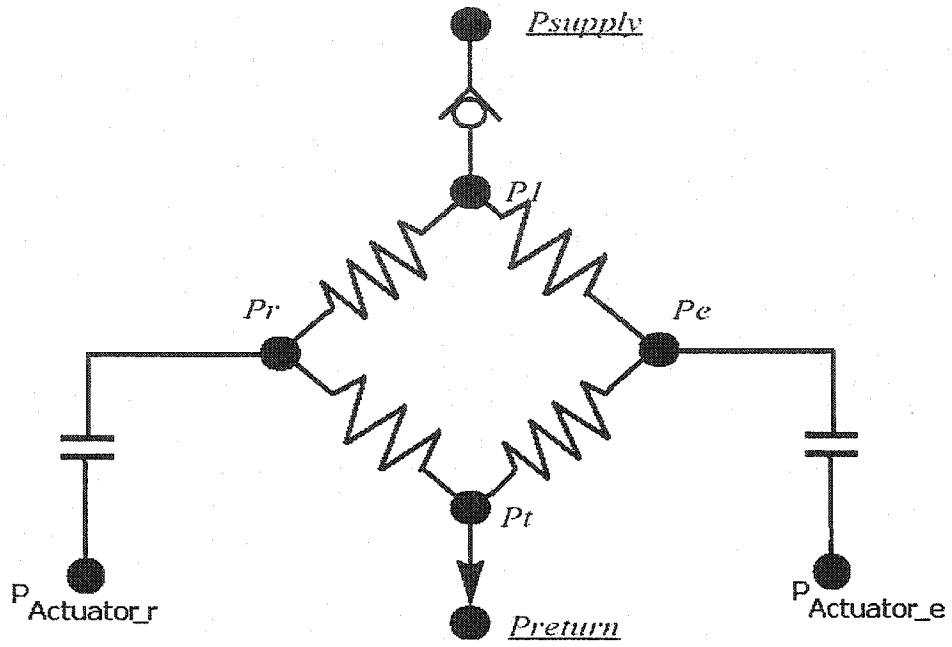

Figure 4.18 – PCU Model Nodal Diagram

Pr and Pe are then used to computes pressures in the actuator chamber ($P_{actuator}$ on *Figure 4.18*). Capacitances on *Figure 4.18* are the best analogy to account for the fluid compressibility, whose effects were discussed earlier with *Eqn. (25)*. The PCU force is used in the model as a force on the PCU actuator.

Details of the computational sequence may be found in Appendix C, but one should remember, that if the equation and assumptions are the same in the two models, the methods to solve these equations is show some interesting differences.

The MatrixX model is formed with discrete block at a sample frequency of 10kHz. It is noticeable in *Figure 4.15* that the solving of the model equations is done in a feedback like manner. The computational sequence is quite different in the nodal approach (see Appendix C), since those equations were already manually solved, and the subroutine is simply computing numerical solutions to those equations. The code is

therefore more numerically stable, hence ensuring good stability and robustness of the overall rudder control model.

4.3.3 Clearance Model

Section 3 reviewed the rudder control system; and showed that it is mainly made up of push-pull roll connectors and cable. Since friction is critical in this type of system, a rod-end usually incorporates a roller bearing and looks similar to *Figure 4.19*.

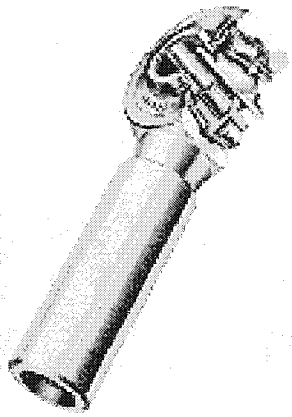

Figure 4.19 – Push-Pull Rod End

In the studied design, it is a double row ball bearing that creates a spherical-like connection in between the two rods.

Even though the system is designed to minimize backlash, there are still a number of locations in the system where backlash is actually present, backlash in the rod end connections having been identified as the most important.

4.3.3.1 Rod End as a Source of Backlash

Figure 4.20 is shows a schematized view of the connection between two rods, and of the potential sources of backlash.

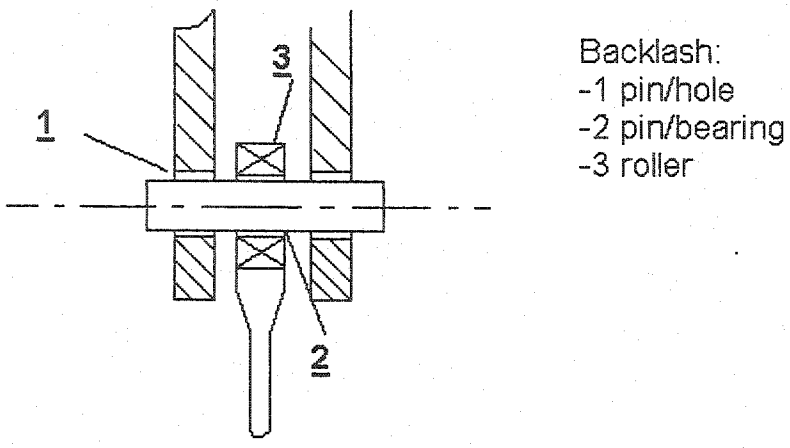

Figure 4.20 – Rod End Schematic

The bearing has an internal clearance estimated at 0.0004 inches in the documentation [25]. A clearance is present between the pin and the bearing, for the load usually present in the system.

Finally, a diametric clearance between the pin and the bore is present due to the tolerance in the manufacturing, and can be estimated to be between 0.0002 inches and 0.0022 inches. This gives a total diametric clearance of between 0.0002 inches and 0.0026 inches.

4.3.3.2 Rod End Clearance Model

The ADAMS/*view* does not incorporate a built-in model of such radial clearances, and it was necessary to develop a methodology to make it to do so.

Since this operation had to be repeated a number of times, an ADAMS macro (a script containing a list of ADAMS/*view* commands), and a dialog box were developed in order to make the process easy and transparent. In addition, this macro had to be capable of creating two different types of joints, revolute and spherical, since some connections in

the mechanism necessitate the extra degree of freedom of the spherical joint. Finally, the object created had to be parameterized, therefore authorizing rapid change of the clearance value while preparing for the study of the system.

The dialog box presented in *Figure 4.21* is directly accessible from the modified ADAMS menu, prompting the user for the necessary information to create the joints with clearance.

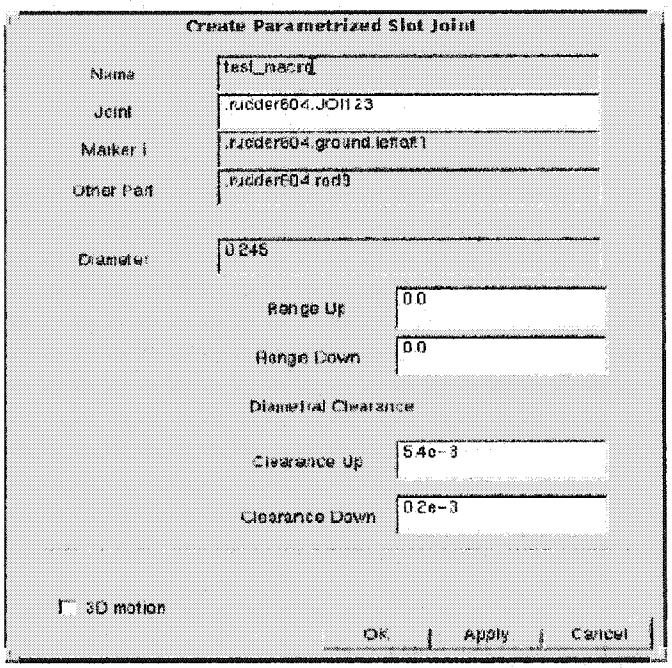

Figure 4.21 – Dialog Box for the Clearance Model

This dialog box drives a macro, which, once activated, will execute the following commands:

1. Create two "design variables": for the diameter and the clearance. Design variable are ADAMS objects that can contain a value and its maximum range of variation.
2. Create two circles/spheres at the joint location (depending if the joint modeled is revolute or spherical), of the specified diameter (as can be computed from pin diameter and clearance values), and with an initial clearance at midpoint.

3. If it is a revolute type of connection requested, create a planar joint on the z-axis of the specified marker in between the two parts, ensuring they do remain in the same plane.
4. Create a contact force in between the two circle/spheres (see Appendix B for a detailed review of this ADAMS/*solver* statement)
5. Deactivate the previous joint

Two extra dialog boxes are provided to the user in order to easily modify these values and return to the previous joint whenever necessary. Aditionnaly, the dialog box presented in *Section 4.2.4* allows the user to simultaneously activate/deactivate all joint clearance models.

Figure 4.22 and *Figure 4.23* illustrate the two types of objects that may be created (Joint and contact forces were hidden on this picture to make the contact circles apparent)

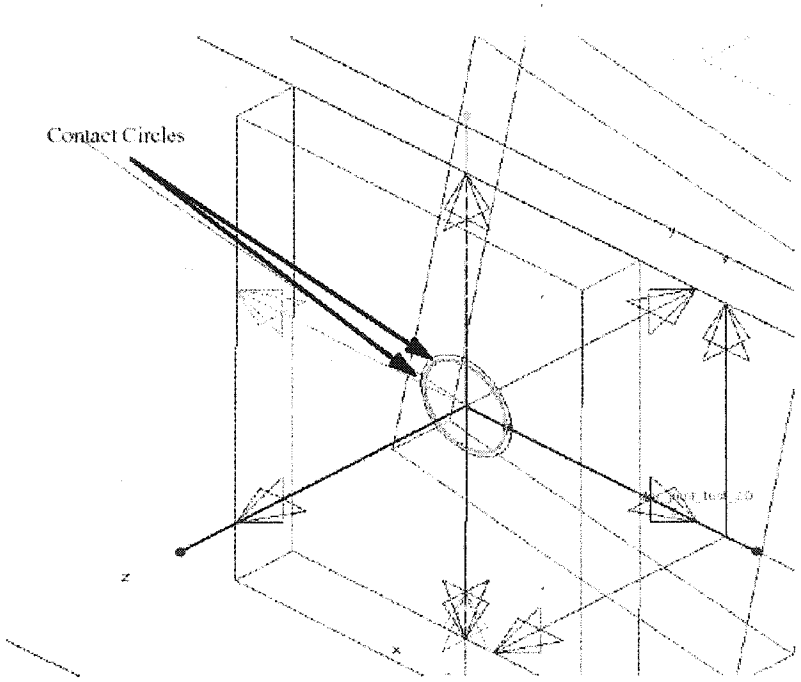

Figure 4.22 – Clearance Model for the Revolute Joint

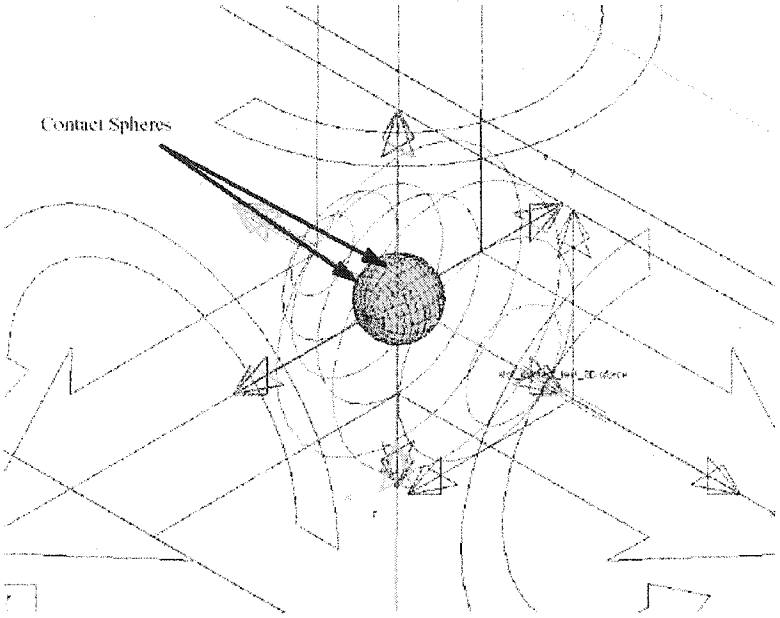

Figure 4.23 – Clearance Model for the Spherical Joint

The major drawback of introducing such an object in the model is a greatly increased simulation time, when the simulation is not simply aborted: the predictor algorithm (see *Section 4.1*) which is part of the ADAMS/*solver*, does not accommodate well with models whose characteristics can change so drastically depending on the contact condition.

The first approach used to reduce simulation time is the choice of a correct contact array (a further discussion of the contact object is available in appendix B) that tries to dampen slightly the contact event. The ADAMS manual does not provide any real methodology for this approach, and the user is left with a lengthy trial and error process. *Table 4.7* is lists the values finally adopted for the project.

Parameter	Value
Stiffness (N/mm)	7.00E+04
Force Exponent	1.1
Damping Factor (N.s/mm)	10
Depth Penetration (mm)	1.00E-09

Table 4.7 – Contact Statement Characteristics

Another way to try and reduce the simulation time is to change the ADAMS/*solver* parameters. ADAMS documentation [26] provides guidelines for such changes: the error tolerance is slightly increased, while the order of the predictor polynomial is limited to one. Also, the maximum number of iteration till convergence is increased. The "memory" of the model's previous configuration is therefore "shortened", allowing the predictor to react faster to the brisk contact event. The optimal parameters are shown in *Table 4.8*:

Parameter	Value
Integrator	Gear
Accuracy	2
Highest Integrator Order	First
Iterations Limit	25
Linear Solver	Harwell

Table 4.8 – Solver Parameter

A macro ensures that the solver automatically adopts these parameters when a clearance model is activated somewhere in the model, and returns the solver to its default characteristics when necessary.

4.3.3.3 Clearance in the Model

Load in the joints are maximal until the secondary feel unit (*Figure 3.4*), since after this point, the PCU's provide the necessary energy to move the rudder.

The clearance between the pin and bore (which is the main contribution) was assumed to be fixed under such low values of the forces at the connection, and was therefore not considered past this point (*Figure 4.24*). The clearances of the summing mechanism were also lumped into a single joint, in order to limit the complexity (each clearance model greatly increases ssimulation time).

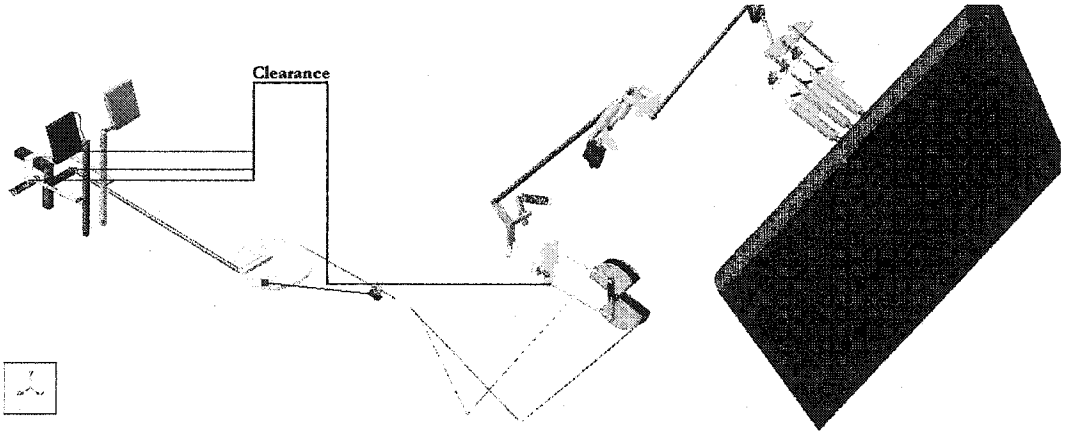

Figure 4.24 – Location of the Clearance Models in the System

4.3.4 Friction Model

Friction appears at the physical interface between two surfaces in contact, and therefore occurs in virtually all mechanical systems. Friction usually refers to a very complex collection of behavior that initiates from a wide range of physical phenomena, engaging elastic and plastic deformation, material science, fluid mechanics and so on.

It is also highly non-linear, and may lead to steady states error, limit cycle oscillations, and poor performances. It is believed that it may be one of the concurrent

causes in yaw kick behavior, and it is therefore crucial for this project to model it in a physically realistic way, that is to model it in a way that reproduces its primary behavior.

4.3.4.1 Friction Characteristics

Behavior of friction was examined extensively during the 20th century in order to try to decipher the complexity of different mechanisms involved in friction phenomena. Below is a list of the most widely recognized behaviors [27]:

A. Steady Velocity Friction

The friction force as a function of velocity for constant velocity motion is called the Stribeck curve, and in particular, the dip in force at low velocities (*Figure 4.25*) is called the Stribeck effect.

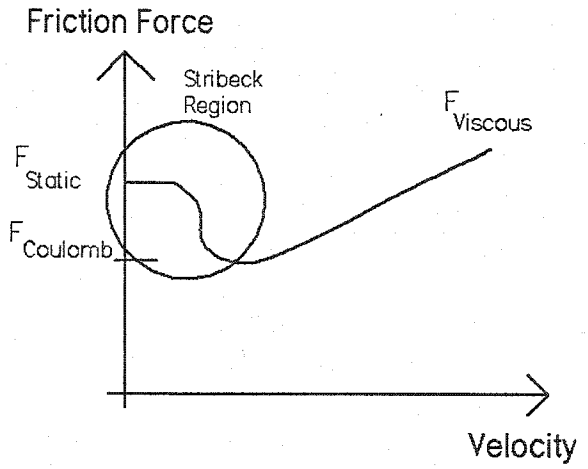

Figure 4.25 – Stribeck Region in the Friction-Velocity Curve

B. Static Friction and Break-Away Force

Static friction, or stiction, is friction when sticking (*Figure 4.25*). The force required to overcome static friction is called the break-away force, and seems to vary with the time spent at zero velocity and with the force application rate.

C. Frictional memory

Frictional memory is the lag observed between the changes in velocity or normal loads and the corresponding change in friction force.

D. Presliding Displacement

Presliding Displacement is the displacement if rolling or sliding contact occurs prior to true sliding, and arises due to elastic and/or plastic deformation; this is often referred to as a spring-like displacement before sliding.

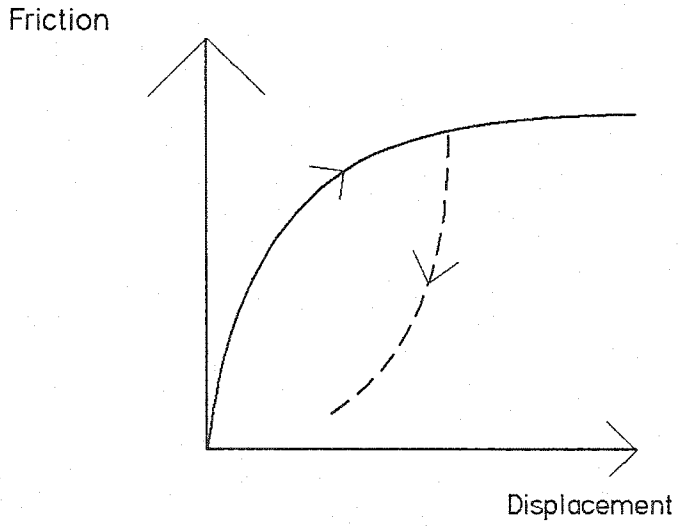

Figure 4.26 – Pre-Sliding Displacement

Table 4.9 aims to give a qualitative evaluation of those phenomenon and their consequences. This work is mainly concerned with the stick-slip transitions where the kick may originate. From *Table 2.1* it appears that of the four, the frictional memory phenomenon is not needed since our model does not include mechanical compliance, wand may significantly simplify the model needed, as well as the number of parameters studied.

Dynamic Friction Phenomenon	Predicted/Observed Behavior
Stribeck Curve	Needed to correctly predict initial conditions and system parameters
Rising Static Friction	Needed to correctly predict the interaction of velocity with the presence and amplitude of stick-slip
Frictionnal Memory	Needed to correctly predict the interaction of stiffness (mechanical or feedback) with the interaction of stick-slip
Presliding Displacement	Needed to correctly predict motion during stick

Table 4.9 – Observable Consequences of Dynamic Friction Phenomena [28]

4.3.4.2 ADAMS Friction Model

ADAMS is providing a complex friction model available for frictional forces on translational, revolute, cylindrical, hook, universal and spherical joints. It is available to the user through the dialog box shown in *Figure 4.27*.

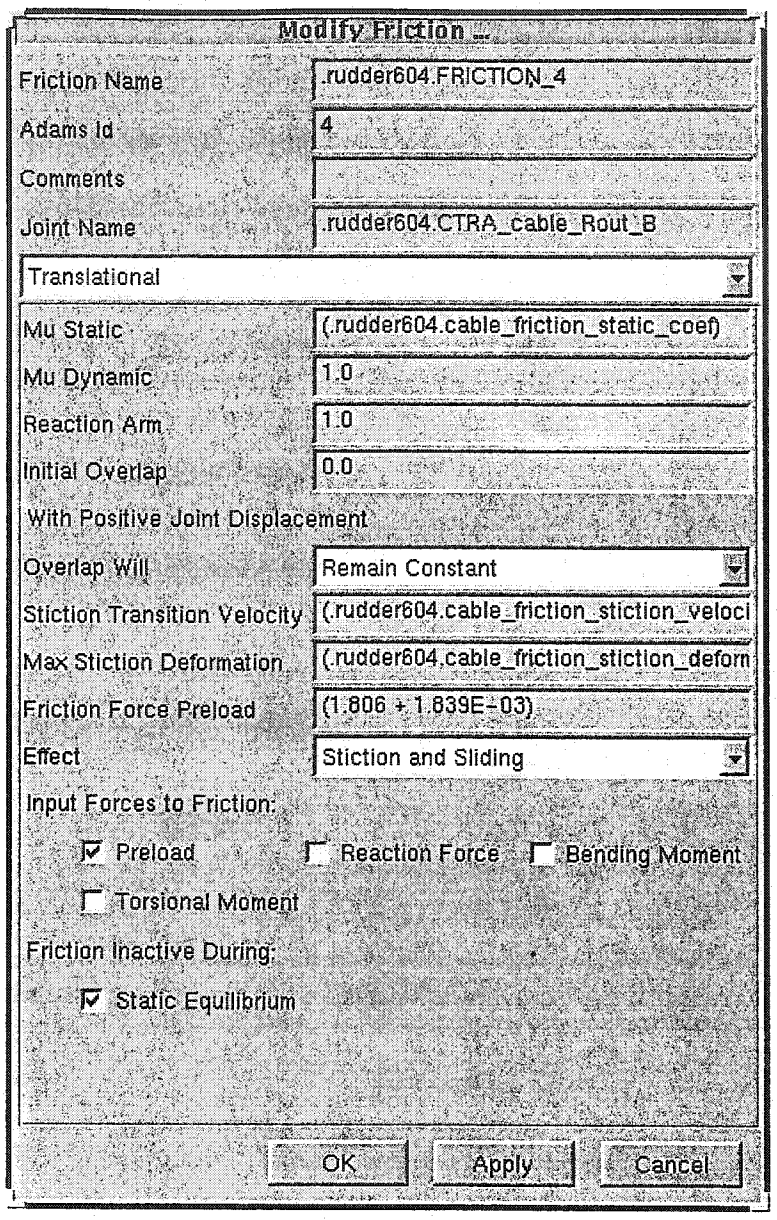

Figure 4.27 – Friction Dialog Box

The following four parameters are of interest for the friction model [26]:

- **Stiction Transition Velocity**: Defines the absolute velocity threshold for the transition from dynamic friction to static friction. If the absolute relative velocity of the joint marker is below the stiction transition velocity, then stiction acts to make the joint stick.
- **Max Stiction Displacement**: defines the maximum displacement that can occur in a joint once the frictional force in the joint enters the stiction regime. The slight deformation allows the ADAMS/*solver* to easily impose the coulomb condition for stiction. It corresponds to the pres-sliding displacement.
- **Mu Dynamic:** Defines the coefficient of dynamic friction
- **Mu Static:** Defines the coefficient of static friction

These values are used to continuously determine the friction regime and magnitude during simulation time. Three friction regimes are permissible in ADAMS:

- **Dynamic Friction:** a joint is in dynamic friction if its joint velocity magnitude exceeds 1.5 times the stiction transition velocity. The dynamic friction coefficient is used in the computation of the frictional forces.
- **Transition between Dynamic and Static Friction:** if the joint velocity is between 1 and 1.5 times the stiction transition velocity, the joint velocity is considered to be transitioning between static and dynamic friction. A STEP function (see Appendix B) transitions the coefficient of friction between the dynamic and static coefficients of friction.

- **Static Friction:** A joint is in static friction when the joint velocity magnitude falls below the stiction transition velocity. The effective coefficient of friction is computed using the joint creep, joint velocity, and static coefficient of friction.

Therefore, joint velocity determines the instantaneous friction regime for a joint. *Figure 4.28* is a block diagram of the friction regime available in the ADAMS/*solver*.

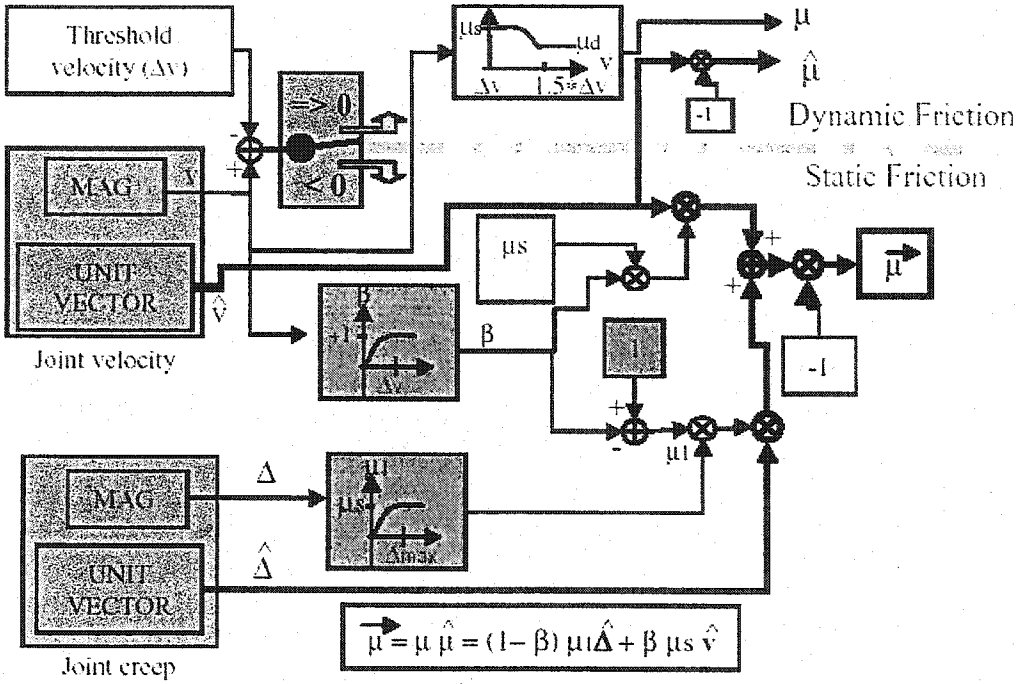

Figure 4.28 –Block Diagram of Friction Regime [26]

Proof that this model exhibits stick-slip behavior is provided in *Section 4.4.2*, while a detailed study of this model and parameters is available in *Section 5.3.2.1*.

4.4 Results Analysis and Model Validation

As with all the primary flight control systems on a new aircraft, the rudder control of concern here was submitted to a number of ground tests aimed at characterizing the cinematic, static, and dynamic behavior of the system.

Different simulation runs have been performed with the model, reproducing the conditions of the experimental tests in order to validate the characteristics of the model.

This model also incorporates original features that are not necessary for the normal performance assessment use, but that were crucial in the progress of this project; for example, the clearance model, and improved friction. This section will therefore aim at developing a justification for the different choices that were made to model this phenomenon.

4.4.1 Clearance Model Validation

Before incorporating the clearance joint within the model, it was necessary to evaluate the behavior of the chosen model with a simpler system. The model in *Figure 4.29* was found suitable for that purpose, and incorporates three rods: two verticals rods connected to the ground through revolute joints, and a middle rod to connect them. The attachment to the right rod was made with a clearance model as can seen in *Figure 4.29*.

A motion is driving the right rod rotation; its rotation being the input angle, while the rotation of the left rod is considered the output angle.

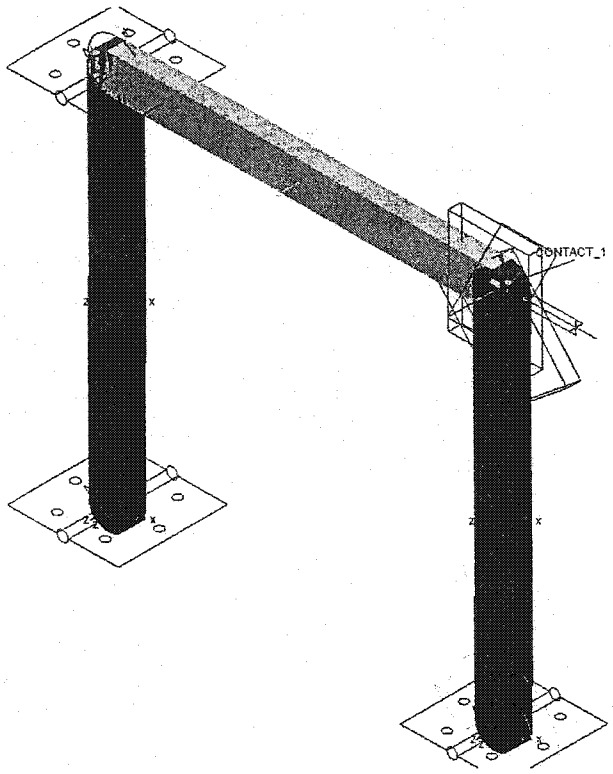

Figure 4.29 – Simple Mechanism for Evaluating Clearance Model

The graph in *Figure 4.30* shows a backlash like shape: the output angle remains at zero until the contact occurs at 0.8 degrees when the rest of the mechanism starts moving. When inversing the motion direction, the output angle will then keep on moving for an equivalent angle due to the forces of inertia.

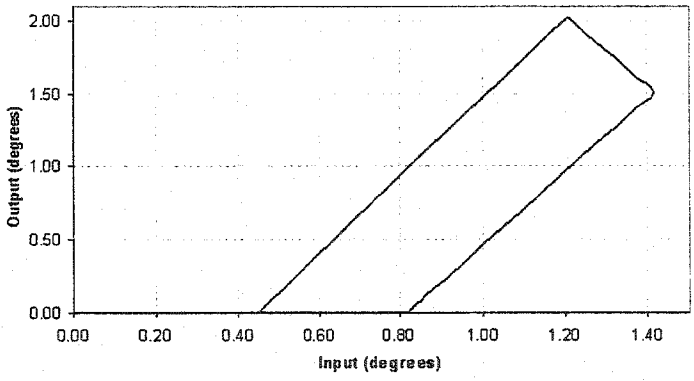

Figure 4.30 – Clearance Simulation Result

4.4.2 Friction Model

Section 4.3.4 discussed the reason that led to the choice of the ADAMS built-in friction model for the purposes of this project. Still, it was estimated necessary in order to fully understand this model, to evaluate the model by using a simpler mechanism, and to demonstrate that it experienced the expected stick-slip behavior.

This was accomplished with the mechanism in *Figure 4.31*, where a mere 1 N weight mass is pulled by a 1 N/m stiffness spring.

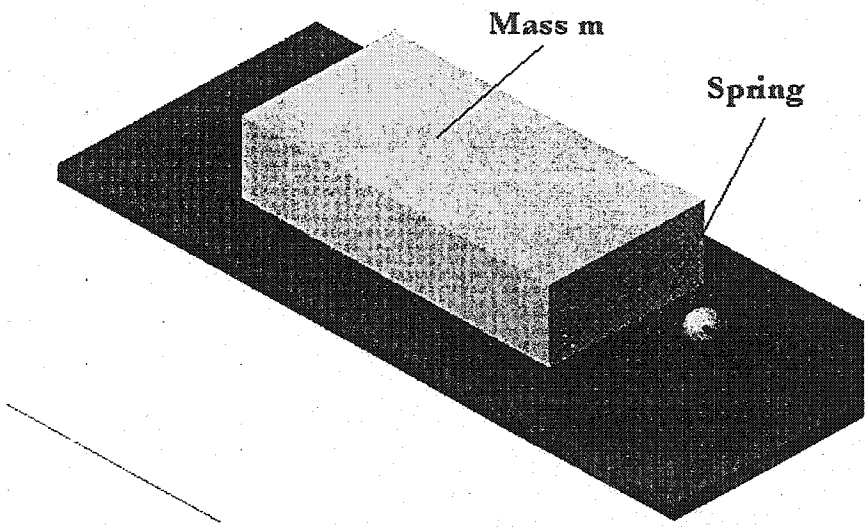

Figure 4.31 – Simple Mechanism for Friction Evaluation

The friction is set at a static friction force of 1 N, while the dynamic friction is 0.9 N. The stiction transition velocity is 0.1 mm/s, while the maximum stiction deformation is 0.01 mm.

For the second experiment, the static friction was increased to 1.5N, while the dynamic friction force is 1N (in order to magnify the effect). An external force is applied to the mass that is gradually increased up to 1.4N and then released. One can observe the

effect of pre-sliding displacement in *Figure 4.32*: a characteristic hysteresis shape of the friction force with displacement, sometimes referred as *Friction Memory*, and recalling experimental results discussed in *Figure 4.26*.

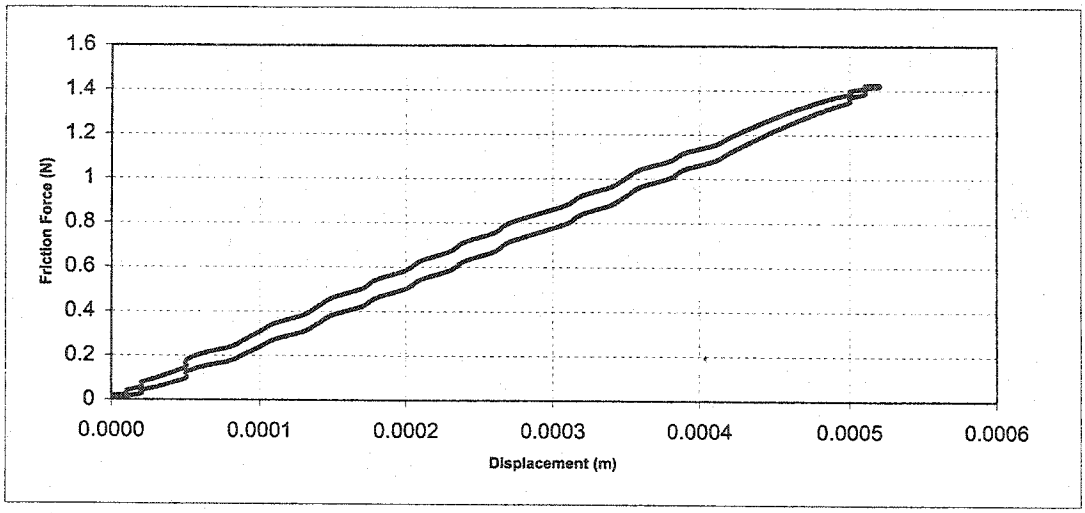

Figure 4.32 – Pre-sliding Displacement

Of crucial importance to this work, demonstrated in *Figure 4.33*, where the end of the spring is pulled out at a constant velocity, with the mass originally at rest. Initially, the friction force counteracts the spring force, and there is only a small displacement. When the friction force reaches the breakaway force (in this case 1N), the mass starts to slide, and the friction decreases rapidly due to the Stribeck effect. The spring counteracts, and the spring force decreases. The mass slows down, and the friction force increases because of the Stribeck effect and finally the motion stops. The phenomenon then repeats itself.

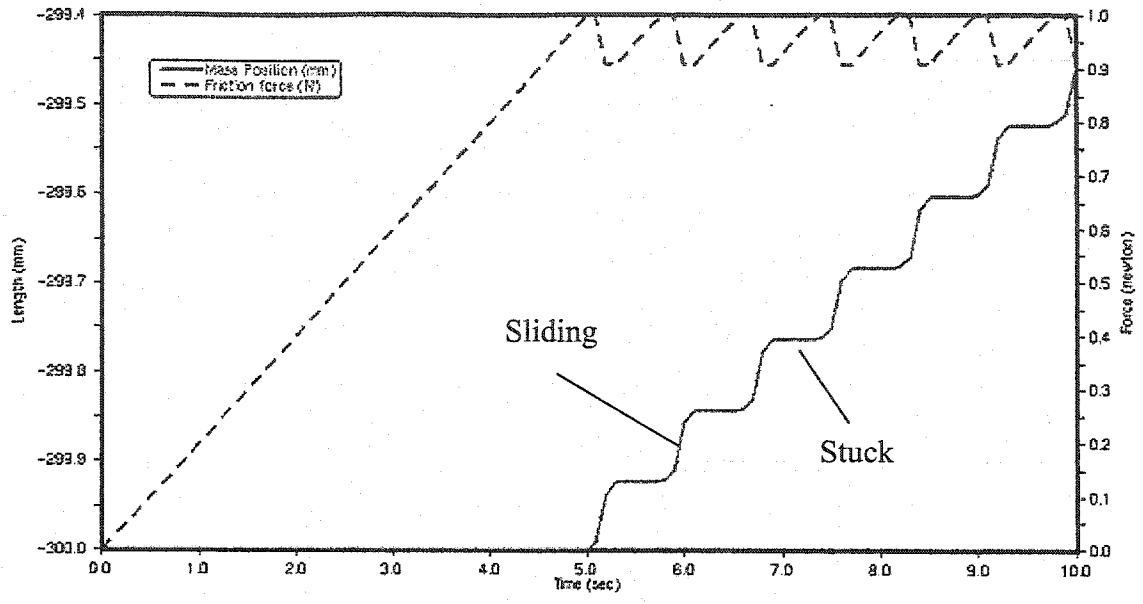

Figure 4.33 – Simulation of Stick-Slip Behavior

It is very important that our model of friction can exhibit this type of behavior, since it is believed that it might be at the source of the yaw kick phenomena.

4.4.3 PCU Model -Validation

Concordia University had developed a detailed PCU model that was validated [4], and whose characteristics were used to fill the PCU model C code template. Nevertheless, differences in the two models (*Section 4.3.2.2*) made necessary an assessment and comparison of their behaviors.

One of the disadvantages of the use of a user-defined subroutine in ADAMS is the difficulty of debugging: the subroutine states are not available from ADAMS/*postprocessor*, and each modification of the C code necessitates the compilation and linkage to the ADAMS *solver* code.

The PCU C code was therefore inserted into the MatrixX PCU model through a Systembuild User Code block, and compared to the MatrixX model (as can be seen in *Figure 4.34*).

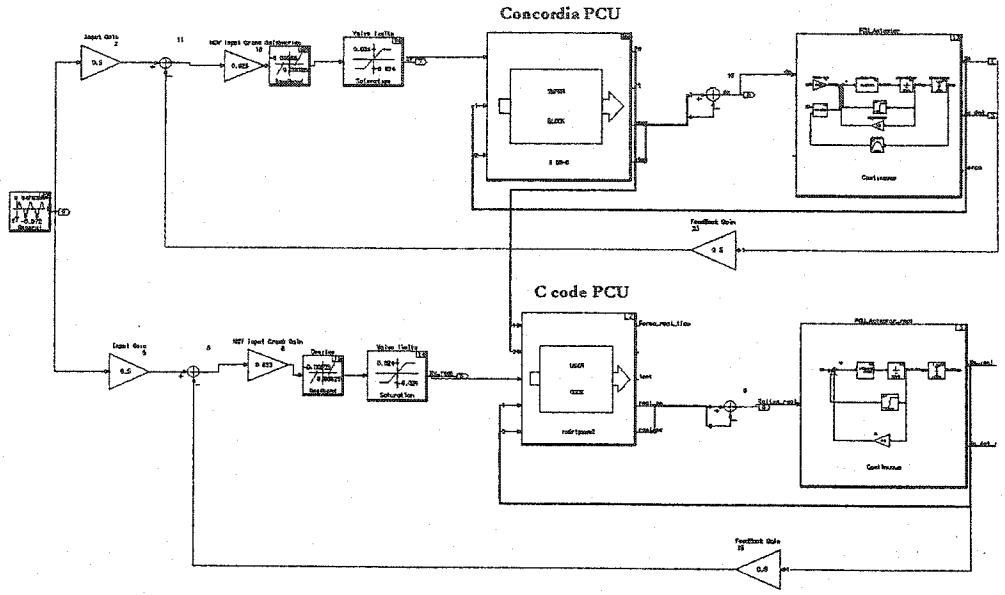

Figure 4.34 – PCU MatrixX Validation

Figure 4.35 presents a trace of the actuator position for a given input command showing no differences in between the two models.

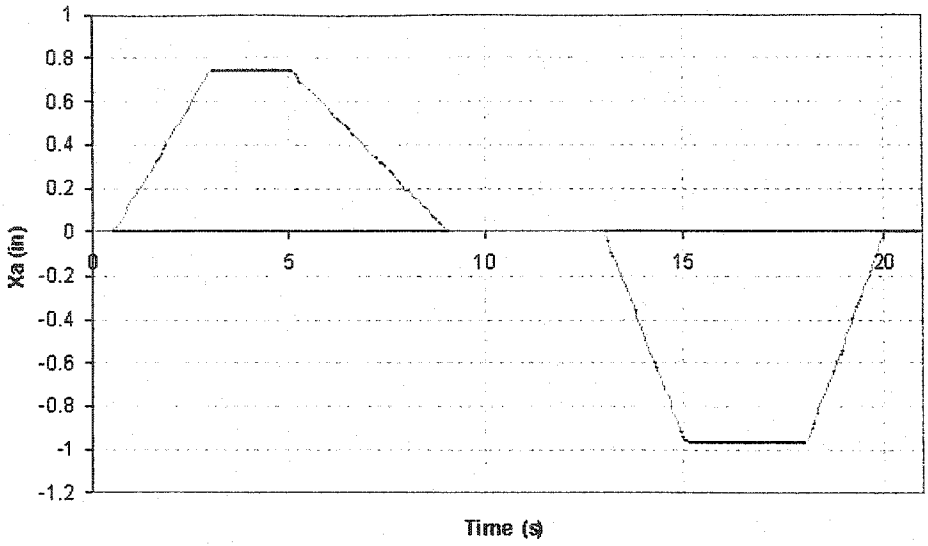

Figure 4.35 – Actuator Position Versus Time

Figure 4.36 illustrates the PCU actuator forces for a full rudder sweep at take off (hinge moment on rudder corresponding to a typical take-off condition).

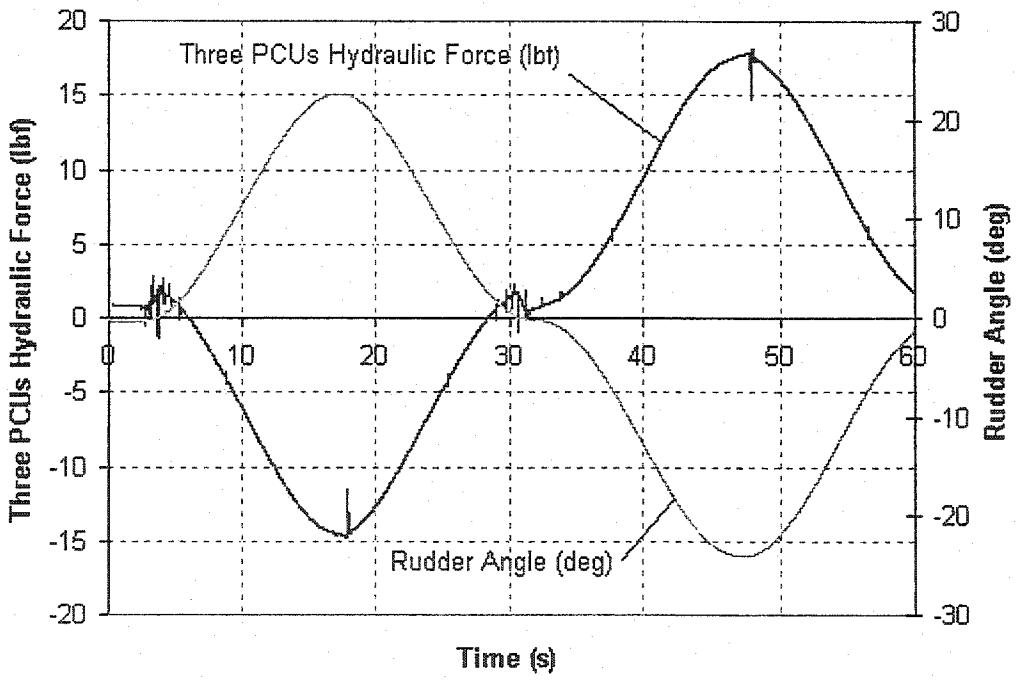

Figure 4.36 – PCU Force for Rudder Sweep

4.4.4 Control Kinematic

Rudder control cinematic is usually assessed in the form of a rudder full sweep while recording rudder rotation versus pedal displacement. The rudder displacement for a given pedal displacement is linear, and the actual gradient was found to be around 6.3 deg/in. This number should be compared to the results of the test on the model in *Figure 4.37*. The gradient on this diagram is found to be 6.8 deg/s. This represents an error of 7.3% between the model and the experiment. As stated in *Section 4.1.1*, the model kinematic was in the original model, but was nevertheless checked prior to any further development. This discrepancy could be the result of an error in a part's dimension, or in the positioning of its attachment to the aircraft structure in the aircraft reference frame. After a careful examination of those dimensions, nothing was found, but:

- It is considered within the tolerances of the VPFCS requirements.
- For the purpose of this work, we are interested in small displacements of the rudder around the neutral position in a region situated in between –1 and +1 degree of rudder displacement. In this region, the error in the rudder position might represent a maximum error of 0.08 deg. Though not completely negligible, this should not affect the qualitative behavior of the system.

Finally, further investigation with the department in charge of the measures has proven that the measure of the pedal displacement in the cockpit is indeed quite difficult and should be taken with caution: the error could therefore be a consequence of measurement and calibration problems.

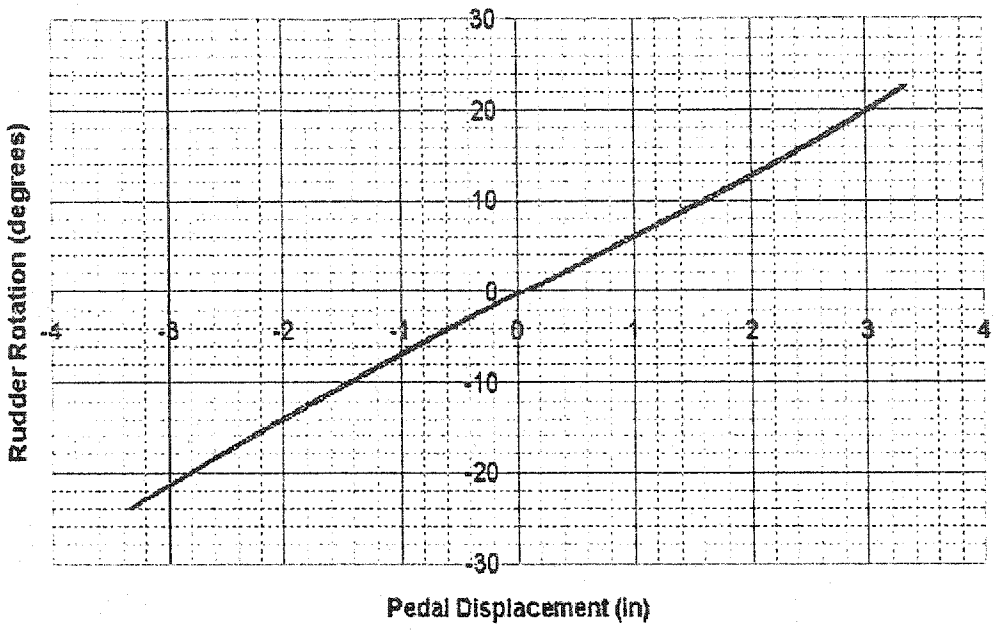

Figure 4.37 – Rudder Control Sweep Simulation (total time of 60 seconds)

4.4.5 Static Control Sweeps

The rudder pedal position sweep input commands (*Section 4.2.4*) are used to generate the results of the static sweep simulation runs. This consists in a full pedal sweep at a time large enough so that dynamic effect can be neglected, therefore recording the static characteristics of the system. Meanwhile, the force at the pedal is recorded versus the pedal position. The main characteristics researched during such a test are summarized in *Figure 4.38*. They include the force gradient of course, but also the break out force, accounting for the capacity of the system to return to the neutral position, as well as the friction force.

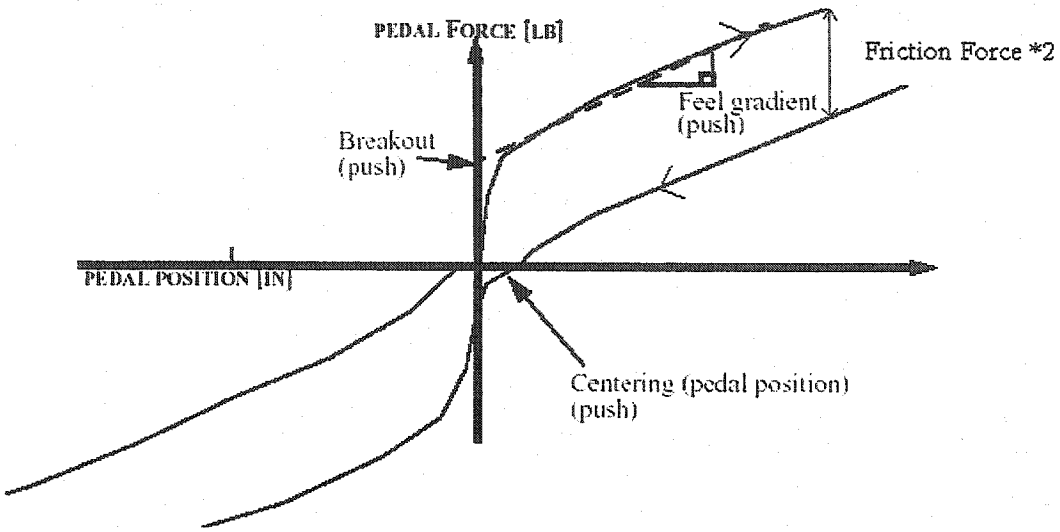

Figure 4.38 – Rudder Static Sweep Characteristics

Table 4.10 summarizes the results of the simulation (see *Figure 4.39*) and compares them to the experimental data. Error at the breakout force could be explained by small discrepancies between the two feel units' cam profiles: a very small error in their alignment or in their curve can have a very large impact on those values. This might also provide a good explanation for gradient error. Still, these values are within 10 % and were found to be within the limits VPFCS standards. Here again, measurement errors and calibration issues might also contribute greatly in the above-mentioned discrepancies. One might also notice in *Figure 4.39*, the characteristic shape of the curve in the vicinity of the neutral position, which conforms to *Figure 4.38*: the cam on the feel unit ensures an higher force gradient in this area, ensuring centering of the control.

Characteristic		Error (%)
Break out force (lbs)		12.50
Push	Gradient (lbs/in)	7.65
	Force @ 3 inches pedal displacement (lbs)	3.04
Pull	Gradient (lbs/in)	9.91
	Force @ 3 inches pedal displacement (lbs)	5.59

Table 4.10 – Static Control Sweep Characteristics

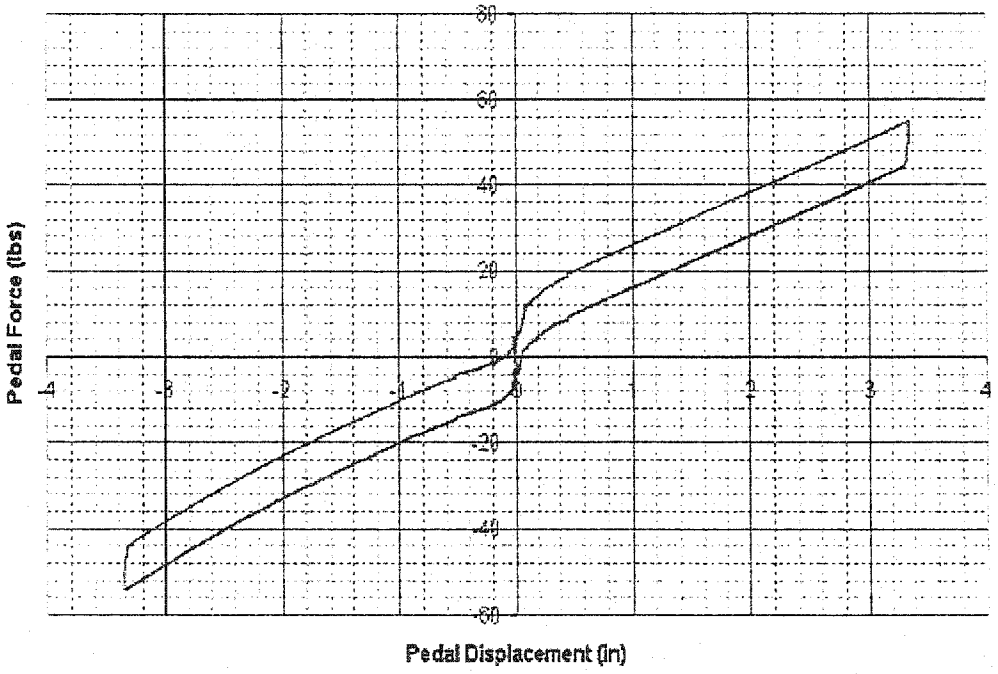

Figure 4.39 - Rudder Static Sweep Simulation (total time of 60 seconds)

4.4.6 Pedal Release Test (Dynamic)

The pedal release command (*Section 4.2.4.1*) is used to generate the simulation of pedal release at 1/3 (*Figure 4.40*) and 2/3 deflection (*Figure 4.41*). This test consists in bringing the rudder surface to one third of its maximum deflection (and then two thirds

respectively), and then to suddenly release the force on the pedal. It is the most common way to assess the dynamic response of the system.

The results are summarized in the *Table 4.11*:

Type		Settle Time (s)	Overshoot (rudder, degrees)
1/3 Pedal Release	Simulation	0.344	0
	Test	0.3	0
2/3 Pedal Release	Simulation	0.4	0
	Test	0.35	0

Table 4.11 - Dynamic Test and Correlation

Here again, the error between experimentation and simulation is reasonable: the general behavior is the same, with globally an over damped response. The very short settle time was very hard to measure considering its magnitude. It should be noted that during the test preformed by an operator, the release of the pedal force is probably not as sharp as might occur when the simulation is performed on ADAMS.

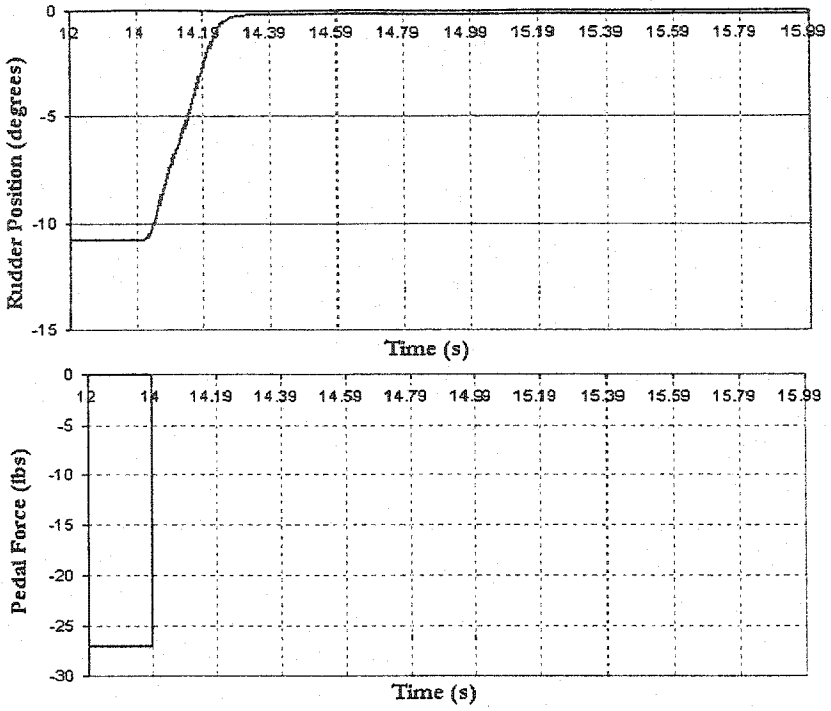

Figure 4.40 – 1/3 Pedal Release Simulation

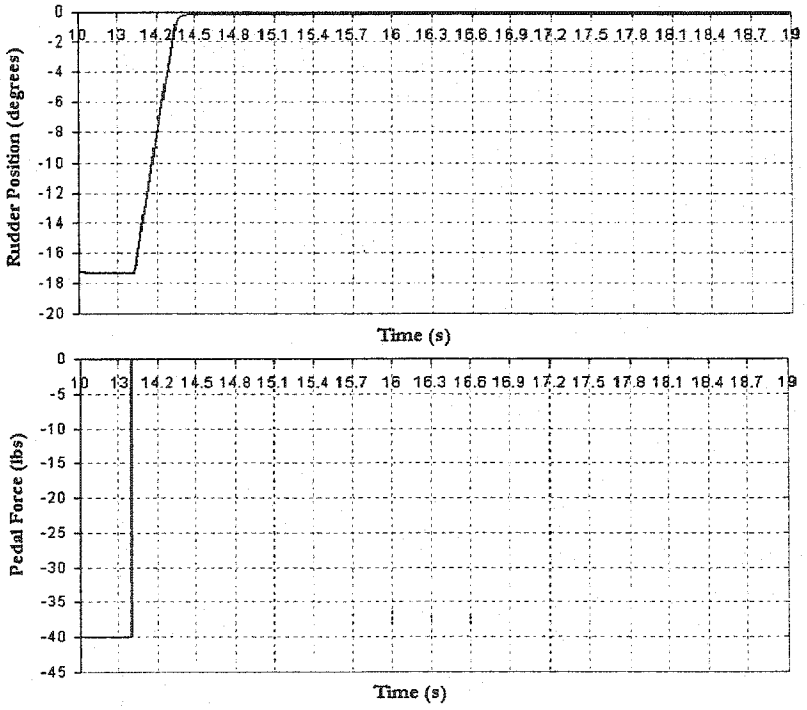

Figure 4.41 - 2/3 Pedal Release Simulation

4.5 Conclusion

A brief study in *Section 3* of the rudder control system exposed its complexity: its modeling was a challenge and proved to be long-term work. *Table 4.12* that list the different parts and joints of the model illustrates the complexity.

Estimated DOF	21
Moving Parts	72
Cylindrical Joints	13
Planar Joints	1
Revolute Joints	33
Spherical Joints	38
Translationnal Joints	10
Fixed Joints	1
Hook Joints	3
Motions	4
Coupler	1
Gears	4

Table 4.12 – Model Characteristics

This section has covered a wide range of topics; first justifying the choice of the modeling platform, and then reviewing the most significant choices made to model the physic of the system. The results were summarized in *Section 4.5*, along with the discussions of the non-linearity modeling in *Section 4.3* that demonstrates fully its fidelity to the system's behavior and physic. This was the test that had to be completed in order to move ahead to the next step of the project: using it to study how this non-linearity might work together to initiate a brisk and slight rudder deflection, leading to a yaw kick. This is discussed in *Section 5*.

5 Analysis and Results

One major difficulty of the investigation into the yaw kick phenomena is the lack of experimental data: only a little data is available about the conditions during which yaw kicks initiate.

We also saw in *Section 1.1.2*, that it is not a problem affecting a particular design, but rather a number of airplanes manufactured according to that design. The solution must therefore lie somewhere in the world of possibilities offered by all of the tolerances that can affect such a complex mechanism.

It is believed that clearance/backlash and stiction might in certain cases store energy in the rudder control system, later releasing it due to the aircraft's structure vibrations.

Both are known to exist on any physical system with joints, and both depend on a wide number of factors. Amongst these factors, many are not controlled since their effect is normally hidden under the normal performance of the system. For instance, lubrification of the bearings in the connection of push-pull rod affects the friction's characteristics. Clearance in the connection between the rods is maintained within a certain limit during their manufacture, but their arrangement in the chain going from the pedals to the rudder might vary from one aircraft to another.

Moreover, their correct measurement is beyond what physics can predict: no perfect model for friction yet exists, and what really does happen in a rod end when different clearances are added to allow a small freedom between the rods is beyond the scope of this work.

Even if it seems impossible to pretend to be able to perfectly assess all of these factors, it does seem reasonable to quantify them. The approach adopted in this work is to vary the values of these non-linearities within realistic/actual tolerances, thereby deriving a number of model sets. Each model set is then 'flown' and subjected to typical realistic corrective rudder pedal inputs in a 'straight-and-level' flight regime. The purpose is to investigate whether in some particular configurations of the system, a yaw kick might initiate. If simulation cannot clearly prove that they are the root factors for yaw kicks, it at least might allow one to conclude whether it is reasonable to consider them as a possible cause, and identify possible issues in design.

The ADAMS parameterization and design of experiment (DOE) functionalities authorize automatic design changes and simulation runs, therefore automating part of the investigation.

Still (*Section 5.1*), this procedure requires careful planning: the complexity of the model makes simulation runs very consuming in terms of computer power, and the true necessity of every single runs must be carefully evaluated, in order to maximize the information gained by each run.

Figure 5.1 illustrates the investigation process: the model has been fully completed and validated, and the next step will be an examination of the model behavior under the yaw kick conditions, as they were defined in *Section 1.1.1*.

The impact of the rod end joint clearance and of the stiction will indeed both be separately examined in an attempt to extract the most prominent factors. These two effects will then be combined, and the ADAMS DOE features will then be used to try to

maximize a possible kick of the rudder. If it appears, additional tests will then attempt to further isolate its root cause and/or eliminate irrelevant factors.

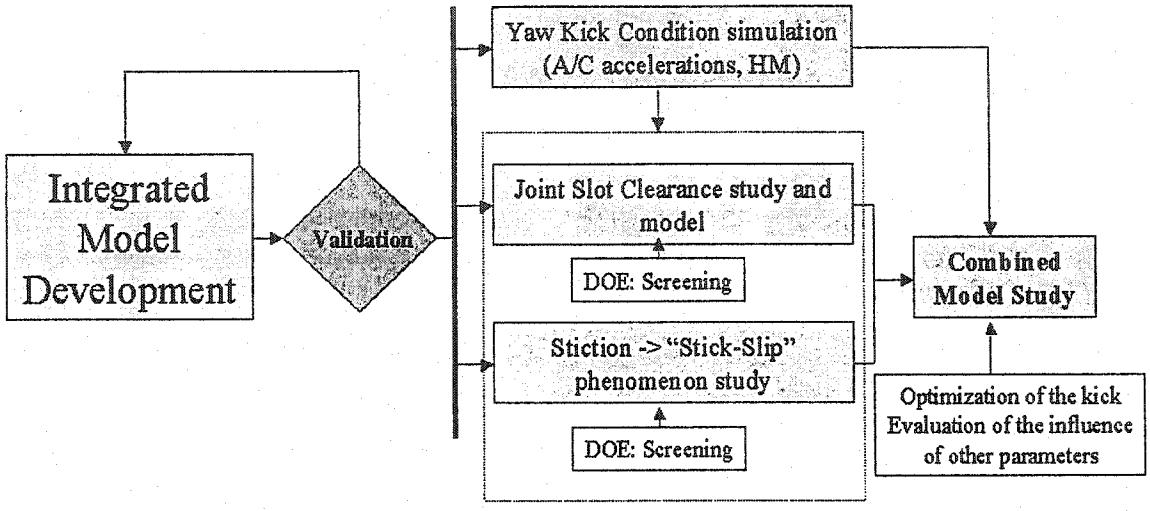

Figure 5.1 – Yaw Kick Investigation Scheme

5.1 Design of Experiment Techniques with ADAMS

Design of Experiment is a way to economically maximize information produced by experiments.

During this process, one or more process variables (or factors) are modified in order to observe the effect the changes have on one or more response variables. The design of experiments procedure plans for these changes so that the data obtained can be analyzed to yield valid and objective conclusions.

DOE begins with determining the objectives of an experiment and selecting the process factors for the study. An experimental design lays out of a detailed experimental plan in advance of doing the experiment. Well-chosen experimental designs maximize the amount of "information" that can be obtained for a given amount of experimental effort.

DOE can be used for different purposes; this work will make use of two of them:

- Screening factors: screening experiments are an efficient way, with a minimal number of runs, of determining the most important factors.
- Maximizing or minimizing a response: DOE can be used to find the set of factor corresponding to the maxima of the response.

Once one has chosen the factors and objective, the next step is the choice of the design matrix. The design matrix describes the different experiments and includes a column for each factor and a row for each run. The matrix entries are the level for each factor for each run.

During this work, we will make use of the so-called two level full factorial designs, which consist in setting all of the input factors at two levels. These levels are called `high' and `low' or `+1' and `-1' respectively, and are standing for maximum and minimal value of the factors.

If there are k factors, each at 2 levels, a full factorial design therefore requires 2^k runs. It is therefore recommended to keep this type of DOE for experiment with 5 factors or less [29]

Table 5.1 shows a 2^3 full fractional design matrix, with the run in standard order.

	Factor		
Run	1	2	3
1	-1	-1	-1
2	1	-1	-1
3	-1	1	-1
4	1	1	-1
5	-1	-1	1
6	1	-1	1
7	-1	1	1
8	1	1	1

Table 5.1 – Design Matrix for a 2^3 two-level, Full Factorial Design [29]

ADAMS/*view* version 10.1 limits DOE study to one response variable, with full fractional design The ADAMS software package normally includes ADAMS/*Insight*, a module specifically devoted to DOE, but which was unavailable, hence limiting the possibilities to full factorial design.

5.1.1 Model Preparation

ADAMS/*view* provides several parameterization methods. This work primarily makes use of the so-called design variable. These are a special type of variable that cannot be changed during simulation and allow for variation of any aspect of a modeling object. When one change the value of a design variable, all objects that refer to it automatically update to reflect the new value. Design variables also include a range for the specific value, allowing the user to restrict which variables may be changed.

5.2 Reproducing Yaw Kick Conditions in the System

Figure 5.1 features a block announcing the development of a yaw kick condition simulation. This work assumes that the actual yaw kick, the brisk yaw motion of the aircraft platform, is the response to a rudder input initiated in the rudder control system.

5.2.1 Flight Model Integration

The project's initial ambition was for co-simulation between the flight model in MatrixX (*Section 2.2*) and the ADAMS model of the rudder control system: the flight model of the aircraft dynamic, in MatrixX, would control the ADAMS model of the

rudder. *Figure 5.2,* illustrates this idea, highlighting the *feedback loop* connection this procedure would imply, and the variables exchanged by the two models.

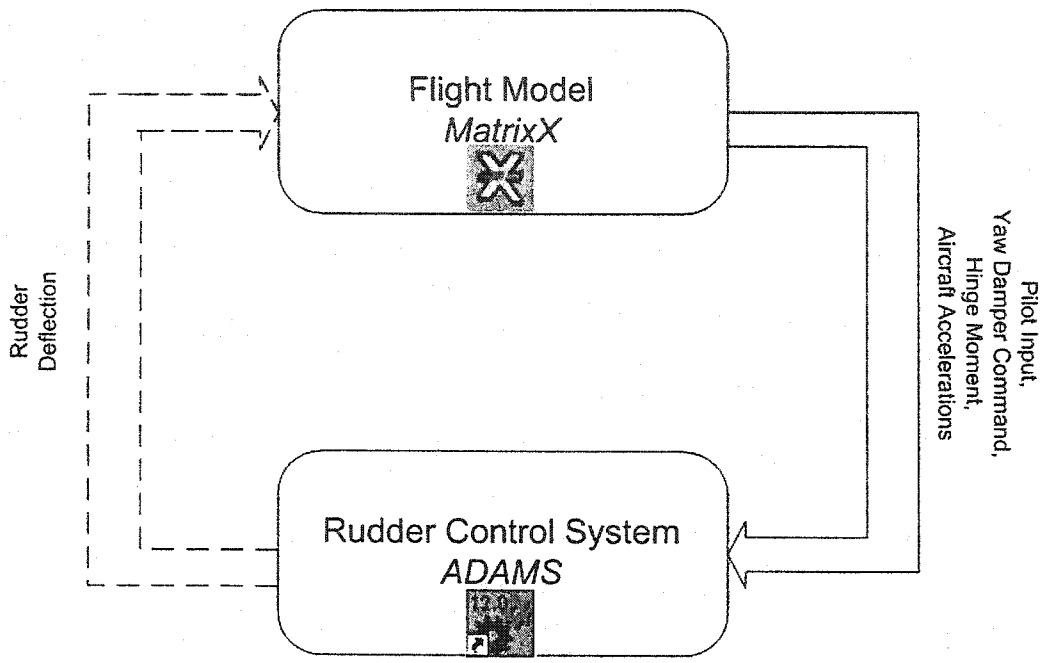

Figure 5.2 – Co-Simulation Procedure

Figure 5.3, details the connection in between the two models, illustrates the place of the rudder control system in the aircraft, and demonstrates the need for the aerodynamic moment and for the yaw damper command in order to correctly reproduce the system behavior and response. *Figure 5.3* also shows that those quantities are available from the flight model.

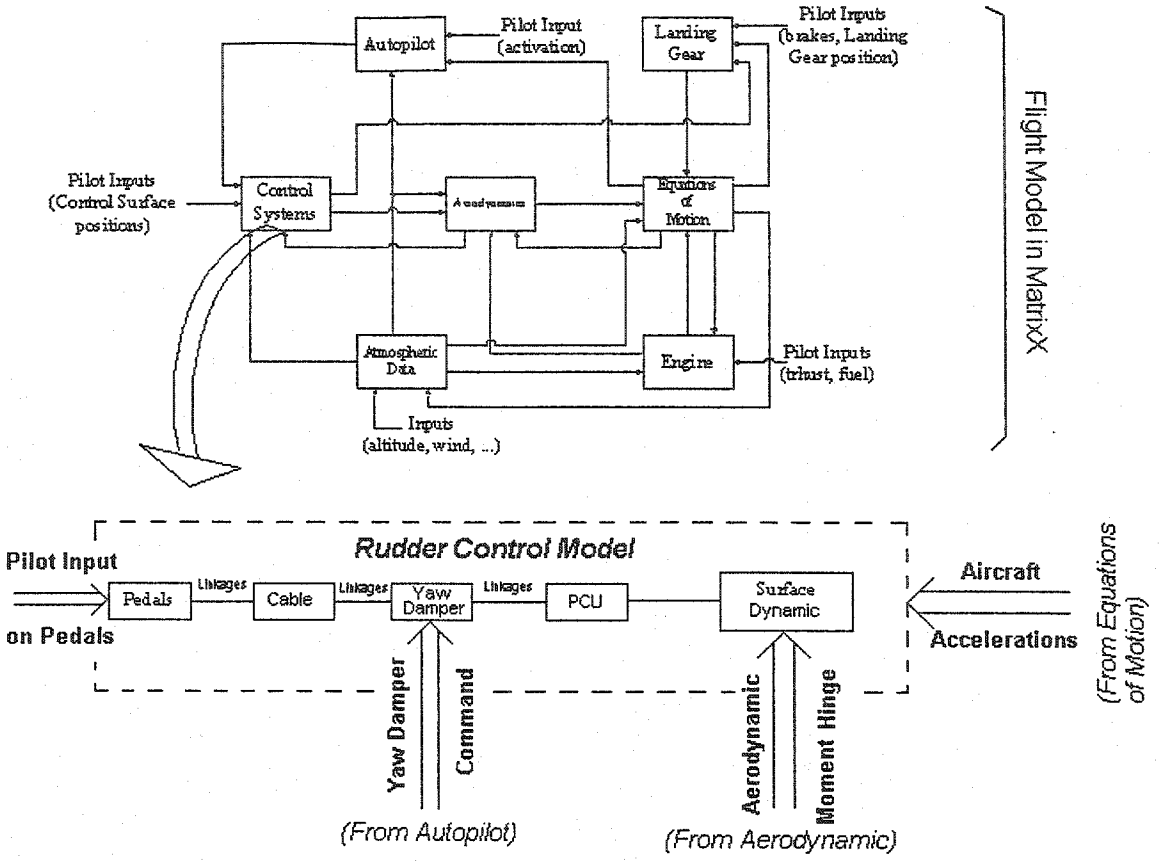

Figure 5.3 – Rudder Control System in the Flight Model

The benefits of this solution were examined and a few tests of the co-simulation procedure were performed. They exposed the difficulty of such a simulation (a detailed review of the co-simulation procedure, and of its difficulties and limitations can be found in *Section 4.3.2*): having the two models and solvers work together on such complicated models proved to be quite a challenge. Moreover, it might have limited the complexity of the model (*Section 4.3.2* i documents the fact Adams CONTACT statement are not well supported in co-simulation) when this work requires a complex and extensive model. Furthermore, the fact that it is the MatrixX/*Solver* which actually controls the simulation would have made the use of ADAMS automatic design change on the model impossible

(*Section 5.1*). Overall, difficulties of such a simulation appear to overweight the benefits it might have brought to this study. However, it might be worthwhile for future work, as discussed in *chapter 6.2*.

5.2.2 Flying the ADAMS Model

This project focuses on the trigger phase of the yaw kick phenomenon and therefore does not require a complete study of what happens *after* yaw kick ignition. Further research on the actual interaction between rudder control and the aircraft dynamic would be necessary for yaw oscillations investigations, and an exact determination of the aircraft's response under the kick ignition might therefore be left for future work. This, together with the reasons stated in *Section 5.2.1*, explains the choice of a "two steps process", for flying the rudder control model under yaw kick trigger condition. These two steps are:

- Fly the flight model subjected to typical realistic corrective rudder pedal inputs in 'straight-and-level flight regime' under the conditions favorable to the initiation of a yaw kick (as defined in *Section 1.1.2*). Simulate and record the aircraft kinematic and dynamic quantities and the yaw damper command, and export them in text files.
- Import these data in ADAMS (using the acceleration macro (*Section 4.2.5.8*) for kinematic and dynamic quantities, as a spline commanding the yaw damper actuator deflection for the yaw damper command see *Section 4.2.4*), and use them to "fly" the rudder control model (as seen in *Figure 5.1*)

Remembering *Figure 5.2*, one can realize that this to-steps process, is neglecting the feedback from the rudder control system model to flight model (see *Figure 5.4*).

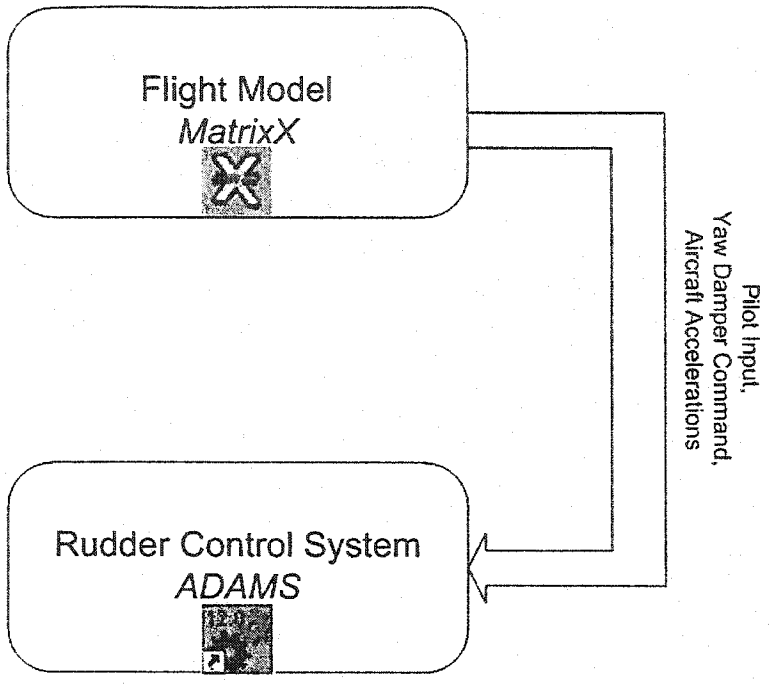

Figure 5.4 – Two-Steps Procedure

Remembering *Figure 5.3* one might also notices the aerodynamic hinge moment is not transmitted to the rudder control system model. A particular hinge moment curve (that is the aerodynamic moment on the rudder surface, in function of the rudder surface deflection) at estimated yaw kick conditions (275 knots and 15000 ft, see *Section 1.1.1*) was also generated from the flight model and imported into the rudder control model following the procedure defined in *4.2.5.7*. Even though this procedure can be considered enough during the motion of small amplitudes, and therefore satisfactory for the study of the yaw kick trigger which is the object of this work, this procedure neglects the interaction between rudder deflection and the aircraft dynamic, or put differently, it considers rudder deflection and sideslip angle to be equal.

5.2.3 Data for the Rudder Control System Model

A particular profile (the curve in *Figure 5.5*) was extracted from test data. This profile had to gather two characteristics:

- Present an initial motion of medium amplitude, in order to be compatible with the type of correction a pilot might perform during a normal flight, while loading energy into the mechanism.
- This initial step must be followed by a long period of time where the system is recorded "at rest": this is the time where we expect to find the configuration of the model where a yaw kick might initiate

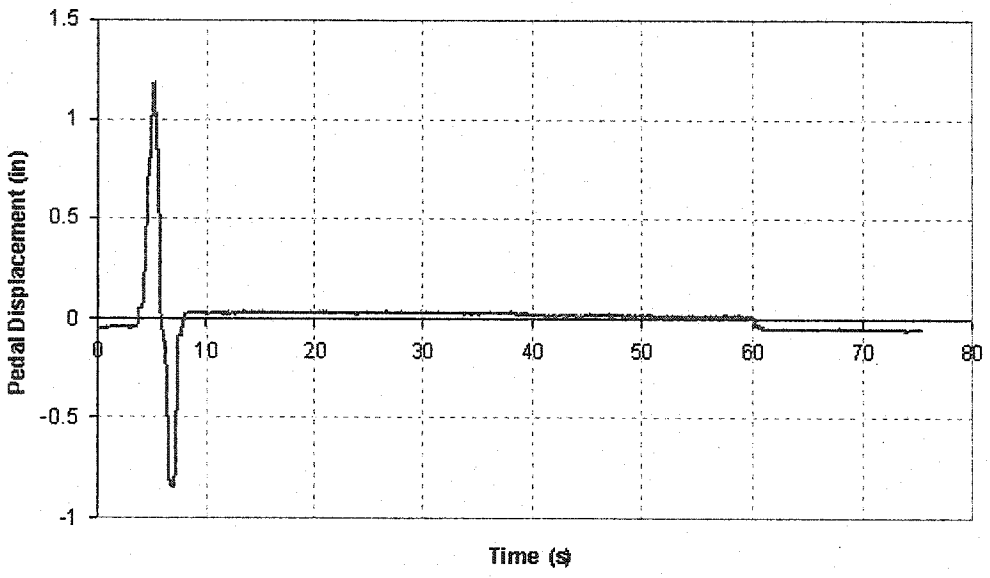

Figure 5.5 – Pedal Displacement Curve

This profile was imported into the flight model, and used to carry out a simulation of the aircraft response. While performing the simulation, the aircraft was submitted to a small amount of energy turbulence (*Section 2.2.3*). It is indeed believed that the kick might initiate from the brutal release of energy stored in the system. By slightly shaking

the aircraft platform, we aim at maximizing the chance of this release to occur. For the same reason, the yaw damper is left active, and its deflection is also exported to the ADAMS model (*Figure 5.7*). Those hypotheses will be justified later on in this document (*Section 5.3.3.2*).

Figure 5.6 is shows the lateral quantities (aircraft lateral acceleration and yaw rate) in response to this particular pedal displacement profile.

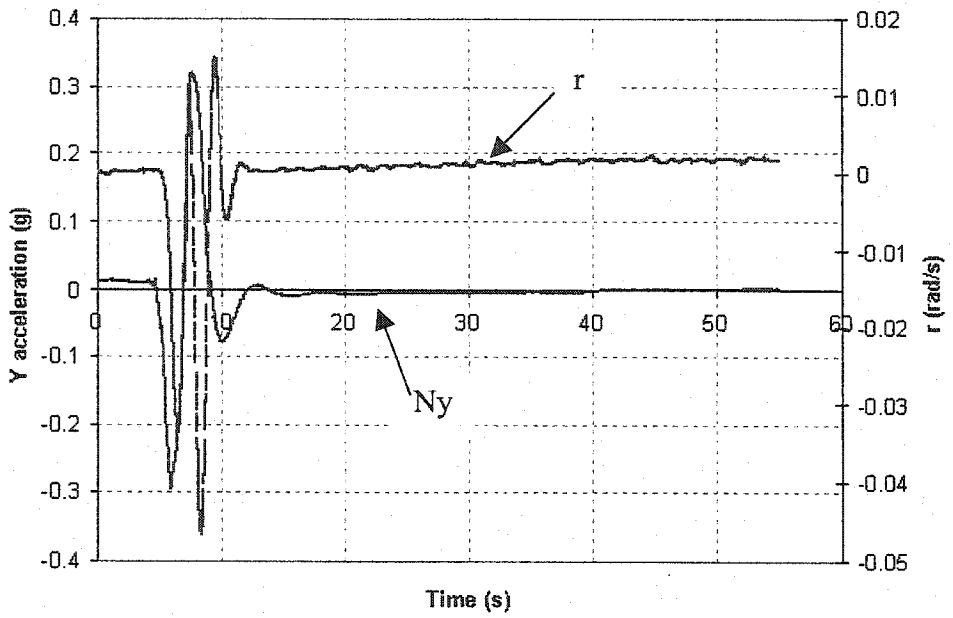

Figure 5.6 – Aircraft Lateral Quantities in Response to the Pedal Displacement

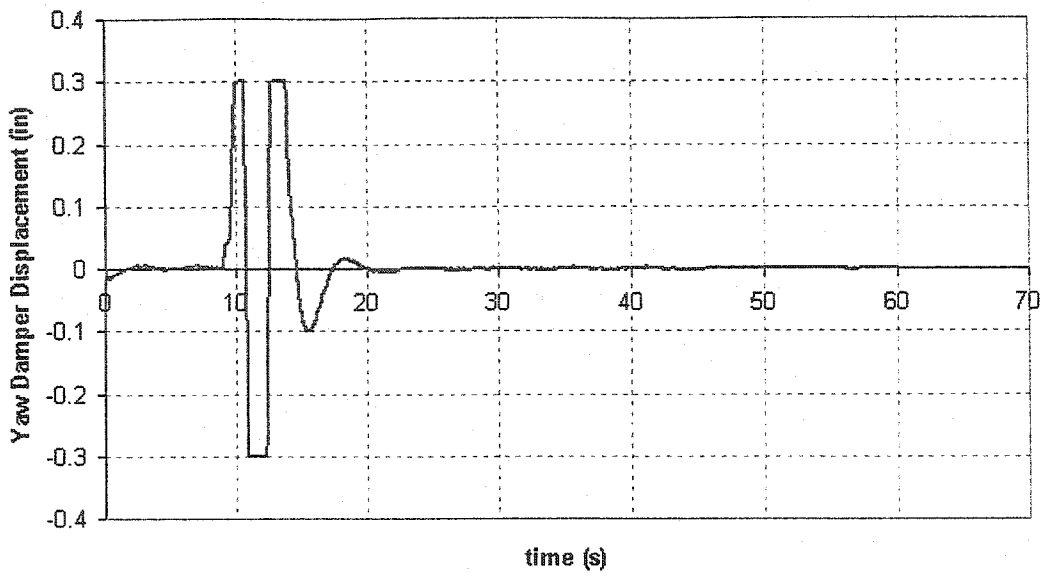

Figure 5.7 – Yaw Damper Deflection

5.3 Model Study

5.3.1 Joint Clearance Study

The first tests were carried out with the clearance model as it is specified in *Section 4.3.3* (friction model of static/dynamic friction is inactive).

The model is not really expected to experience a kick in these conditions, but this first step was judged necessary in order to evaluate the relative importance of the different clearance on the rudder motion and to notice any possible cross effects.

The objective is to study the difference between rudder motion without clearance, and rudder motion with clearance, and is only examined after the initial pedal motion occurs.

Of the four different clearances stated in *Section 4.3.3.3*, three were retained for this analysis (*Figure 5.8* locates them in the mechanism): the force was applied to the left

pedal, the right pedal therefore only reacts to the system's motion. As a result, the backlash at this point was not studied but left at maximum. A two level full fractional design was applied to the other three values of the clearance; factor 1, accounting for the clearance in the complete summing mechanism (from *Section 4.3.3.3* one can remember that it is the one that was given most weight).

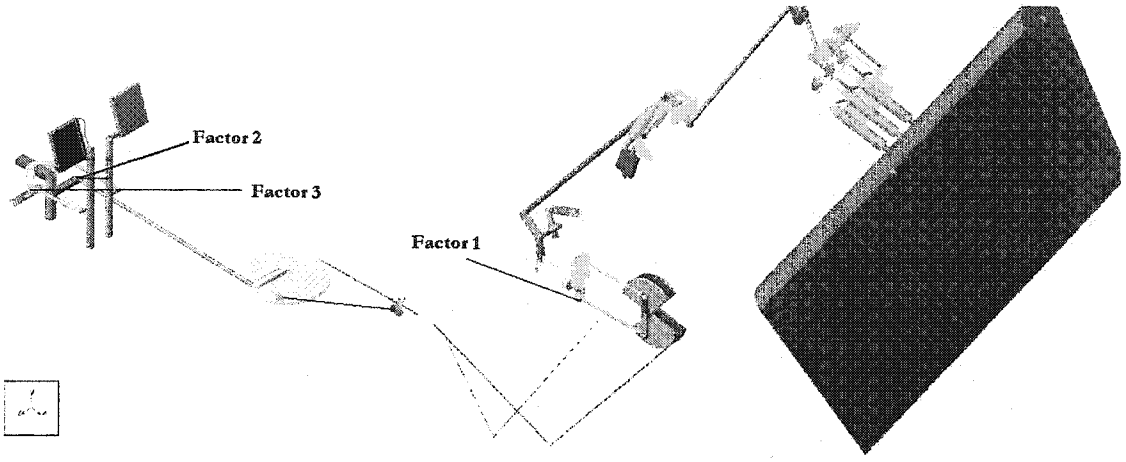

Figure 5.8 – Factor for the Clearance Analysis

As expected, none of the runs produced an actual kick, but simply experienced a small discrepancy with the motion without clearance that stayed at a fix value after the pedal motion.

Figure 5.9 displays on the same graph the maximum value of the objective and the three factors as a function of the iteration.

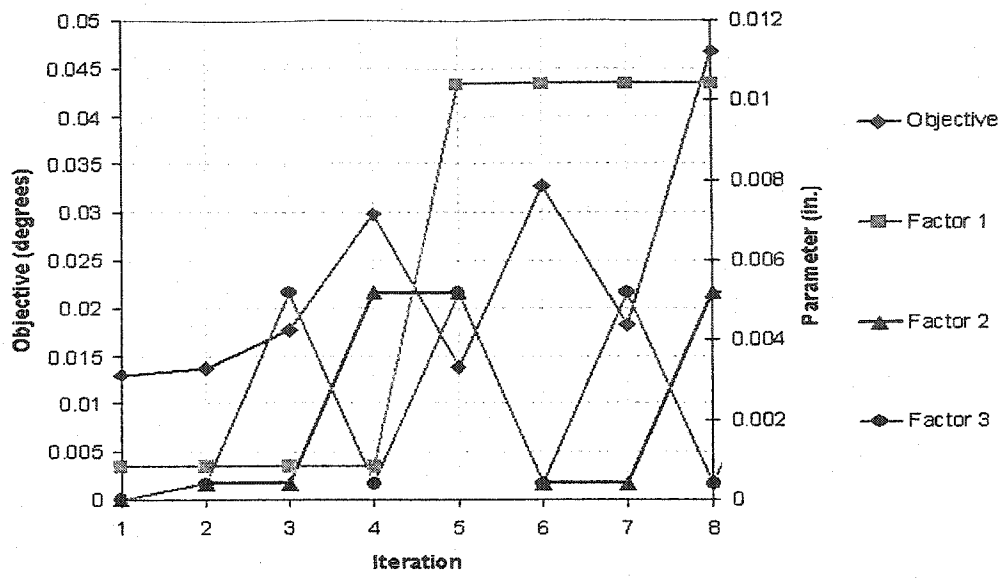

Figure 5.9 – Clearance Analysis Result

As expected, the maximum value of the objective corresponds to the maximum clearance, and suggests that this the factor has the most important impact on the objective.

Of the three, the second factor is found to be less important, and will therefore stay fixed at its maximum value for later experiments.

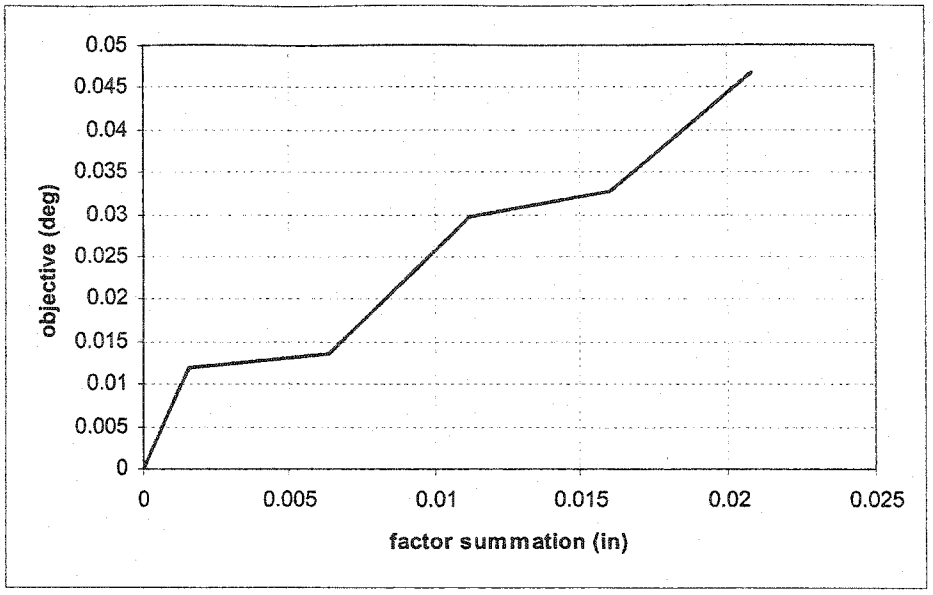

Figure 5.10 – Backlash Model Convergence

Another piece of information that may be extracted from *Figure 5.9* is the fact that the objective decreases uneventfully with decreasing tolerance (sum of all the factors). This is observable in *Figure 5.10*, built using data from this experiment: the objective absolute value is decreasing with the sum of all the tolerances. This therefore justifies the increased solver tolerance discussed in *Section 4.3.3.2* that was necessary to decrease simulation time.

5.3.2 Stiction Study

5.3.2.1 Simple Model

Following the scheme developed in *Figure 5.1*, the stiction phenomena has been studied separately. As seen in *Section 4.3.4*, stiction and the Stribeck effect were found to be the main factors responsible for stick-slip motion, and the friction model adopted was built around 4 parameters. Since the experiment on the model was found to be consuming

a lot of computer time, a preliminary study was performed with the simple mass-spring model, as displayed in *Figure 4.31* (*Section 4.4.2*). This simple experiment intends to assess the effect of these parameters on the intensity of the stick-slip behavior, and to possibly eliminate unimportant factors in later studies.

[28] provides us with a reasonable range for the value of those four parameters: with a static friction of 1.1 to 1.5 times higher than the dynamic friction, a pre-sliding displacement between 1 and 5 micrometers (2e-4 to 4e-5 inches) and a very large range for the stiction transition velocity, from 0.01 to 0.00001 m/s (0.4 to 0.0004 inches) is used.

This time, the objective was to investigate the mass average kinetic energy. This was found to give a very good separation of the different result, and of the intensity of the energy release when the slip occurs.

The results of the DOE can be better explained in the format of a table, as seen in *Table 5.2*.

Trial	Maximum of Kinetic Energy (newton-mm)	Displacement (m)	Static Friction Coefficient	Stiction Transition Velocity (m/s)
1	0.00013928	0.0000394	1.1	0.0004
2	5.4362E-06	0.0000394	1.1	0.4
3	0.00001	0.0000394	1.5	0.0004
4	0.0014256	0.0000394	1.5	0.4
5	0.0001386	0.0002	1.1	0.0004
6	0.000030187	0.0002	1.1	0.4
7	0.00001	0.0002	1.5	0.0004
8	**0.0014247**	**0.0002**	**1.5**	**0.4**

Table 5.2 – Stiction Study on Simple Model, Results

From this study, the main impacting parameter has logically been identified as static friction; the higher the static friction, the bigger the kicks (as can be seen in *Figure*

5.11). The transition velocity also appears to have a positive impact on the kick intensity, and it will be kept at its maximum value of 0.4 in/s for the rest of the analysis. Finally the value of the initial displacement is of a relatively small and negative importance, and will therefore stay fixed at 0.0002 in for the rest of the analysis.

Fixing these two values allows us to make the stick-slip behavior a function of a single parameter, while ensuring that the intensity of the kicks will stay maximal and thereby prepare the field for further analysis.

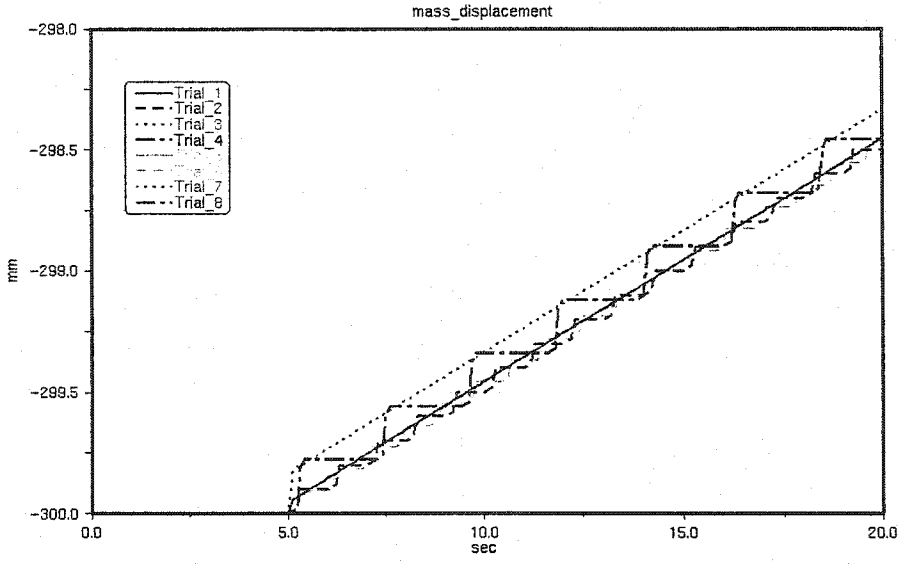

Figure 5.11 - Stiction Study on Simple Model, Curves

5.3.2.2 Rudder Control Model Study

Returning to the complete model, the next analysis will study how interaction between stiction effects in the model might affect the stick-slip behavior.

The flag for the clearance model was inactive, whereas this time, the friction model, as specified in *Section 4.4.2* is activated. This analysis is not performed with the conditions as defined in *Section 5.2*: in order to decrease simulation time, the model is

submitted to a constant rate sweep (using the simulation driver as defined in *Section 4.2.4.1*), reproducing the experiment as it was performed in *Section 5.3.2.1* but this time on the complete model. The simulations lasts a short time, in order to stay the neutral position of the system, which is the operating point of interest for this work. The value of the motion rate is to chosen to be of a magnitude that corresponds to the Root Mean Square of the pedal displacement after the initial motion (basically after 10 seconds, as seen in *Figure 5.5*). This attempts to recreate sufficiently similar conditions (with reference to the conditions created by the pedal displacement input of *Section 5.2.3*) while eliminating the need of long simulation. From the experiment in *Section 5.3.2.1* three factors were retained: those are the static friction coefficients for added friction (factor 1), cable friction (factor 2), and valve friction (factor 3).

The objective of this experiment is to find the maximum kinetic energy of the rudder. *Table 5.3* shows the objective versus the factor for the different iteration. It does not show any cross-effect between the three factors, and the biggest energy is logically gained when the static coefficients are maximal.

Trial	Objective (lb-in)	Factor 1	Factor 2	Factor 3
1	0.0155	1.1	1.1	1.1
2	0.0162	1.1	1.1	1.4
3	0.0168	1.1	1.4	1.1
4	0.0169	1.1	1.4	1.4
5	0.0159	1.4	1.1	1.1
6	0.0158	1.4	1.1	1.4
7	0.0169	1.4	1.4	1.1
8	**0.0171**	**1.4**	**1.4**	**1.4**

Table 5.3 – Stiction Interaction Study

Figure 5.12 illustrates a value of the rudder angle and kinetic energy versus time, the stick-slip behavior, though less striking than for the simple model is still clearly noticeable, with marked oscillations of the rudder kinetic energy corresponding to oscillation of its position.

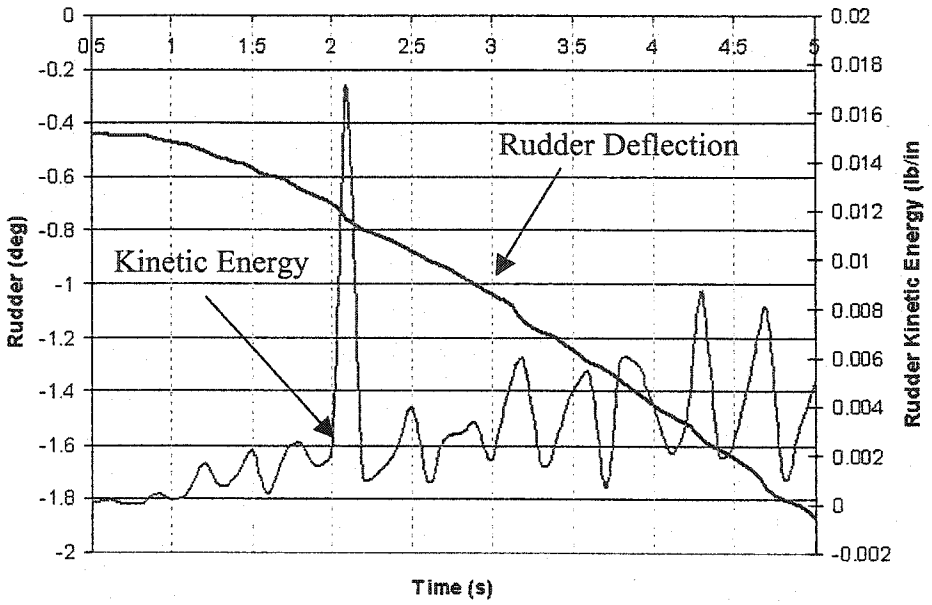

Figure 5.12 – Stick-Slip Behavior of the udder Model

5.3.3 Study of the Complete Model

Having identified the parameters of interest for our study, we are now ready to conduct experiments on the complete model, the rudder control system model, with the friction and clearance model activated. The question now is whether a kick will initiate after the initial small pedal kick, and how stiction and backlash affects the system. From *Section 5.3.2* we sorted out two main parameters for the friction model:

- The cable static friction coefficient (**factor 1**)
- The valve static friction coefficient (**factor 2**)

While *Section 5.3.1* allowed us to identify two main parameters for the clearance:

- The clearance in the summing mechanism referred to as **factor 1** in Figure 5.8, and referred to as **factor 3** in this study.
- The clearance in the input mechanism referred to as **factor 3** in Figure 5.8, is referred to as **factor 4** in this study.

The problem of studying these 15 parameters was reduced to the study of 4 of them. From *Section 5.1* we know that any DOE experiments on this model will require 2^4=16 runs.

The only thing left to do to complete this study is the relevant objective. The system is expected to produce a kick: a brisk, small amplitude motion of the rudder. This kick should initiate after the initial pedal kick (it was explained in *Section 5.2* how this initial kick was selected in order to "load" the system), a high-speed rotation of the rudder, whose amplitude should be as big as possible.

Since ADAMS/*view* only allows DOE runs for a single objective, initial tests were done with a linear combination of these two values. It quickly led to the conclusion that our factor has a small impact on rudder rotation, and that the best results were attained while using the same difference objective as defined in *Section 5.3.1*: the maximum of the absolute value of the difference in between the rudder deflection with and without non-linearity (clearance and stiction). *Table 5.4* shows the result for such an experiment.

Trial	Objective	Factor 1	Factor 2	Factor 3	Factor 4
1	0.10311	1.05	1.05	0.0008	0.0004
2	0.13154	1.05	1.05	0.0008	0.0052
3	0.11613	1.05	1.05	0.0104	0.0004
4	0.14068	1.05	1.05	0.0104	0.0052
5	0.095711	1.05	1.4	0.0008	0.0004
6	0.12419	1.05	1.4	0.0008	0.0052
7	0.11804	1.05	1.4	0.0104	0.0004
8	**0.14111**	**1.05**	**1.4**	**0.0104**	**0.0052**
9	0.10622	1.4	1.05	0.0008	0.0004
10	0.12987	1.4	1.05	0.0008	0.0052
11	0.11587	1.4	1.05	0.0104	0.0004
12	0.14121	1.4	1.05	0.0104	0.0052
13	0.10634	1.4	1.4	0.0008	0.0004
14	0.1276	1.4	1.4	0.0008	0.0052
15	0.12349	1.4	1.4	0.0104	0.0004
16	0.14079	1.4	1.4	0.0104	0.0052

Table 5.4 – DOE for Complete Model

The *Figure 5.13* illustrates this difference variable in function of time for the configuration of trial 8 in *Table 5.4*. A small 0.14 degree kick, on a two second period, appears 10 seconds after the beginning of the simulation, and tended to appear in all configurations, though maximal value in trial 8. It is maximal for the maximal clearance: we can therefore deduce that though this kick necessitates stiction to appear, the main influence on its amplitude is from the clearance. Trial 16 is found to produce a slightly faster kick (the rise time is approximately equal to 2 seconds), while limiting its final value to 0.125 degrees.

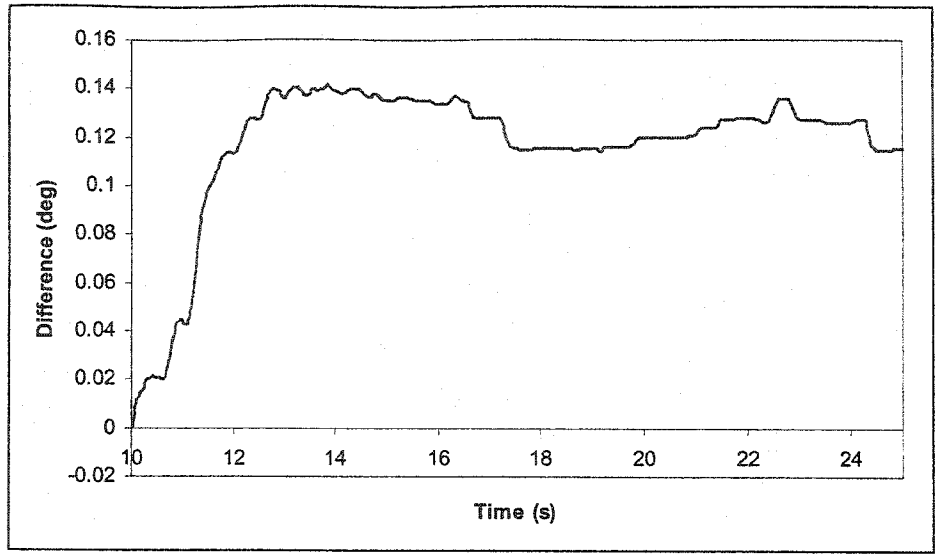

Figure 5.13 – Difference Objective of Combined Model

With the objective of giving an "energetic map" of this kick simulation, *Figure 5.14* reproduces *Figure 5.13*, adding the potential energy in the feel units (the main sources of stiffness in the system) along with the kinetic energy of the rudder.

One might notice the primary feel unit is the main energetic contribution to the kick, while a careful examination of the cable stretch (not shown here) shows a small impact of the cable stretch in the kick. These graphs locate the main energetic source of the kick on the front part of the mechanism.

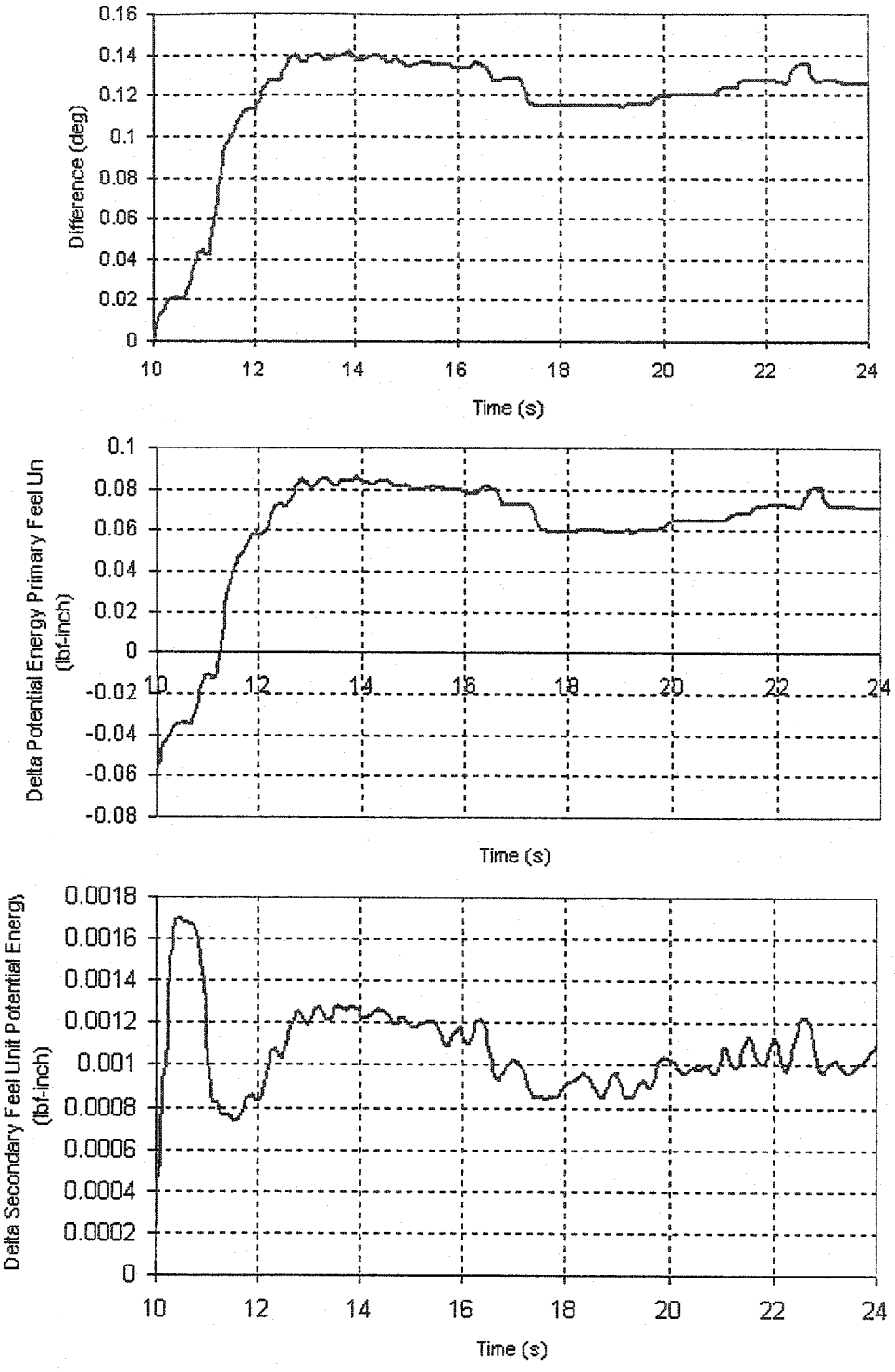

Figure 5.14 – Yaw Kick Simulation, Energy-1

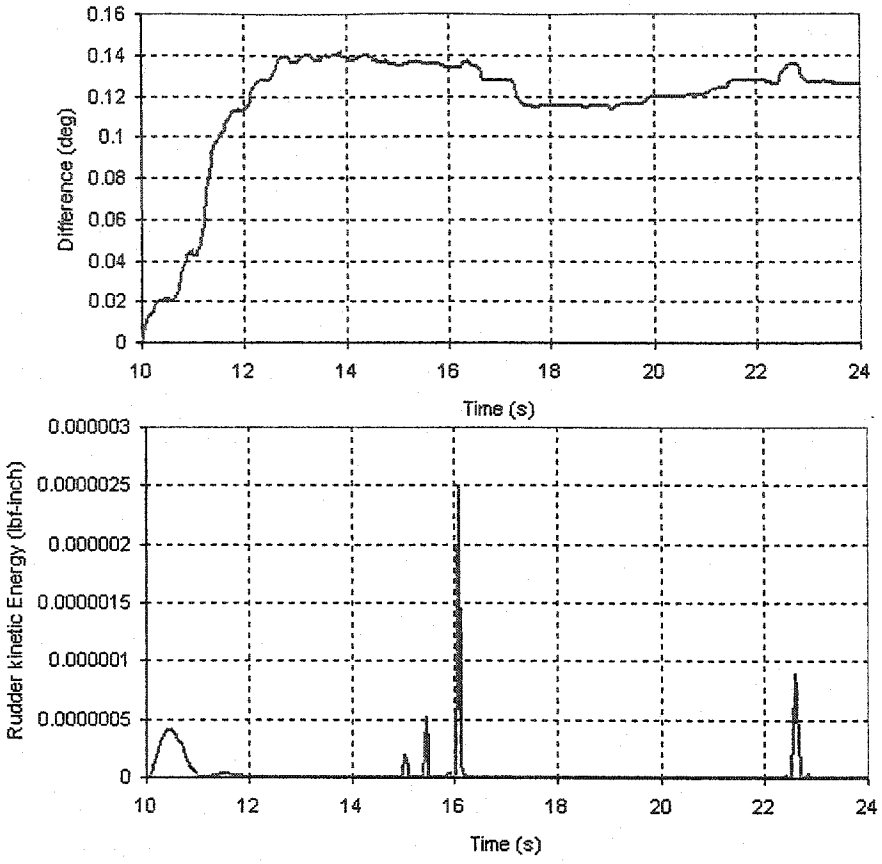

Figure 5.15 - Yaw Kick Simulation, Energy-2

For more details about the energy involved during stick-slip phenomenon in the system, the reader might report to Appendix D, which provides an energetic map of the model in this consideration, in response to a constant rate pedal displacement.

5.3.3.1 Findings

In the configuration of trial 8, our model is producing something that we can relate to the 0.5 degrees rudder step input identified in *Section 1.2* as the probable cause of the yaw kick. Before making any further comments on this result, it is important to understand the chronology of this phenomenon, which might be obvious when one looks at *Figure 5.16.* The *"pedal input start"* and *"Pedal Input Finishes"* correspond o the

initial pedal motion of *Figure 5.5,* while the two "*Yaw Damper*" labels correspond to the yaw damper correction as shown in *Figure 5.7.*

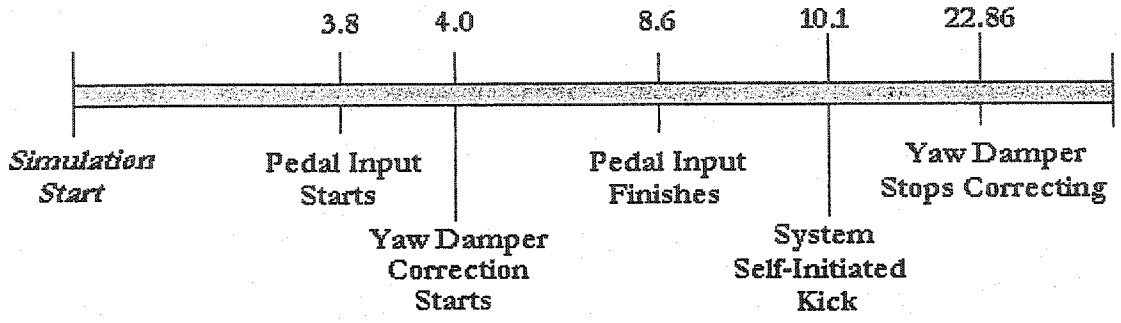

Figure 5.16 – Events Chronology of the Simulation

First, it should be noted that the aircraft dynamic data used in this model, as well as the yaw damper reaction and the hinge moment are somehow "static": they were generated in the flight model, and imported in the rudder control model. Hence, everything that happens after the kick initiation is only an estimate of what might happen: for instance, the yaw damper reaction to the yaw kick is not modeled, and to do so would probably require modeling of its complete control law and physical dynamic.

Still, it appears that if this kick is self-initiating after the end of pedal input, it occurs while the yaw damper is still reacting to the pilot's initial kick. It should be reminded a this point that there are no experimental data allowing to acknowledge the state of the yaw damper during yaw kick. Though it seems to exist in all configurations, the value of this kick appears to primarily depend on valve stiction effects. It is also dependent on the clearance in the mechanism, since the setting of two clearance parameters reduces the kick amplitude by 35% (one should note that the model includes a small amount of clearance in all configurations (see *Section 5.3.1*)).

It is therefore of crucial importance to examine how the system would behave if the yaw damper is kept inactive.

5.3.3.2 Without Yaw Damper

The experiment was repeated under the same conditions with the yaw damper inactive. *Figure 5.17* shows rudder rotation during the same time period when the yaw damper is not active. Clearly the kick shown by *Figure 5.13* is no longer present.

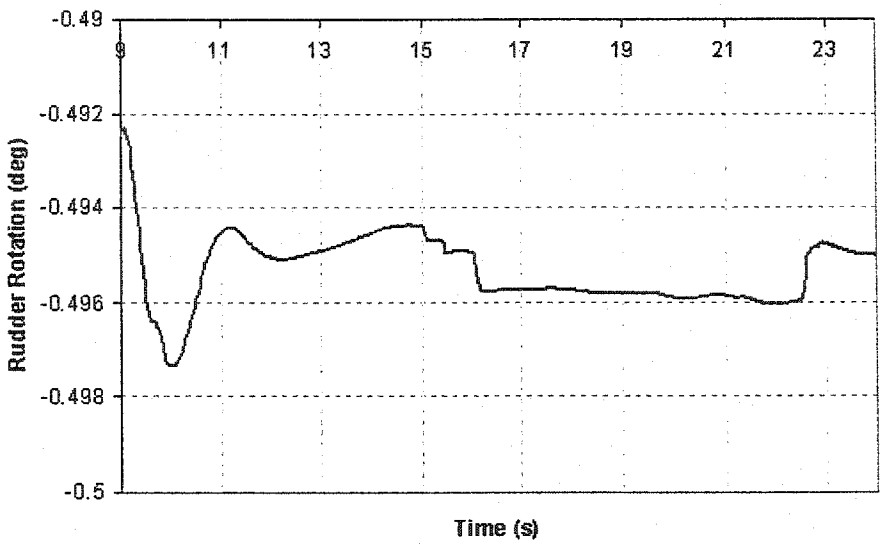

Figure 5.17 – Rudder Position with Yaw Damper Off

It therefore seems that if the backlash/stiction effects are responsible for storing a small amount of the energy applied to the system during the initial pedal motion, the yaw damper motion is responsible for releasing this energy during the simulation (*Figure 5.16*). Yet, it does not say anything concerning the role of the yaw damper during yaw kick initiation, since this release of energy might also appear due to aircraft structure vibration or any external cause in flight.

5.3.3.3 Without Aircraft Acceleration

With the goal to achieve a better understanding of how the mechanism might initiate this motion, and of the interactions between the aircraft platform dynamic and the rudder system behavior, the same experiment was repeated but with the acceleration macro (see *Section 4.2.5.8*) setting to gravity. The influence of acceleration on the aircraft platform on the mechanism's behavior is therefore neglected.

The result is observable in *Figure 5.18*: the kick initiates in this configuration with amplitude slightly diminished, but within a smaller time frame.

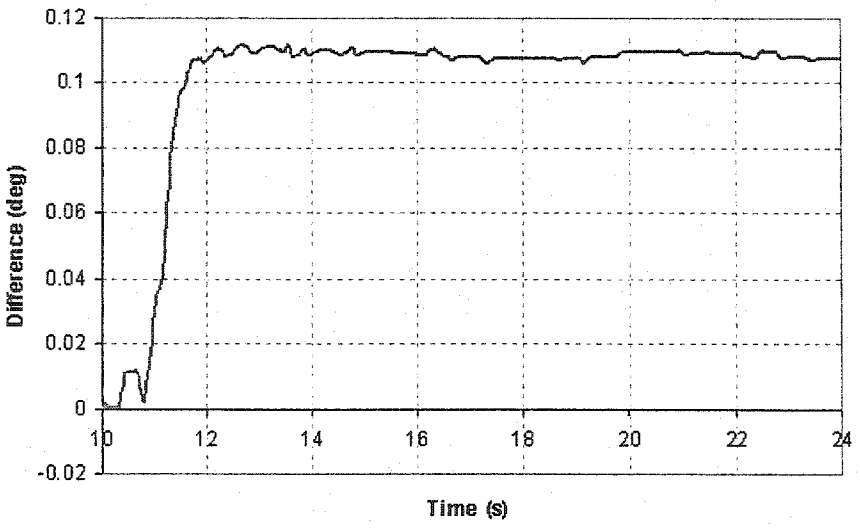

Figure 5.18 - Difference Objective of Combined Model without A/C Accelerations

5.4 Conclusion

This section presented a detailed review of the investigations as they were performed on the model whose characteristics were developed in the *Section 4*.

Though this investigation cannot pretend to be fully comprehensive, it should be considered an attempt to apply rational critical thinking in order to analyze and provide an answer to the yaw kick issue.

Overall, the results are ambivalent: it appears that under maximum conditions of clearance and stiction effects, a small kick is triggered during yaw damper operation.

Still, even though the amplitude is of the same order as what was defined in *Section 1.2*, this study could not succeed in reaching the *0.5 deg* expected.

The next section, while trying to summarize the results of this work, will also prepare the field for further investigation.

6 Conclusions, Recommendations, and Future Work

6.1 Conclusions

The objectives of this thesis, as stated in *Section 1*, were twofold. One goal was to produce a computer model of the overall rudder control system that is compliant with Bombardier Aerospace standards, while still presenting all the features necessary to pursue the main goal of this thesis, that is to find a root cause to the yaw kick phenomenon.

The steps leading to the development of the model were presented in *Section 4* of this document, based on a detailed description of the system as given in *Section 3*. Development involved the detailed modeling in ADAMS of a complex multibody system, encompassing mechanical linkages, cables, and hydraulic servo actuators, and appears to be a success. Lessons learned by Concordia in the development and validation of a detailed PCU model were capitalized: even though the initial project of a model direct integration within ADAMS was discarded, the solution applied is still a derivate of Concordia's previous work, also including Bombardier's experience in the domain.

This model is now part of the Bombardier System Simulation Group's library of models, ready to be used as a tool for evaluating future design changes, or to investigate possible failure cases of the system. It includes parameterized models of the clearances in the rod ends and of the stiction phenomenon, both being necessary for the performance of the yaw activity investigations.

This work therefore perfectly fulfills the requirements of the first objective.

The second objective was then to carefully investigate whether particular arrangements of the non-linearities might cause the system to self-initiate a rudder position step of the amplitude that was found using the flight model to be necessary for the yaw kick to be initiated.

Detailed reasoning of the investigations as they were performed is given in *Section 5*. It was found that if a kick was self-initiating when the yaw damper was on, and under condition of maximum backlash and stiction, its amplitude was too low. This might be explained in different way. Backlash in the system might have been underestimated or/and other phenomenon not considered in this analysis, like mechanical compliance in the system or in the supporting structure might amplify it. The aircraft's dynamics, and the rudder control system reaction to this dynamic (particularly the yaw damper) might also be invoked. Finally, one might also be tempted to reconsider the 0.5 degrees: this figure was derived from what an average human being might find noticeable, and therefore should not be taken for granted, but rather as an estimation, whose tolerance is hard to estimate. However, if this study demonstrates that a particular combination of backlash/stiction may induce a self-generated brisk motion of the rudder of the order of magnitude necessary to generate a yaw kick, to obtain a conclusive proof that those non-linearities are at the origin of yaw kick would require a more detailed study and availability of more flight test data.

6.2 Recommendations for Future Work

This project might be used to inspire future work on the subject. As they are stated in *Section 6.1*, explanations for the lack of positive affirmative results from this

work are underlining the necessity of additional experimental data. These data would be necessary for a more accurate characterization of the yaw kick conditions, as well as for validations or invalidations of a number of assumptions. More generally, they would greatly contribute to help investigations go beyond the "theoretical bubble" they have been contained in, also nourishing further questioning.

Furthermore, collaboration from the yaw damper supplier, in the form of a detailed model and/or control laws seems to be compulsory if the system is to be fully understood.

Further work might also imply the improvement of the rudder control system model by adding mechanical compliance, certain linkages, and/or the supporting structure. Bending of the whole vertical fin structure, or simply of the structure supporting the PCU's have already been identified as potential culprits, since it might create an error in the input link thus creating an input to the PCU.

MSC, the developer of ADAMS, has provided ADAMS users with a module referred to as ADAMS *flex* for a few years now, which makes this type of model perfectly feasible. It implies importing modal analysis of the suspected part from a third party FEM software, which is used to draw and mesh the part, and perform the modal analysis. Macro for the creation of this type of file required by ADAMS is provided for most common FEM solution, such as NASTRAN, I-DEAS, ANSYS and ABAQUS [30]. With version 12, MSC also offers ADAMS/*Autoflex*, which has the same function as the above-mentioned FEM software but with limited capabilities, and built within ADAMS/*view*.

Finally, a major work is left with the integration of the ADAMS model to the MatrixX flight model, which would be necessary for further investigation of the dynamic of the kick, as for yaw oscillations studies. Difficulties anticipated for this type of work were already discussed in *Section 5.2*, so this last section will therefore deal with a proposed solution.

The current model was done on version 9 of ADAMS and this is already an old version of the software; many improvements have been put in place in the field of co-simulation. For instance, ADAMS 12.0 is coming out with a completely revised approach for this type of model. ADAMS *Control* is now coming out as an add-on to ADAMS/*view* and is therefore no longer a separate entity, making the debugging process more straightforward. Also, many improvements have been made to ADAMS/*solver,* which is now expected to behave better for co-simulation. Finally, a new feature referred to as *control system import* offers an alternative and appealing approach that would eliminate the problem of communication in between the two solvers, and greatly simplify debugging. It involves the generation of C code of a Matlab Simulink model by a Matlab Real-time workshop, which can be later on imported as a subroutine within ADAMS/*solver* (this process was also subsequently improved). Though it is at the cost of the extra step of moving the flight model from MatrixX to Matlab, the idea of transferring the flight model directly within ADAMS sounds very promising.

Returning to the idea of a controller (recall *Figure 1.2*), Concordia intends to conduct more detailed research on the possibility of counteracting stick-slip phenomena in such a system, by automatically releasing the energy in a controlled

manner when necessary. The present document includes, in Appendix E, a review of a simplified model for MatLab, which integrates the results of this work, a PCU model [3], and a simplified flight model. This simplified model includes the main elements detailed in this work, and should therefore present an interesting platform from which to conduct further research.

REFERENCES

1 Investigation of the limit-cycle oscillation problem in Flight Control System Design, Bombardier/Concordia Project, Phase 1 report

2 Jacques Thibaudeau, "A Proposal for a Yaw Activity Production Specification", Bombardier Flight Operations, Montreal, January 2000, pp.3

3 ISO-6897-1984: guidelines for the evaluation of the response of occupants of fixed structures, especially buildings and offshore structures to low frequency horizontal motion.

4 Davaze E., "Investigation of Flight Control System Non-Linearities", M.A.Sc. Thesis – in progress, Concordia University, Montreal, 2003

5 John H. Blakelock, "Automatic Control of Aircraft and Missile", John Wiley & Sons, New York, USA, 1965, pp. 181

6 Bandu N. Pamadi, "Performance, Stability, Dynamics, and Control of Airplanes", NASA Langley Research Center, Virginia, US, 1998, pp. 4.1 –4.5, pp. 6.3

7 Donald McLean "Automatic Flight Control Systems", Prentice Hall International, London, UK, 1990, pp. 299

8 http://www.allstar.fiu.edu/

9 Peter H.Zipfel, "Modeling and Simulation of Aerospace Vehicle Dynamics", 2000, AIAA Education Series, Virginia, United Stated, pp. 10.2

10 Frederic M. Hoblit, "Gust Loads on Aircraft: Concepts and Application", AIAA Education Series, Washington, USA, 1988, pp. 4.1-4.7

11 "MatrixX version 61.3" User Help

12 Peter Dietz, "Coordination MEMO ECM-604-BA/CU-AERO-001", Coordination memo from Bombardier Flight Science Group to Concordia University, 26 of July 2002, pp. 4

13 http://www.carolinaaircraft.com/afs/n88nm/ckpt.html

14 Ian Moir & Allan Seabridge, "Aircraft Systems", Longman Scientific and Technical, London, UK, 1992, chapter 3

15 Darrol Stinton, "The Design of the Aeroplane", Van Nostrand Reinhold Company Inc., 1983, pp. 430

16 Special Federal Aviation Regulations, SFAR 23, Sec. 29.695, "Power Boost and Power-Operated Control System"

17 George R Keller, "Hydraulic System Analysis", Industrial Publishing Company, Cleveland, Ohio, 1974, pp. 167, 168

18 – Bombardier Aerospace, "Challenger Maintenance Training Manual", 1995, pp. 11-8, 11D-3

19 Ahmed A. Shabana, "Dynamics of Multibody Systems, Second Edition", Cambridge University Press, USA, 1998, pp. 3.0, 3.6

20 James B. McConville and Joseph F. McGrath, "Introduction to ADAMS Theory", Mechanical Dynamics Inc., Ann Harbor Michigan, 1998, pp. 1,28

21 Boeing Design Manual, 606.1 Mechanical Controls, 11-3-78

22 Francois R. Godin, "Aircraft Flight Control System Modeling – Cable Construction Kit-", International ADAMS user Conference, Orlando, June 19-21, 2000

23 MSC, "Getting Started Using ADAMS/*controls*", ADAMS 12 documentation

24 http://www.aero-rexnord.com/Prod3/Rod.htm

25 MS 21151 (military) Specification sheet for bearing, ball, rod end, double row, precision, external thread, self-aligning, airframe type II

26 MSC, "ADAMS/*solver* documentation"

27 H. Olsson, K.J. Astrom, C. Canudas de Wit, M Gafvert, P. Lischinski, "Friction Model and Friction Compensation", European Journal of Control, Dec. 1998, No. 4, pp. 176-195.

28 B. Armstrong and C. Canudas de Wit. CRC Controls Handbook, chapter "Friction Modeling and Compensation" Boca Raton: CRC Press, 1995, Invited Book Chapter.

29 *NIST/SEMATECH e-Handbook of Statistical Methods*, http://www.itl.nist.gov/div898/handbook/, November 2002, pp. 5.1 to 5.4

30 MSC, "ADAMS/*flex* 12.0 User Guide"

Appendix A: Von Karman Turbulence Model

Gust loads, whether due to discrete gusts or continuous turbulence, are ordinarily considered to be the result of a change in angle of attack due to a component of gust velocity at right angles in the flight path. (*Figure A.1*).

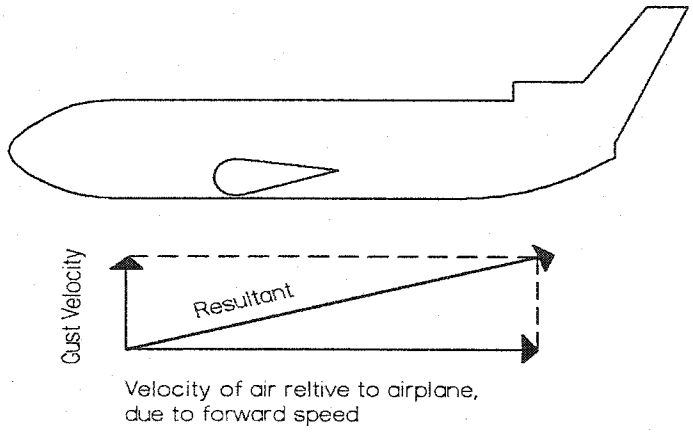

Figure A.1 – Gust Turbulence

Gust profiles (*Figure A.2*) are usually continuous and irregular: they are therefore referred to as turbulence. Beside, they usually tend to be isotropic: their profile will present the same characteristics (peak value, distribution, frequency content), along vertical, lateral or longitudinal direction.

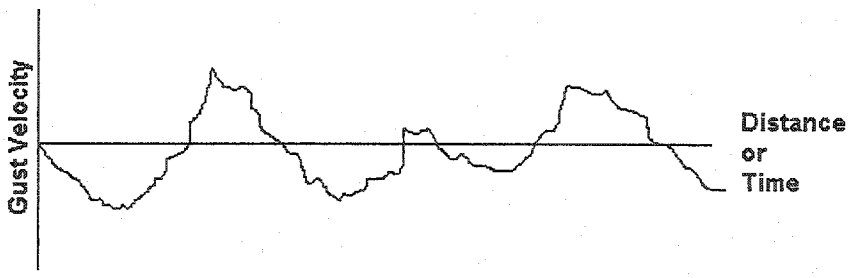

Figure A.2 - Gust Profile

They are usually idealized as being a **"stationary Gaussian random process"** as this idealization:

- Produces gust profiles very close to test data
- Easy-to-apply mathematical techniques are available to use with this idealization

But this only defines the magnitude of the gust profile. In order to complete it statistical description, a definition of its frequency content is also required.

This can be done with a power-spectral density (psd) function, which provides a complete continuous description of the process in the frequency domain.

Von Karman left his name to a gust velocity *psd* commonly used in design. Its mathematical expression (for vertical and lateral gust) is:

$$\Phi(\Omega) = \sigma_w^2 \frac{L}{\pi} \frac{1 + \frac{8}{3}(1.139L\Omega)^2}{[1 + (1.139L\Omega^2)]^{11/6}}$$

with:

- $\Omega = \frac{2\pi f}{v}$ as the spatial frequency (cycles / feet)
- L is the scale of the turbulence (a common value is 2500 ft)
- σ_w is the root mean square of the gust velocity

Figure A-3 gives a plot of the Von Karman distribution. The Von Karman spectrum is the standard for design use.

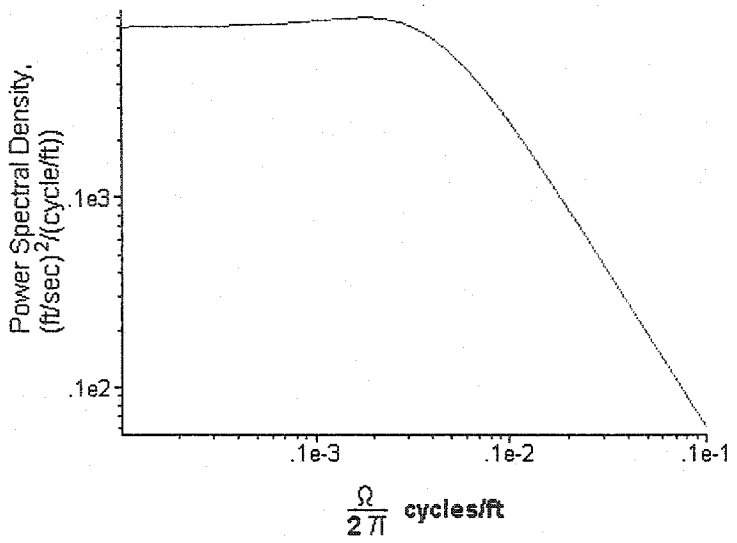

Figure A-3 Von Karman Gust psd

Reference:

Frederic M. Hoblit, "Gust Loads on Aircraft: Concepts and Application", AIAA Education Series, Washington, USA, 1988, pp. 4.1-4.5.7

Appendix B: ADAMS/*Solver* Important Statement

B.1 Contact

B.1.1 Definition

The CONTACT statement lets you define a two- or three-dimensional contact between a pair of geometric objects. ADAMS/*Solver* models the contact as a unilateral constraint, that is, as a force that has zero value when no penetration exists between the specified geometries, and a force that has a positive value when penetration exists between two geometries.

The CONTACT statement supports:

- Multiple contacts
- Dynamic friction
- Contact between three-dimensional solid geometries

Once the contact kinematics are known, contact forces, which are a function of the contact kinematics, are applied to the intersecting bodies. Failure to enforce planarity will result in a run-time error, when the bodies go out of plane during a simulation.

B.1.2 Contact Normal Force Calculation

Two models for normal force calculations are available in ADAMS/*Solver*: IMPACT function model and the coefficient of restitution or the POISSON model .Both force models result from a penalty regularization of the normal contact constraints. Penalty regularization is a modeling technique in mechanics, in which a

constraint is enforced mathematically by applying forces along the gradient of the constraint. The force magnitude is a function of the constraint violation. Contact between rigid bodies theoretically requires that the two bodies not penetrate each other. This can be expressed as a unilateral (inequality) constraint. The contact force is the force associated with

enforcing this constraint. Handling these auxiliary constraint conditions is usually accomplished in one of two ways, either through introduction of Lagrange multipliers or by penalty regularization. For contact problems, the latter technique has the advantage of

simplicity; no additional equations or variables are introduced. This is particularly useful when treating intermittent contact and algorithmically managing active and inactive conditions associated with unilateral constraints. Additionally, a penalty formulation is easily interpreted from a physical standpoint. For example, the magnitude of the contact reaction force is equal to the product of material stiffness and penetration between contacting bodies, similar to a spring force. For these reasons, ADAMS/*Solver* uses a penalty regularization to enforce all contact constraints. The disadvantage of the penalty regularization, however, is that you are responsible for setting an appropriate penalty

parameter, that is, the material stiffness. Furthermore, a large value for the material stiffness or penalty parameter can cause integration difficulties.

Before presenting the contact normal force models in ADAMS/*Solver*, it is helpful to clearly define the contact constraints and associated kinematic and kinetic quantities. First, impenetrability of two approaching bodies is measured with a gap function g,

where a positive value of g indicates penetration. Next, we denote the normal contact force magnitude as Fn, where a positive value indicates a separation force between the contacting bodies. With this notation in hand, the auxiliary contact constraints are defined as *Eqn. (B.1)-(B.4)*:

$$g \geq 0 \qquad \textit{Eqn. (B.1)}$$

$$Fn > 0 \qquad \textit{Eqn. (B.2)}$$

$$Fn * g = 0 \qquad \textit{Eqn. (B.3)}$$

$$F_n * \frac{dG}{dt} = 0 \qquad \textit{Eqn. (B.4)}$$

The first three equations reflect:

- The impenetrability constraint
- Separating, normal force constraint
- Requirement that the normal force be nonzero only when contact occurs.

The fourth condition is called the persistency condition and it specifies that the normal force is nonzero only when the rate of separation between the two bodies is zero. The last constraint is particularly important when you are interested in energy conservation or energy dissipation.

We obtain the IMPACT force model by replacing the first three auxiliary contact conditions with the following *Eqn. (B.5)*:

$$Fn = k * (g **e) \qquad \textit{Eqn. (B.5)}$$

where k (stiffness) is a scalar penalty parameter. The penalization becomes exact as k approaches infinity, but otherwise allows small violation of the impenetrability constraint. It is important to note that ill conditioning of the governing

equations, and ultimately an integrator failure, will result as the stiffness becomes excessively large. Therefore, k must be appropriately selected while preserving the stability of the solution.

You can also approximate the compliance of a body by correlating k to the body's material and geometric parameters; however, in doing so, you should recall the earlier remark concerning ill conditioning. In an effort to incorporate general material constitutive relationships for the contacting bodies, as well as facilitate time integration, ADAMS/*Solver* augments the previous expression with nonlinear displacement-dependent, viscous damping terms. The general form of the IMPACT force function is then given by *Eqn. (B.6)*:

$$Fn = k*(g**e)*STEP(g,0,0,d_{max},c_{max},\frac{dG}{dt}) \qquad \textit{Eqn. (B.6)}$$

where:

- g represents the penetration of one geometry into another.
- $\frac{dG}{dt}$ is the penetration velocity at the contact point.
- e is a positive real value denoting the force exponent.
- d_{max} is a positive real value specifying the boundary penetration to apply the maximum damping coefficient cmax.

Clearly, for cmax = 0 and e = 1, the original penalization is recovered.,The POISSON force model is derived from the persistency condition, $F_n * \frac{dG}{dt} = 0$. A penalty regularization of the fourth contact constraint yields:

$$Fn = p*\frac{dG}{dt} \qquad \textit{Eqn. (B.7)}$$

where p is a scalar penalty parameter. Again, the penalization is exact as $p \to \infty$, which carries the risk of ill conditioning. In the context of dynamic contact problems, the POISSON model is more consistent with conservation laws and conserves/dissipates energy appropriately. You can optionally provide a coefficient of restitution e to model inelastic contact. In this case, the POISSON force model computes the normal contact force as follows:

$$Fn = p * [(\frac{dg}{dt})_+ - (\frac{dg}{dt})_-] \qquad \textit{Eqn. (B.8)}$$

here the subscripts $(\cdot)_-$ and $(\cdot)_+$ denote values immediately before and after contact.

B.2 BISTOP

The BISTOP function models a gap element. *Figure B.1* illustrates the BISTOP force. The gap element consists of a slot which defines the domain of motion of a Part I located in the slot. As long as Part I is inside the slot and has no interference with the ends of the slot, it is free to move without forces acting on it. When Part I tries to move beyond the physical definition of the slot, impact forces representing contact are created by the BISTOP function. The created force tends to move Part I back into the slot.

The BISTOP force has two components: A stiffness component dependent on the penetration of Part I into the restricted Part J and a damping or viscous component that may be used to model energy loss.

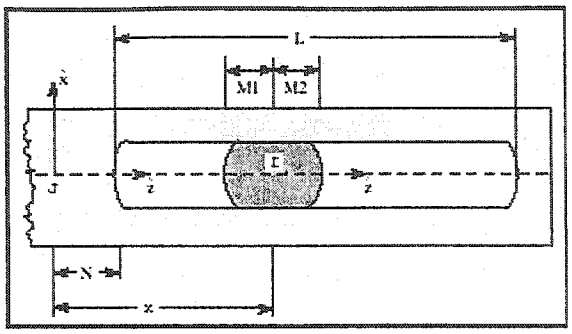

Figure B.1 –BISTOP Force

To prevent a discontinuity in the damping force at zero penetration, the damping coefficient is defined as a cubic step function of the penetration. Thus at zero penetration, the damping coefficient is always zero. The damping coefficient achieves a maximum, cmax, at a user-defined penetration, d.

The BISTOP force can be mathematically expressed as in *Eqn. (B.9):*

$$Bistop = \begin{cases} \text{Max}(k*(x_1 - x)^e - \text{STEP}(x, x_1 - d, c_{max}, x_1, 0)*x', 0) : x < x_1 \\ 0 : x_1 \le x \le x_2 \\ \text{Max}(k*(x - x_2)^e - \text{STEP}(x, x_2, 0, x_2 - d, c_{max})*x', 0) : x > x_2 \end{cases} \quad \textit{Eqn. (B.9)}$$

B.3 STEP

The STEP function approximates the Heaviside step function with a cubic polynomial. It has continuous first derivatives. Its second derivatives are discontinuous at. *Figure B.2* illustrates the STEP function.

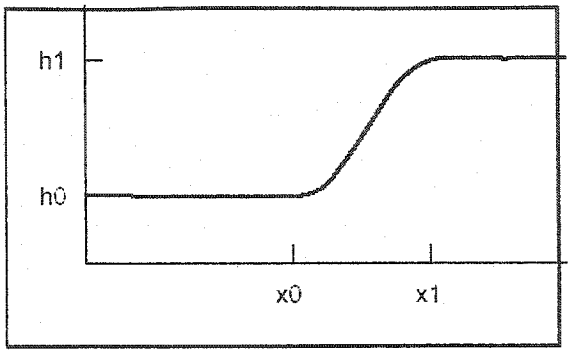

Figure B.2 – STEP Function

The equation defining the STEP function are given in *Eqn. (B.10)-(B.12):*

$$a = h_1 - h_0 \qquad \textit{Eqn. (B.10)}$$

$$\Delta = \frac{x - x_0}{x_1 - x_0} \qquad \textit{Eqn. (B.11)}$$

$$STEP = \begin{cases} h_0 \, for x \le x_0 \\ h_0 + a\Delta^2(3 - 2\Delta) \, for x_0 < x < x_1 \\ h_1 \, for x \ge x_1 \end{cases} \qquad \textit{Eqn. (B.12)}$$

Reference:

Mechanical Dynamic, "Using ADAMS/*Solver*" for ADAMS 12, 2002, Mechanical Dynamics, Incorporated.

Appendix C: PCU C code model

This appendix intends to detail the procedure developed by Bombardier while developing its C code template for the PCU model (refer to *Section 4.3.2* in the document "Investigation of Aircraft Yaw Motion"). The choice of a C code offers many advantages in opposition to the other software available to develop this type of model:

- Portability between different platforms (Unix, Windows....) at the simple cost of a recompilation
- Portability between different "host software" (ADAMS, Matlab), at the cost of a few known code modifications
- The code can be optimized to run efficiently

The latest point being supported by the fact that the code presented below was used for real time simulation of flight control.

The fact that the PCU hydraulic diagram is converted to its electrical equivalence was discussed in the main document. In this appendix, we will therefore only recall this diagram (*Section 4.3.2*):

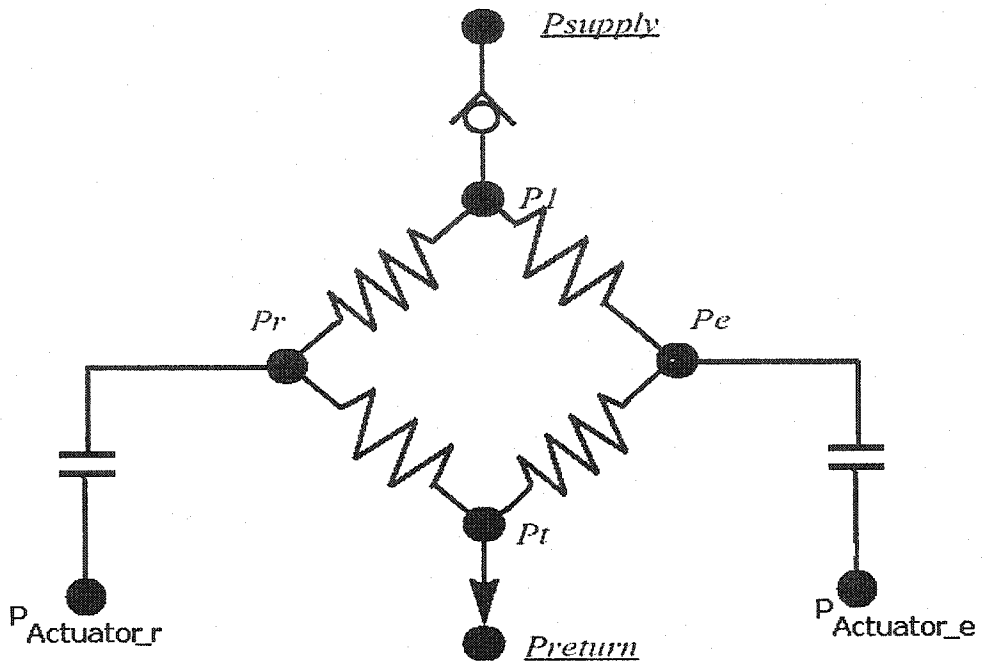

Figure C.1 – PCU Nodal Diagram (remember *Figure 4.18* of main document)

The pressure at the nodes P_e, P_l, P_r and P_t is evaluated knowing summation of flows (mass conservation) at control volumes.

Flow is modeled a using standard orifice flow equation, assuming turbulent flow (recall *Eqn. (14)* from main document):

$$Q = A * C_d * \sqrt{\frac{2 * \Delta P}{\rho}} \qquad \textit{Eqn. (C.1)}$$

The code then formulates this equation using the electrical equivalence, defining the admittance across the orifice:

$$Q = ADM * \Delta P \qquad \textit{Eqn. (C.2)}$$

with ADM the admittance across the orifice (in3/sec psid) and ΔP the differential pressure (psid).

Hence, the admittance is used to define the conductivity across orifice C (in3/sec $\sqrt{psi}$) as in *Eqn. (C.3):*

$$ADM = \frac{C}{\sqrt{\Delta p}} \qquad \textit{Eqn. (C.3)}$$

Compressibility effects in the actuators chamber (inductance on *Figure C.1*) are taken into account by *Eqn. (C.4).*

$$Q = C\frac{dp}{dt} \qquad \textit{Eqn. (C.4) [C.1]}$$

with C the hydraulic capacitance (volume/ bulk modulus) and $\frac{\partial P}{\partial t}$ the pressure rate of change)

The program execution procedure is self-explanatory and is illustrated in the flow chart *Figure C.2.* One should also note on the diagram the variable exchange with the host software.

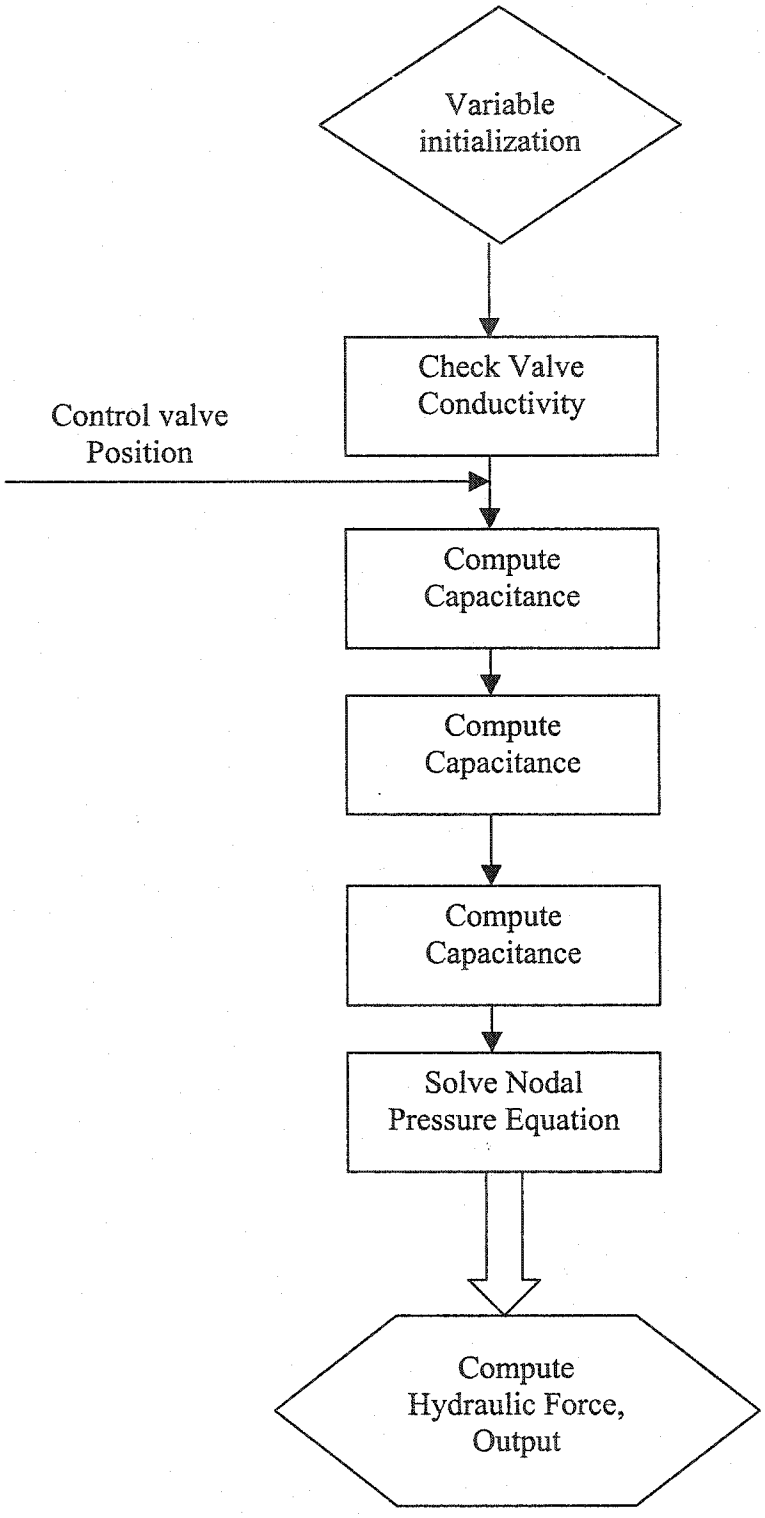

Figure C.2 – C Code PCU Program Flowchart

One might also notice the main procedure difference between the MatrixX PCU model and the one discussed in the present document. When the MatrixX PCU model is using a negative feedback loop to find a solution to the hydraulic equations, this model simply computes numerical values for the linear equations system, whose analytical solutions is already known.

Reference:

C.1 George R Keller, "Hydraulic System Analysis", Industrial Publishing Company, Cleveland, Ohio, 1974

Appendix D: Stick-Slip Simulation

The figures D.1 on the next page detail different energetic parameters (kinetic for the main inertia contributions, potential for the main stiffness contribution) for the model configuration as it is detailed in the main document, in *Section 5.3.3.1*, during a simulation with a constant rate pedal displacement (this rate is chosen to be close to pedal rate displacement during the yaw kick simulation, *Section 5.2.3* in the body). It therefore illustrates the energy involved during stick-slip phenomena in the system.

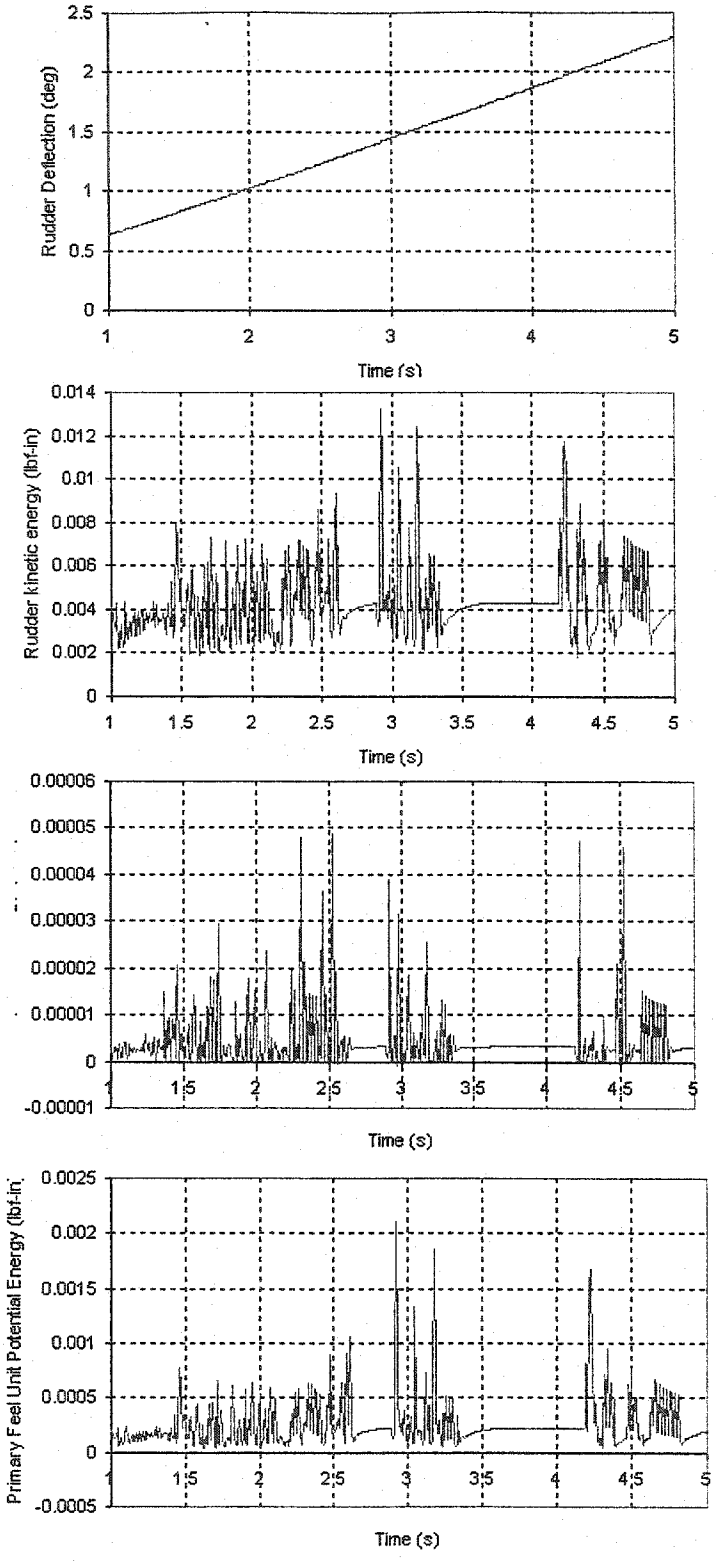

Figure D.1 – Stick-slip Simulation

Appendix E: Simplified Rudder Control Model

The present appendix is detailing the characteristics of a simplified rudder control model. Also including a state-space model of the aircraft dynamic, this model, built around data extracted from the detailed model presented in the body part of this document, should be seen as a research tool for further study on the phenomena detailed in the body. It is therefore presenting its main characteristic, while attempting to correctly reproducing its behaviors.

The model was developed in Matlab/Simulink, a software package commonly available in universities.

The linkage parts, is represented by two simple translating masses (for the front and aft part of the mechanism), separated by a cable model (*Figure E.1*).

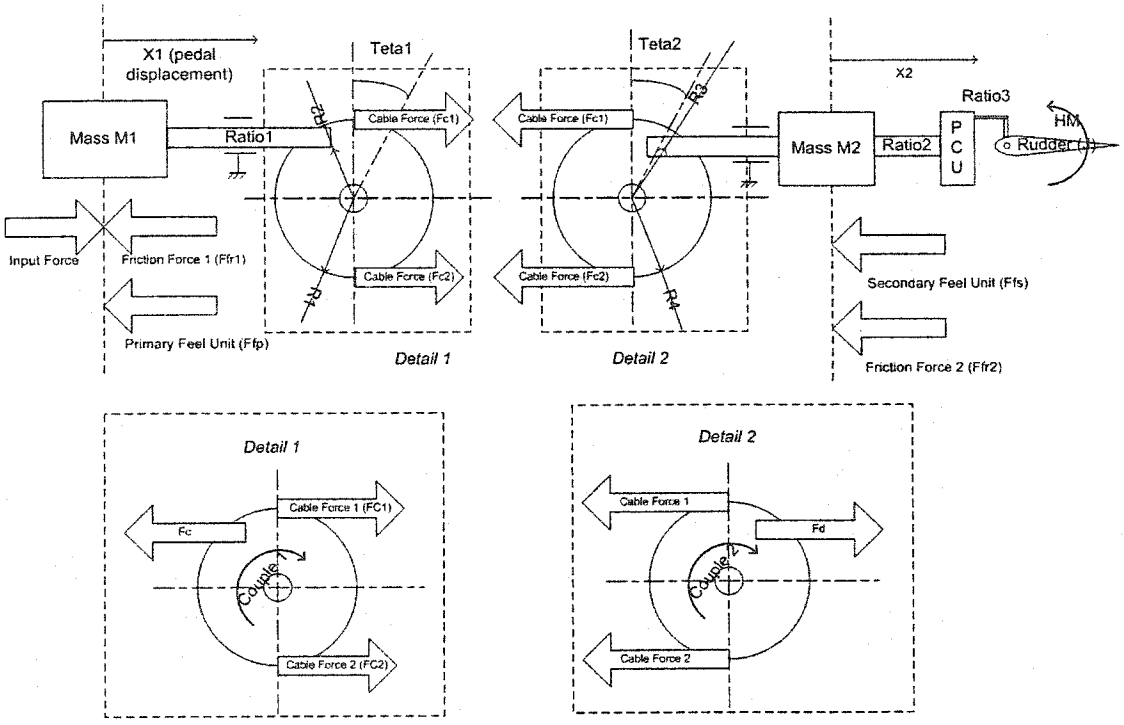

Figure E.1 – Simplified model

Each of them is subjected to friction forces (*Section 4.2.5.6* in the body of this document), but also feel forces, represented in Simulink in the form of look-up tables. Not included in *Figure E.1* are two Simulink deadband blocks at the position output of each mass, figuring the backlash in the system, as discussed in *Section 4.3.3* of the main document.

Table E.1 is presenting the variable name and value for each element of the model, as extracted from the ADAMS model, and presented in *Figure E.1*. Mass M1 and M2 were computed lumping the most significant masses of (respectively) front and aft part of the mechanism at the pedal and aft quadrant (respectively).

The position output of the mass M2 is used to command the PCU model developed by Concordia [E.2], translated from SystemBuild to Simulink (one should note this model, along with the hinge moment blocks, were developed and are still in imperial units). This model is outputting a rudder position in degree, used to drive the state-space aircraft lateral dynamic model. The PCU model is also requiring a hinge moment torque: the corresponding block of the MatrixX flight model was converted and imported in MatLab.

Type	Variable	Value	Unit
Equivalent Mass front mechanism	M1	16.9	kg
Ratio Teta1 and X1	ratio1	4.122047	rad/m
Radius of Forward Quadrant groove	R1	0.1524	m
Radius of forward Quadrant to rod attachment	R2	0.1397	m
Radius of aft Quadrant groove	R4	0.161544	m
Radius of aft Quadrant to rod attachment	R3	0.1016	m
x2 to command to PCU	ratio2	0.079813	m/rad
Equivalent Mass front mechanism	M2	17.6	kg
Rudder rotation for PCU actuator displacament	ratio3	13.94451	rad/in
PCU command for Yaw damper input	ratio4	0.532855	m/m
Backlash front	0.000866667		m
Backlash aft	0.000254		m

Table E.1 – Model characteristics

E.1 Mass Dynamic Equations

Equations for the mass dynamic are derived using Newton's law (*Eqn. (E.1)&(E.2)*) (referring to the conventions of *Figure E.1*):

$$M_1 * \ddot{x}_1 = F_I - F_{fr1} - F_{fp} - F_c \qquad \textit{Eqn. (E.1)}$$

$$M_2 * \ddot{x}_2 = -F_{fr2} - F_{fs} + F_d \qquad \textit{Eqn. (E.2)}$$

with F_I representing the pedal force (in Newtons), F_{r1} and F_{r2} frictions, and F_{fp} and F_{fs} respectively primary and secondary feel unit force, in function of the mass displacement.

E.2 Cable Model Equations

The Matlab cable model is based on the same equation as discussed in *Section 4.3.1* of the main document and are reproduced here with equations *Eqn. (E.3)&(E.4):*

$$F_{c1} = K[R_4\theta_2 - R_1\theta_1 + l_{init}]*l_c \qquad \textit{Eqn. (E.3)}$$

$$F_{c2} = K[R_1\theta_1 - R_4\theta_2 + l_{init}]*l_c \qquad \textit{Eqn. (E.4)}$$

with l_{init} the cable elongation at installation and l_c the total cable length. The reader might report to *Figure E.1* for the meaning of the other variables involved in these equations. K is actually depending on the instantaneous equation and was modeled using a look-up table, built around the same data as *Figure 4.14* of the main document.

Using Fc1 and Fc2, forces on M1 and M2 can be computed as in *Eqn. (E.5)&(E.6):*

$$F_C = \frac{-R_1(F_{c1} - F_{c2})}{R_2} \qquad \textit{Eqn. (E.5)}$$

$$F_C = \frac{R_4(F_{c2} - F_{c1})}{R_3} \qquad \textit{Eqn. (E.6)}$$

E.3 Friction Model

[E.1] presents a new model for friction than can be used for friction compensation, and exhibits all the friction phenomena that were presented in *Section 4.4.2.*

At microscopic level, contact surfaces are very irregular: it can actually be though of as a number of asperities in contact, therefore reducing the contact area. The model visualizes this as two rigid bodies with bristle in contact, as illustrated in *Figure E.2.* Bristle will deflect like torsion spring with increasing tangential forces, till they deflect so much than the bodies will slip.

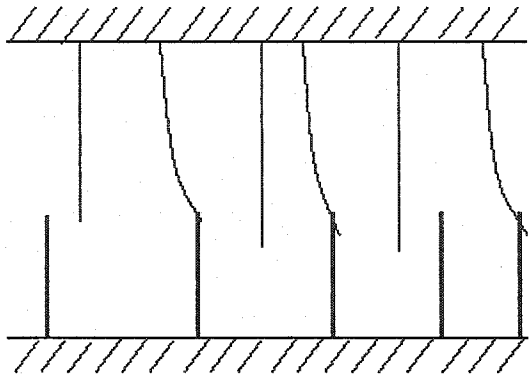

Figure E.2 – Friction Interface Bristle model (lower part seen rigid for simplicity)

The model of [E.1] is based on the average deflection of the bristle denoted z and is modeled by *Eqn. (E.7)*:

$$\frac{dz}{dt} = v - \frac{|v|}{g(v)} z \qquad \textit{Eqn. (E.7)}$$

the first term ensures the deflection is proportional to velocity, while the second state is used to compute the steady state average deflection as seen in *Eqn. (E.8):*

$$z_{ss} = g(v) * sign(v) \qquad \textit{Eqn. (E.8)}$$

g is dependant on many factors, but is globally accounting for the Stribeck effect if it is decreasing monotonically with velocity [E.1]. In this report, we will use the parameterization of *Eqn. (E.9):*

$$g(v) = \alpha_0 + \alpha_1 e^{-(\frac{v}{v_0})^2} \qquad \textit{Eqn. (E.9)}$$

Finally, the friction force generated by the deflection of the bristle is described as:

$$F = \sigma_0 z + \sigma_1 \frac{dz}{dt} + \sigma_2 v \qquad \textit{Eqn. (E.10)}$$

with σ_0 the stiffness, σ_1 the damping coefficient, and σ_2 accounting for viscous friction.

Eqn. (E.6), (E.7) and *(E.10)* are therefore providing a complete model of the friction based on the six parameters σ_0, σ_1, σ_2, α_0, α_1 and v_0. This model is dependant on the previous state and is therefore accounting for the friction memory

The pertinence of this model might be demonstrated by simulating the system of *Figure E.3*, where a unity mass is attached to a spring of stiffness 2N/m. The end of the spring (position y) is pulled out at a constant velocity 0.1 m/s.

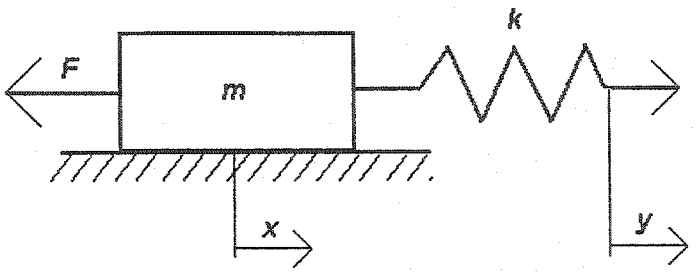

Figure E.3 – Stick Slip Simulation Set-up

As can be seen on *Figure E.4*, the model exhibits a stick-slip behavior, as discussed in more details in *Section 4.4.2* of the body part of this document.

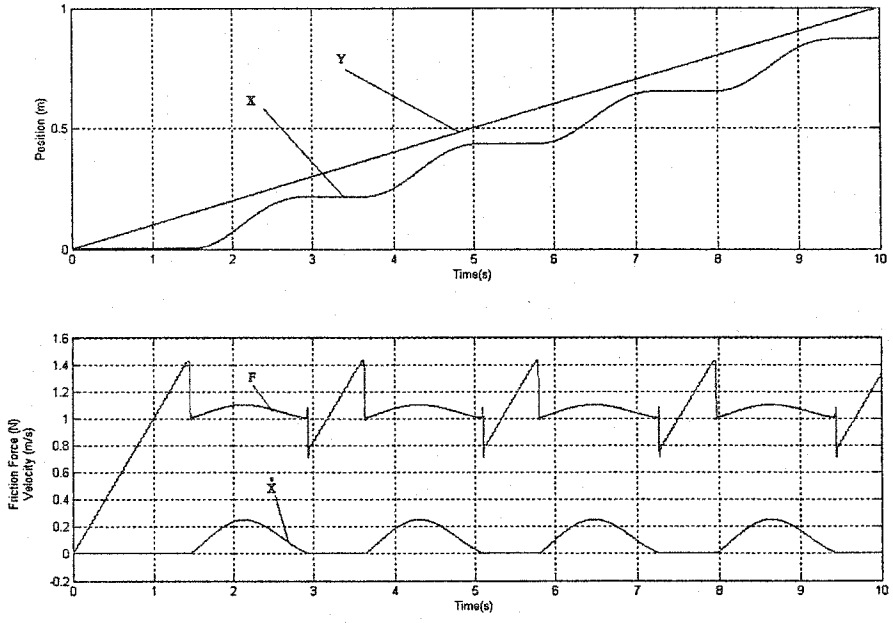

Figure E.4 – Stick- Slip Behavior

E.4 A/C lateral Dynamic Model

Details for the derivation of a linearized lateral flight model are given in the main document, *Section 2.1.3.4*. The present model includes this state-space model, for an aircraft in the conditions of *Table E.2*.

Flight Conditions		Unit
altitude	11278	m
speed	218.1	m/s
Woe	12292	kg
passengers (8)	762.0153492	kg
fuel weight	2267.902825	kg
m	15321.91817	kg

Table E.2 – Simplified Flight Model conditions

Detailed calculations of the state-space model, presented in the form of an Excel worksheet, allow fast modifications of these parameters, which are resulting in matrices A and B, necessary for the model presented in a state space form.

The resulting state-space model can then easily be imported in the Matlab workspace: the in Simulink, the user is prompted for double-clicking a block. This runs a number of Matlab commands (in the file *load_aircraft.m*), that in turns make sure the proper matrices are loaded in the Matlab workspace. *Table E.3* is comparing the Dutch roll characteristics of the response of the two flight models to a rudder step input, is proving the state-space model to be a reasonable approximation.

Detailed Flight Model	Damping ratio	0.033525
	Wn	1.737018
State Space Approximation	Damping ratio	0.032903
	Wn	1.762754

Table E.3 - Comparison

E.5 Simplified Model

The simplified model therefore consists in:

- A Simulink *.mdl file containing the simplified model, that is:
  - Model of cable and linkages as seen in *Figure E.1*
  - A PCU model [E.2]
  - A lateral dynamic model (*Section E.4*)
  - An hinge moment model, as extracted from the MatrixX flight model
- A folder named "picture components" with the bitmap files for the masks in the above-mentioned file.
- A Matlab command file "load_aircraft.m" that can be run form the Simulink model and that is importing the results of the "aircraft.xls" file.
- An "aircraft.xls" file, detailing the computation of matrices A and B for the lateral dynamic model. This file can be used to easily produce model for different aircraft configurations.
- A number of files "animinit.m", "draw_aircraft_top.m", "draw_aircraft_front.m", "circle.m", "aircraft_animation.m", used to animate a small drawing of the aircraft during the simulation. Thought not essential, they somehow enhance the user perception of the aircraft behavior.

The resulting model, as presented in Simulink, can be seen in Figure E.3

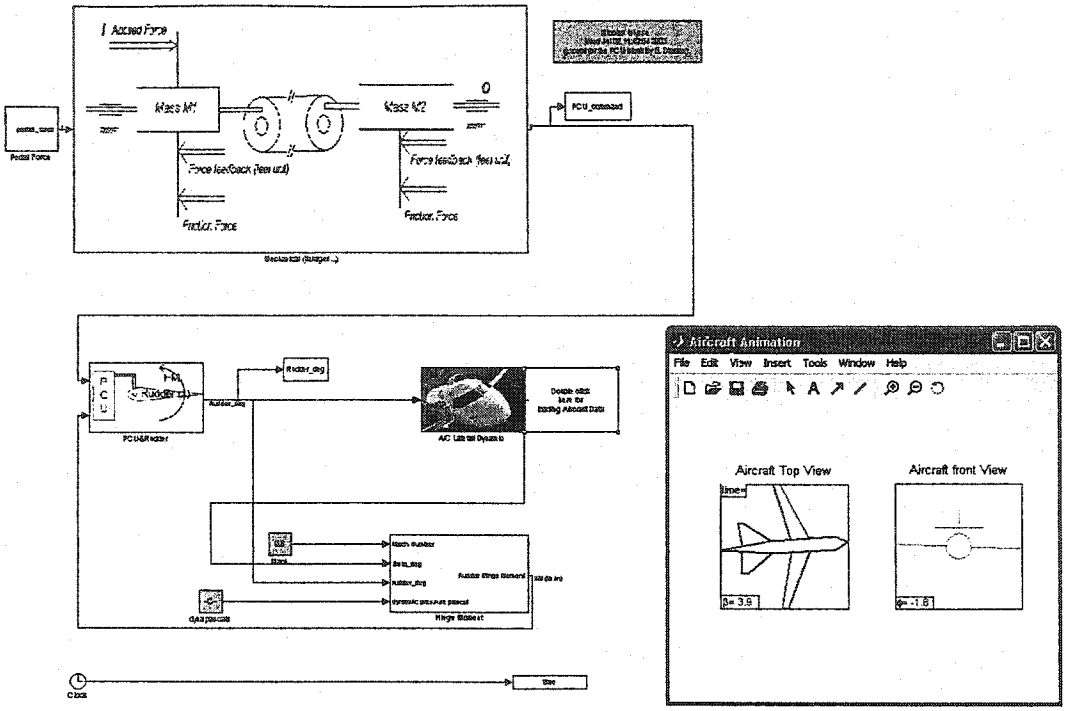

Figure E.5- Yaw Control System Simplified Model

Figure E.6 - E.8 are reproducing the simulation tests of *Section 4.4* in the body of this document (the choice of imperial units is justified by the will to ensure easy comparison). They demonstrate that the simplified model is reproducing the system behaviors with a reasonable fidelity.

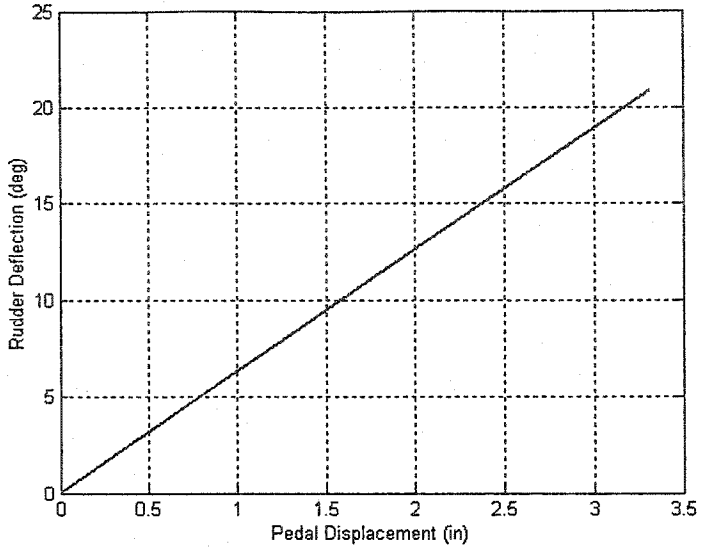

Figure E.6 – Simplified Model, Kinematic (Simulation time: 30s)

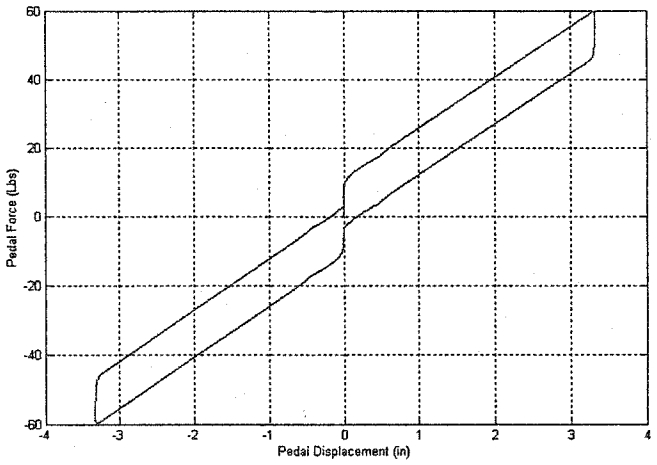

Figure E.7 – Simplified Model, Static (Simulation time: 120s)

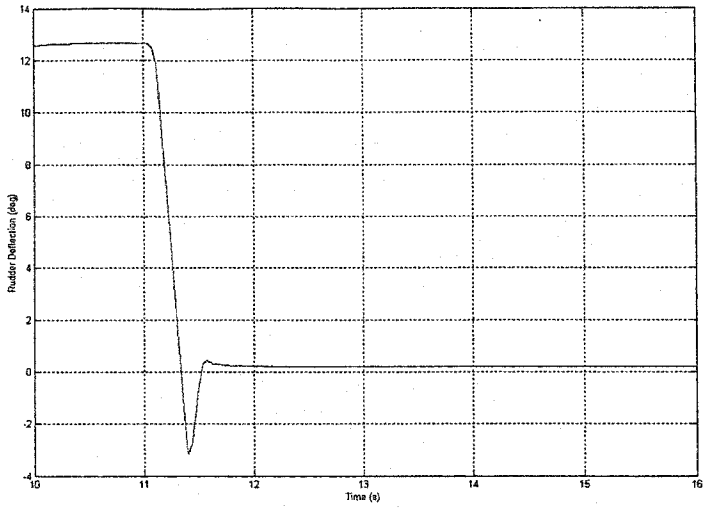

Figure E.8 – Simplified Model, Dynamic (Simulation time: 120s)

References:

E.1 C. Canudas de Wit, H. Olsson, K.J. Astrom, P. Lischinski, "A New Model for Control of Systems with Friction", IEEE Transaction on Automatic Control, Vol. 40, No 3, march 1995

E.2 Davaze E., "Investigation of Flight Control System Non-Linearities", M.A.Sc. Thesis – in progress, Concordia University, Montreal, 2003